INTERACTION BETWEEN MICRO AND NANO PATTERNED POLYMERIC
SURFACES AND DIFFERENT CELL TYPES

A THESIS SUBMITTED TO
THE GRADUATE SCHOOL OF NATURAL AND APPLIED SCIENCES
OF
MIDDLE EAST TECHNICAL UNIVERSITY

BY

HAYRİYE ÖZÇELİK

IN PARTIAL FULFILLMENT OF THE REQUIREMENTS
FOR
THE DOCTOR OF PHILOSOPHY
IN BIOLOGY

AUGUST 2012

Approval of the thesis:

INTERACTION BETWEEN MICRO AND NANO PATTERNED POLYMERIC SURFACES AND DIFFERENT CELL TYPES

submitted by **HAYRİYE ÖZÇELİK** in partial fulfillment of the requirements for the degree of **Doctor of Philosophy in Department of Biology, Middle East Technical University** by,

Prof. Dr. Canan Özgen   _____
Dean, Graduate School of **Natural and Applied Sciences**

Prof. Dr. Musa Doğan   _____
Head of Department, **Biotechnology**

Prof. Dr. Vasıf Hasırcı   _____
Supervisor, **Biological Sciences Dept., METU**

Dr. Celestino Padeste   _____
Co-Supervisor, **Paul Scherrer Institut,**
LMN Laboratory, Villigen Switzerland

Examining Committee Members:

Prof. Tülin Güray   _____
Biological Sciences Dept., METU

Prof. Dr. Vasıf Hasırcı   _____
Biological Sciences Dept., METU

Assoc. Prof. Dr. Can Akcali   _____
Mol. Bil. and Genetics Dept., Bilkent Uni.

Assist. Prof. Dr. Can Özen   _____
Biotechnology Dept., METU

Assist. Prof. Dr. Ergin Tönük   _____
Mechanical Eng Dept., METU

Date: 24.08.2012

I hereby declare that all information in this document has been obtained and presented in accordance with academic rules and ethical conduct. I also declare that, as required by these rules and conduct, I have fully cited and referenced all material and results that are not original to this work.

Name, Last name: Hayriye Özçelik

Signature:

ABSTRACT

INTERACTION BETWEEN MICRO AND NANO PATTERNED POLYMERIC SURFACES AND DIFFERENT CELL TYPES

Özçelik, Hayriye

Ph.D., Department of Biology

Supervisor: Prof. Dr. Vasıf Hasırcı

Co-Supervisor: Dr. Celestino Padeste

Micro and nanopatterned surfaces are powerful experimental platforms for investigating the mechanisms of cell adhesion, cell orientation, differentiation and they enable significant contributions to the fields of basic cell and stem cell biology, and tissue engineering. In this study, interaction between micro and nanopatterned polymeric surfaces and different cell types was investigated. Three types of micropillars were produced by photolithography (Type 1-3), while nanometer sized pillars were produced in the form of an array by electron beam lithography (EBL). Replica of silicon masters were made of polydimethylsiloxane (PDMS). Polymeric [P(L-D,L)LA and a P(L-D,L)LA:PLGA blend] replica were prepared by solvent casting of these on the PDMS template and used in *in vitro* studies. The final substrates were characterized by various microscopic methods such as light microscopy, atomic force microscopy (AFM) and scanning electron microscopy (SEM).

In order to investigate deformation of the nucleus in response to the physical restrictions imposed by micropillars, Type 1 and Type 2 pillars were used. These substrates were covered with pillars with different interpillar distances. While Type 1 is covered with symmetrically (in X-Y directions) distributed pillars, Type 2 pillars were distributed asymmetrically and the inter-pillar distances were increased. Nuclei deformation of five cell

iv

types, two cancer cell lines (MCF7 and Saos-2), one healthy bone cell (hFOB1.19), one stem cell (bone marrow origined mesemchymal stem cells, BMSCs) and one standard biomaterial test cell type, (L929) fibroblasts was examined by using fluorescence microscopy and SEM. The nuclei of Saos-2 and MCF7 cells were found to be deformed most drastically. Nucleus deformation and intactness of nuclear membrane was examined by Anti-Lamin A staining. The interaction of the cells with micropillars was visualized by labelling focal adhesion complexes (FAC). Wettabilities of patterned and smooth surfaces were determined. As the patterns become denser (closer micropillars, Type 1) the hydrophobicity increased. Similar to water droplets, the cells were mostly spread at the top of the Type 1 pillars. The number of cells spread on the substrate surface was much higher on Type 2 patterned films. In order to support these qualitative findings, nucleus deformation was quantified by image analysis. Frequency of nucleus deformation was determined as the ratio of deformed to the total number of nuclei (%). In order to quantify the intensity of nuclei deformation, their circularity was evaluated. In addition to nucleus deformation, alterations in the ratio of cell area-to-nucleus area in response to micropillars were determined by image analysis. The results indicated that cancerous cells were more deformable. The qualitative microscopic evaluation and the data obtained by quantification of the nucleus and cellular deformation were in good agreement. In addition, the findings were consistent with expectations which suggest that cancerous cells are "softer".

In the second part of the research the force applied by the cells on arrays of micropillars with high aspect ratios (Type 3 substrates) during tugging at the pillars was investigated. Micropillars were produced using P(L-D,L)LA as well as a 60:40 blend of P(L-D,L)LA with PLGA. The blend is a material with lower stiffness than P(L-D,L)LA. The mechanical properties of the two materials were determined by tensile testing of solvent cast films. Deformation of Type 3 micropillars by the cellular tugging force of Saos-2 and L929 was studied by fluorescence and SEM microscopy, both on stiff and softer substrates. Displacements of the centers nodes of the pillars were evaluated from SEM micrographs. On the stiff surface, the two cell types bent the pillars to the same extent. On the other softer substrate (blends), however, the maximum displacements observed with Saos-2 cells were higher than the ones caused on the stiffer substrate or the ones caused by L929 cells. It is reported that stiffness of the substrate can determine stem cell lineage commitment. In order to examine the effects of change of substrate stiffness on osteogenic differentiation of BMSCs, osteopontin (OPN) expression was determined microscopically. It was found that osteogenic differentiation is enhanced when BMSCs are cultured on P(L-D,L)LA Type 3 pillars.

In the last part of research, arrays of nanopillars whose interpillar distances systematically varied to form different fields were examined in terms of adhesion and alignment in order to determine the differential adhesion of BMSCs and Saos-2 cells. The difference in their adhesion preference on nanopillar arrays was quantified by image analysis. It was observed that BMSCs and Saos-2 cells behaved in an opposite manner with respect to each other on the fields with the highest density of nanopillars. The BMSCs avoided the most densely nanopillar covered fields and occupied the pattern free regions. The Saos-2, on the other hand, occupied the most densely nanopillar covered fields and left the pattern free regions almost unpopulated. It was also found that both BMSCs and Saos-2 cells aligned in the direction of the shorter distance between the pillars. Both BMSCs and Saos-2 cells started to align on the pillars if the distance in any direction was >1.5 µm. To better understand the effects of chemical and physical cues, protein coating and material stiffness were tested as two additional parameters. After fibronectin coating, the surfaces of P(L-D,L)LA films with the highly dense pillar covered fields, which were avoided when uncoated, were highly populated by the BMSC. Similarly, decreasing the stiffness of a surface which was normally avoided by the BMSCs made it more acceptable for the cells to attach.

Key words: Micro and Nanopatterned Surfaces, Nucleus Deformation, Cell Adhesion, Cell Alignment, Tugging Force, Substrate Stiffness, Nanopillar Array.

ÖZ

MİKRO VE NANODESENLİ POLİMERİK YÜZEYLERLERLE FARKLI HÜCRE TİPLERİ ARASINDAKİ ETKİLEŞİM

Özçelik, Hayriye

Doktora, Biyoloji Bölümü

Tez Yöneticisi: Prof. Dr. Vasıf Hasırcı

Ortak Tez Yöneticisi: Dr. Celestino Padeste

Ağustos 2012, 139 sayfa

Mikro ve nanodesenli yüzeyler hücrelerin tutunma (yapışma), yönlenme ve farklılaşma mekanizmalarını incelemekte kullanılan ve temel hücre biyolojisi, kök hücre biyolojisi ve doku mühendisliği alanlarına önemli ölçüde katkı olanağı tanıyan güçlü deneysel araçlardır. Bu çalışmada mikro ve nanodesenli polimerik yüzeylerle farklı hücre tipleri arasındaki etkileşimler incelenmiştir. Fotolitografi yöntemiyle üç tip mikro sütun üretilirken, nanometre boyutundaki sütunlar bir dizi biçiminde, elektron ışını litografisi (EBL) yöntemiyle üretilmiştir. Orjinal silisyum şablonların polidimetilsiloksan (PDMS) kopyaları yapılmıştır. *In vitro* çalışmalarda kullanılacak poli(L-D,L-laktik asit) [P(L-D,L)LA] ve poli(L-D,L-laktik asit): poli (laktik-co-glikolik asit) [P(L-D,L)LA:PLGA] karışımı polimerik filmler çözücü uçurma yöntemiyle hazırlanmıştır. Elde edilen filmler ışık mikroskobu, atomik kuvvet mikroskobu (AFM) ve taramalı elektron mikroskobu (SEM) gibi yöntemlerle incelenmiştir.

Mikro sütunların yarattığı fiziksel kısıtlamalara (etkilere) maruz kalmaları sonucu hücrelerin çekirdeklerinde oluşan deformasyonu incelemek amacıyla Tip 1 ve Tip 2 sütunlar

kullanılmıştır. Bu yüzeyler birbirine uzaklığı farklı sütunlarla kaplıdır. Tip 1 simetrik (X ve Y yönünde) dağılım gösteren sütunlarla kaplıyken, Tip 2'de sütunlar asimetrik olarak dağılmış ve sütunlar arası uzaklık artmıştır. Beş hücre tipindeki, iki kanser hücre hattı (MCF7 ve Saos-2), bir sağlıklı kemik hücresi hattı (hFOB1.19), bir kök hücresi (kemik iliği kökenli mezemşimal kök hücresi, BMSC) ve biyomalzeme testi standartı olan fibroblast (L929), çekirdek deformasyonu floresan mikroskobu ve SEM kullanılarak incelenmiştir. Saos-2 and MCF7 hücrelerinin çekirdeklerinin en çok deformasyona uğrayan çekirdekler olduğu bulunmuştur. Çekirdek deformasyonu ve çekirdek zarının bütünlüğü Anti-Lamin A boyması ile incelenmiştir. Hücrelerin mikro sütunlarla ilişkisi fokal adhezyon kompleksi (FAC) boyanarak gösterilmiştir. Desenli ve düz yüzeylerin ıslanabilirliği belirlenmiştir. Desen yoğunlaştıkça (Tip 1'de birbirine yakın duran sütunlardaki gibi) hidrofobik özellik artmıştır. Su damlasının davranışında olduğu gibi, hücreler en çok Tip 1 sütunlarının üstünde yayılmışlardır. Film taban alanına yayılan hücrelerin sayısı Tip 2 üstünde daha yüksektir. Elde edilen nitel (kalitatif) bulguları destelemek için çekirdek deformasyonu görüntü analizi yoluyla ölçülmüştür. Deforme olan hücrelerin sıklığı (frekansı) deforme olanların toplam hücre sayısına oranı olarak belirlenmiştir. Çekirdek deformasyonunun şiddetini ölçmek için çekirdeklerin yuvarlaklığı (circularity) değerlendirilmiştir. Çekirdek deformasyonuna ek olarak mikro sütunların etkilediği hücrelerde çekirdek alanının hücre toplam alanına oranı görüntü analiziyle belirlenmiştir. Sonuçlar kanser hücrelerinin daha çok deforme olabildiklerini göstermiştir. Mikroskobik değerlendirmeler, hücre ve çekirdek deformasyonu ölçümlerinde elde edilen verilerle uyum içindedir. Buna ek olarak, sonuçlar kanser hücrelerinin daha yumuşak olduklarını öngören beklentilerle de uyumludur.

Araştırmanın ikinci kısmında hücrelerin yüksek en-boy oranına sahip Tip 3 mikrosütun dizileri üstünde, mikro sütunları çekerken (veya mikro sütunlara asılırken) uyguladıkları kuvvetler incelenmiştir. Tip3 mikro sütunlar hem P(L-D,L)LA hem de 60:40 oranında P(L-D,L)LA ve PLGA karışımı kullanılarak üretilmiştir. Her iki malzemenin mekanik özellikleri çözücü uçurma tekniğiyle yapılan filmlerde çekme testiyle belirlenmiştir. Hücresel çekme (asılma) davranışı sonucu Tip 3 mikrosütunlarındaki deformasyonlar sert ve daha yumuşak filmlerde, floresan mikroskobu ve SEM ile çalışılmıştır. Sütunların tepe merkez noktalarının yer değiştirmesi SEM fotoğrafları kullanılarak ölçülmüştür. Sert yüzeyde her iki hücre tipi mikrosütunları aynı ölçüde eğmiştir. Öte yandan, daha yumuşak olan karışım yüzeyinde, sütunlardaki en büyük yer değiştirme Saos-2 hücresinde gözlenmiştir. Bu değer hem hücrenin sert yüzeyde neden olduğu yer değiştirmeden hem de L929 hücresinin neden olduğundan daha yüksektir. Yüzey sertliğinin kök hücresinin farklılaşacağı hücre tipini belirleyebildiği rapor edilmiştir. Yüzey sertliğinin BMSC'nin kemiğe farklılaşmasındaki

etkilerini incelemek amacıyla ostepontin üretimi mikroskobik olarak belirlenmiştir. BMSC P(L-D,L)LA sütunları üstünde çoğaltıldığında, bu hücrelerde kemiğe farklışmanın arttığı bulunmuştur.

Araştırmanın son kısmında, farklı bölgeler oluşturmak amacıyla birbirine uzaklığı sistemli bir biçimde değiştirilmek süretiyle elde edilen nano sütunlardan oluşan diziler, BMSC ve Saos-2 hücrelerinin ayrımsal tutunmalarını (yapışmalarını) belirlemek için hücre tutunması ve yönlenmesi bağlamında incelenmiştir. Bu hücrelerin nano sütun dizileri üstündeki yapışma tercihleri görüntü analiziyle ölçülmüştür. BMSC ve Saos-2 hücreleri nanosütunların yoğun olduğu bölgelerde birbirinin tamamen tersi biçimde davrandıkları gözlenmiştir. BMSC en yoğun nanosütun kaplı bölgelerden kaçınıp desensiz bölgeleri kaplamıştır. Öte yandan Saos-2, en yoğun nanosütun kaplı bölgelerde çoğalıp desensiz bölgeleri neredeyse tamamen boş bırakmıştır. Ayrıca, BMSCs and Saos-2 hücrelerinin sütunlar arası kısa uzaklık yönünde uzanım gösterdikleri bulunmuştur. Hem BMSCs hem de Saos-2 hücreleri sütunlar arası uzaklığın, x veya y yönünde >1.5 µm olduğunda yönlenmeye başlamaktadır. Fiziksel ve kimyasal ipuçlarının etkilerini daha iyi anlamak amacıyla yüzeyin proteinle kaplanması ve malzeme sertliğinin değiştirilmesi iki ek parametre olarak test edilmiştir. Fibronektin kaplaması sonrasında, P(L-D,L)LA film yüzeyinde kaplamadan önce hücrelerin kaçındığı yoğun sütun kaplı bölgeler BMSC hücreleri tarafından doldurulmuştur. Benzer biçimde, yüzey sertliğinin azaltılması, öncesinde BMSC hücrelerinin kaçındığı bölgeleri tutunma için daha kabul edilebilir hale getirmiştir.

Anahtar Kelimeler: Mikro ve Nanodesenli Yüzeyler, Çekirdek Deformasyonu, Hücre Tutunması (Yapışması), Çekme (Asılma) Kuvveti, Malzeme (Yüzey) Sertliği, Nanosütun Dizisi.

To my family...

ACKNOWLEDGEMENTS

TABLE OF CONTENTS

LIST OF TABLES

TABLES

LIST OF FIGURES

FIGURES

xvi

LIST OF ABBREVIATIONS

2D	Two Dimensional
3D	Three Dimensional
AFM	Atomic Force Microscope
BMSC	Bone Marrow Stem Cell
BSA	Bovine Serum Albumin
Cyt D	Cytochlasin D
DMEM	Dulbecco's Modified Eagle Medium
DPN	Dip Pen Nanolithography
ECM	Extracellular Matrix
ERK	Extracellular Signal Regulated Kinase
EUV	Extreme UV Light
FAC	Focal Adhesion Complex
FIB	Focused Ion Beam
Fn	Fibronectin
MAPK	Mitogen Activated Protein Kinase
MSCs	Mesenchymal Stem Cells
OPN	Osteopontin
P(L-D,L)LA	Poly(L-D,L-lactic acid)
PBS	Phosphate Buffer Saline
PDMS	Polydimethylsiloxane
PLGA	Poly(lactic-co-glycolic acid)
RIE	Reactive Ion Etching
SEM	Scanning Electron Microscope
SPL	Scanning Probe Lithography

CHAPTER 1

INTRODUCTION

Richard P. Feynman, the famous Nobel Laureate physicist given the landmark lecture on December 29th 1959, at the annual meeting of the American Physical Society. The title of his lecture was "There's Plenty of Room at the Bottom-An invitation to enter a new field of physics". For the first time "nanotechnology" was acknowledged as a new field of research by his proposal of development of molecule sized machines. Feynman believed that new and material properties on the level of atoms and molecules should be explored and the ability to control material properties by assembling such materials at the nanoscale could be exploited for research and device application.

In the past several decades, the advances in nanomaterial research provided the basis for innovations in the biomaterials field, regenerative medicine and nanobiotechnology. Just like conventional or micron sized materials, nanomaterials were produced from metals, ceramics, polymers, and composites, and in the forms of nanoparticles, nanocrystals, nanotubes, nanofibers, nanowires, nanorods, nanofilms, etc. In tailoring materials at the micro and nanoscale various industries have developed several top-down and bottom-up techniques such as phase separation, self-assembly, thin film deposition, chemical vapor deposition, chemical etching, nano-imprinting, photolithography, scanning probe lithography and electron beam lithography, etc.

All the cells in the human body are surrounded by topographical and chemical signals, these mainly consist of domains and biomolecules organized in different arrangements such as nanopores, nanofibers, nanocrystals. It is therefore possible to tailor nanoscale topographical surface cues to regulate cell function in much the same way the ECM does. In 1964, it was first proposed that cells react to the topography and to their environment (Curtis and Varde, 1964). Since then various substrates, carrying micro and nanofeatures (grooves, ridges, steps, pores, wells, pillars, and fibers) were produced. Studies have

shown that many cell types react strongly to these features by changes in adhesion, morphology, orientation, proliferation, migration, gene expression and differentiation. In addition, parameters such as surface chemical and mechanical properties (coating with compounds and substratum stiffness) were also shown to regulate cellular functions (Engler et al., 2006, Jing et al., 2011, Huang et al., 2011, Yu et al., 2012). Today, design and construction of substrates with well controlled physical and chemical properties, and micro and nano architecture is becoming an important tool in the construction of tissue-engineered replacements that stimulate cell growth and guide tissue regeneration. Medical devices are currently being engineered at the molecular levels for diagnostic and therapeutic purposes. Furthermore, by incorparation of microfluidics, researchers are able to create well perfused nano-scale environments to perform novel microassays. Thus, cellular biosensors and biomedical devices which can detect pathologic states are becoming logical applications of nanobiotechnology.

The aim of this study was to find a correlation between the size of physical cues (micro and nano pillars) with three main cellular responses: 1. Deformability, 2. Force applied by the cells on the pillars, 3. Adhesion. The first response involves the elucidation of difference in the deformability of cancer cells and their healthy counterparts and mesenchymal stem cells on the micropillar patterned polymeric films. The term deformability was used to explain the morphological changes in the nucleus and cell body in response to physical presence of micropillars. In other words, it does not refer to any detrimental effects of topographic features. Second one is about force with which cells tug at the underlying substrate covered with pillars. The stiffness of polymeric substrates and deflection of the central nodes of micropillars have taken into consideration. Finally, preference of the cells in adhering on an array of nanopillar covered field and the gaps in between. Influence of surface chemistry and stiffness on this was also studied. It should be noted that, "micro and nanopatterned" surfaces were used to mean surfaces covered with nano and micron sized structures. In the literature, the same phenomenon can be found to be expressed as micro and nano structured" surfaces.

1.1   Micro and Nanofabrication Techniques

1.1.1   Photolithograpy

Photolithograpy involves a writing process by the use of light, on a substrate (Schellenberg, 2003). The basic of photolithography is shown in Figure 1.1. Silicon wafers commonly used

2

in many devices are produced by this technique. Typically, layers of oxide, nitride, metal or any additive film are deposited and/or photoresists are coated on top. By exposure to a high energy light source (eg. UV) the patterns on the mask are transferred to the photoresist layer. Photoresist is an organic, light-sensitive material that can be either stabilized by crosslinking or degraded as a result of the reaction with the light. If the exposed portion is degraded, it is removed (positive photoresist) or stabilized, it is left behind (negative photoresist) after a developing process that dissolve the soluble resist. Thus, it is followed by etching of the exposed areas deposition of a new layer (eg. protein) step follows. Etching can be wet (chemical) or dry (reactive ion etching, RIE. In other applications, the additional layers can be deposited through the open areas of the photoresist film. This photolithographic process is performed with high accuracy and precision of the dimensions.
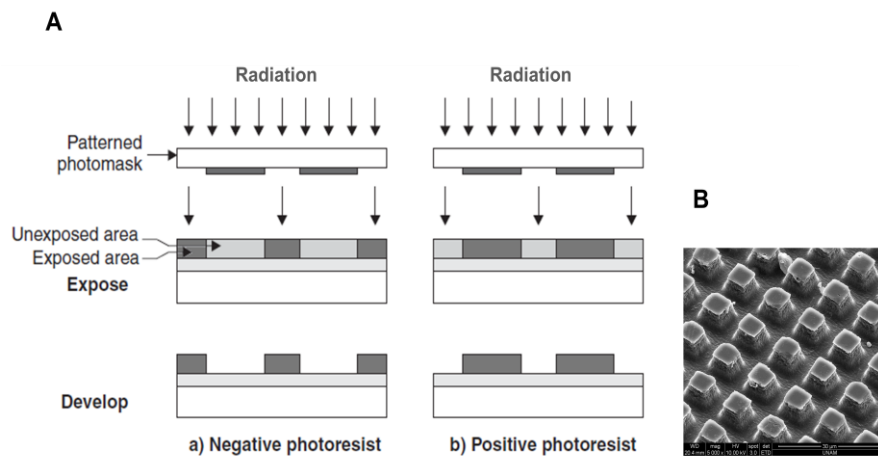
Figure 1.1. Illustration of the basic steps involved in photolithographic process (http://www. 2009.igem.org) (A), SEM micrograph of rectengular prism shaped micro-pillars produced by photolithograpy in Bilkent University, Physics Laboratory (B).

In lithography, the resolution of features is determined by the wavelength of beam used. The resolution of conventional lithography technique is about 1 µm using light of 400 nm (Gates et al., 2005, Shingi et al., 2003) Due to this reason, the conventional lithographical system with UV source results micron level resolution at most. To overcome the current

limitation in resolution, shorter wavelength exposure sources such as EUV (extreme ultraviolet lithography, wavelength ~10 nm) or X-ray wavelength ~1 nm) can be preferred. In another approach, Gates et al (2005) inserted a lens between the mask and the wafer in order to image the mask onto the surface of the resist. Other improvements include "immersion lithography" and "double pattern" lithography. In "immersion lithography" the space between the lens and the wafer is filled with water to take advantage of the higher index of refraction for achievement of smaller feature pitch (French and Tran, 2009) in which a subset of the final pattern is exposed and processed, followed by the exposure of the remaining patterns in a subsequent process in order to complete the pattern. This eliminates interference of very closely spaced patterns (Moon et al., 2004).

1.1.2 Electron Beam Lithograph

The resolution of this approach to photolithography is controlled by the wavelength of the radiation source, therefore a short-wavelength beam is more suitable. For this purpose, radiation sources such as extreme ultraviolet (EUV) and X-ray can be used. However, due to the inherent diffraction and lens aberration in optical system EUV and limitation in image reduction ratio and difficulty in generating mask patterns (X-ray), a direct beam writing method such as that with an electron beam (E-beam) or with an ion beam lithography have also been used (Chiu and Shaw 1997). It has been developed based on the same principles of scanning electron microscopy to write large and complex patterns with nanometer details.

EBL uses a direct write approach for forming patterns in a layer of material and generates the designs from a data file instead of a mask. The e-beam is moved across the surface under computer control using a pattern generator program. After creating the pattern on the resist on the substrate, the conventional lithographic procedures are employed. Though it is possible to focus the e-beam onto a sample with a resolution of 0.5 nm, the properties of the polymeric resist limits the final resolution achiavable to approximately 5 nm. The schematic cross-section of the column is presented in Figure 1.2. The complete e-beam column consists of the following building blocks: an electron source or gun, a first lens system to generate a square shaped beam, a second lens system to provide illumination of individual square sections -subfields- of reticle with square beam of essentially the same size, deflectors and correctors to scan the beam over multiple subfileds with minimal loss of image quality and to control exposure timing. Lenses, deflectors and correctors all use magnetic fields to position the beam, whereas the exposure is controlled with high speed

electric deflectors moving the beam on and off a beam stop with a pass-through aperture. The third lens system projects the reticle subfields reduced in size onto the wafer, including the means to maintain image quality and accurate stitching. Located between the illumination and imaging sections is the reticle mounted on movable stage in a chamber; the wafer is mounted on a similar stage below the imaging section.
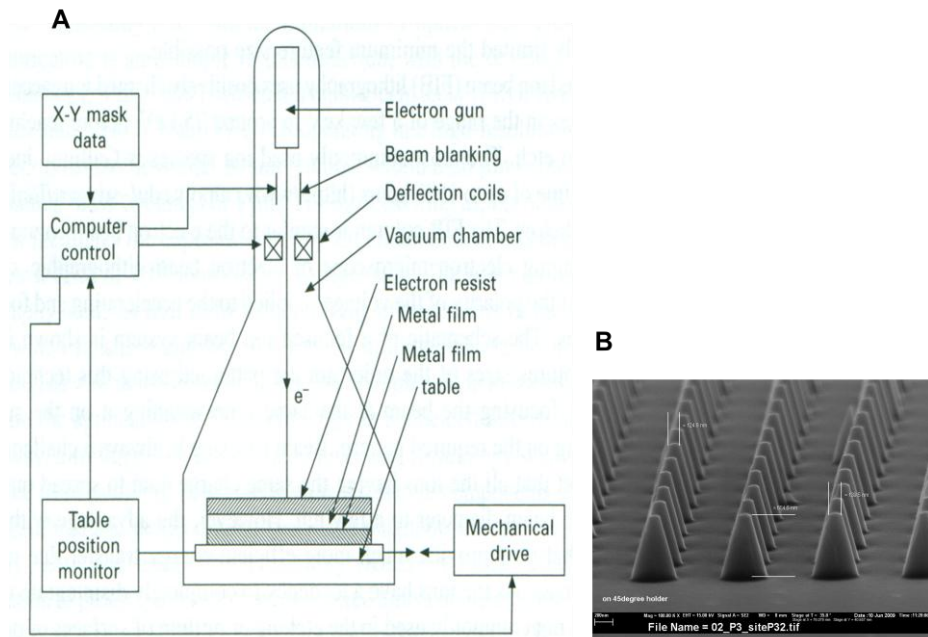
Figure 1.2. Presentation of mask preparation approach using e-beam etching (Wiederrecht 2010) (A), SEM micrograph of pyramidal nanopillars produced by EBL in PSI-LMN Laboratory (B).

Column and stage chambers are under vacuum (10^{-5} torr), requiring appropriate reticle and wafer load/unload system to connect to the outside. Except the vacuum requirements, the column and mechanical system closely resembles optical scanners that one in widespread use today. The electronic control system, however, is much more sophisticated.

1.1.3   Focused Ion Beam Lithography

Ion beams have long been used for surface modifications of materials and thin films through doping or etching. One of major advantages of focused ion beams is that the ions

suffer very little back scattering compared to the electrons and this constitutes a major limitation of EBL.

Focused ion beam (FIB) lithography uses positively charged ions accelerated to energies in the range of a few keV to around 75 keV, before reaching the sample to etch. The most commonly used ion species is Gallium due to its long lifetime up to 1500 hours. A liquid metal source provides Ga atoms. The gallium reservoir is in contact with a sharp tungsten needle and wets its tip. A high extractor voltage (around 10 kV) induces a high electric field of more than 10^{10} V/m at the tip. A sharp cone of Ga atoms forms at the tip and Ga atoms are ionized then emitted. The FIB column is similar to the electron beam column of scanning electron microscope or electron beam lithographic system, except for the polarity of the voltages applied to accelerating and focusing electrodes. The schematic view of a typical FIB system is shown in Figure 1.3.
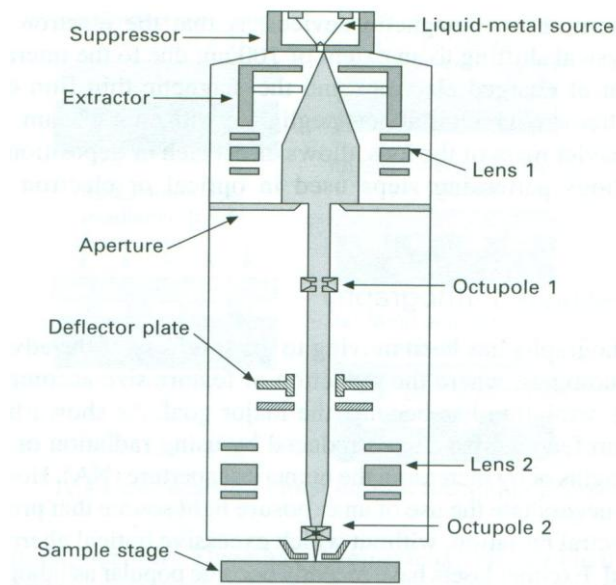
Figure 1.3. Schematic cross-sectional view of FIB system. (Wiederrecht 2010).

1.1.4 Soft Lithography

Soft lithography is another high resolution patterning technology, first proposed by George Whitesides at Harvard University to categorize which used a soft elastomeric stamp or mould (usually PDMS (poly(dimethylsiloxane)) that transfers the pattern to a substrate

(Kumar and Whitesides, 1993, Whitesides and Stroock, 2001, Rogers and Nuzzo, 2005). This method usually employs a microscale replica of the original produced by molding PDMS. Soft lithography covers a wide range of techniques such as, microstamping, stencil patterning, microcontact printing, replica molding, microtransfer molding, phase shift photolithography, cast molding, embossing, microfluidic patterning and inkjet molding (Xia and Whitesides 1998).

The major advantage of the soft lithography is the ease of fabrication. The softness of the materials used in the process allows the fabrication of features two orders of magnitude smaller than those fabricated by conventional silicon micro-machining and lithographic technologies. More importantly, these are not limited by diffraction effects as commonly seen in conventional photolithography, which extends the attainable minimum feature sizes below 30 nm level. However, it may be noted that the master used in all soft lithographic techniques needs to be produced using EBL or another high-resolution photolithographic techniques.

1.1.5   Scanning Probe Lithography (SPL)

Scanning probe lithography (SPL) is the term used for describing an atomic scale writing process based on scanning tunneling microscopy (STM), which was initially developed at the IBM Zurich Lab in the early in 1980s. The STM can generate images using a sharpened conducting tip over the surface with a constant tunneling current. A typical STM has sub-angstrom vertical resolution and sub-nanolateral resolution but, low throughput. Solutions have been suggested to improve these situations such as multiple tip operation and scan speed enhancement by integrated control (Minne et al., 1998, King et al., 2001).

The most important member of SPM family is Atomic Force Microscope (AFM). AFM was developed based on STM principles and by the same research group (Binning et al., 1986). The AFM is made of a cantilever beam with a sharp tip at its free end which scans over the surface (Figure 1.4). The deflection of the beam varies, depending on the attractive and repulsive interaction between the tip and the surface. By measuring the deflection, topographical images can be obtained. For nanofabrication, the same tools are used to deposit, remove and modify the materials on the surface.

AFM can achieve for the high resolution profiling of nonconducting surfaces, is nondestructive and does not require any specific sample preparation. Imaging in liquid

allows the study of live biological samples. The vertical resolution of AFM images is generally dictated by the interaction between the tip and the surface and the lateral resolution is determined by the size of the tip and can be at the level of electron microscope.
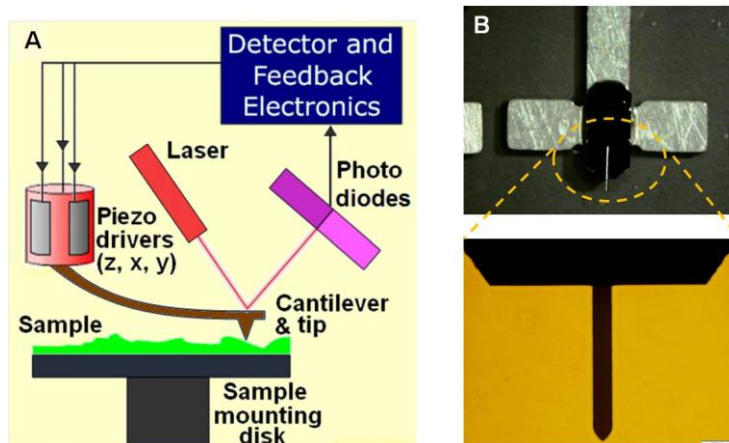
Figure 1.4. Basics of atomic force microscope. (A) A cantilever with a very fine probe, moves along the surface and experiences atomic forces. Laser and photodiode are used to measure those forces (Tseng 2011), (B) A closer view of a cantilever. Scale bar is 100 µm.

The best known additive nanofabrication technique achieved using scanning probe is dip pen nanolithography (DPL) that was developed by Chad Mirkin and coworkers in 1999. SPL approach allows deposition of nanoparticles or molecules, selectively, onto a surface. This method has capability to pattern lateral features with dimensions of down to 100 nm. DPN is a direct write technique that is used to create nanostructures on a substrate by delivering molecules via capillary effect from AFM tip to the surface. The migrated molecules are then immobilized by self assembly (Figure 1.5). DPN has evolved as a versatile method for producing multicomponent arrays of SAM (Self assembled monolayer) as well as other molecules viruses, proteins, oligonucelotides, phopholipids and nanomaterials (Ginger et al., 2004).
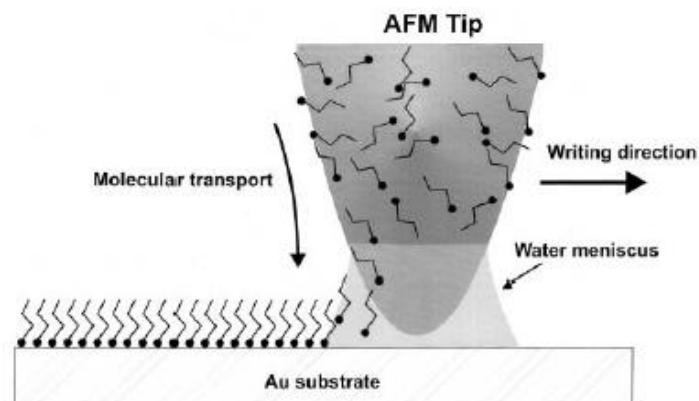
Figure 1.5. Schematic presentation of DPN showing the transfer of 1-octadecanethiol (ODT) to gold surfaces (Piner et al., 1999).

1.1.6   Comparison of Micro and Nanofabrication Techniques

Nanofabrication has become one of the the most rapidly growing field of nanotechnology in the last decade, and can be achieved by two general routes: bottom up and top down (Table 1). Bottom-up techniques refer to well-controlled building up of nanomaterials and devices by putting individual units alongside and on top of other units. These techniques include atomic layer deposition, sol–gel nanofabrication, molecular self assembly, vapor-phase deposition (Huie 2003, George S.M., 2010, Xiu et al., 2008, Dervishi et al., 2009). Top down techniques, on the other hand involve reshaping of existing materials. They include lithographic techniques such as optical, electron beam, soft, nanoimprin and scanning probe, lithography which have been discussed in the previous sections. The border line patterning capability of top down methods was suggested as ≤ 100 nm in multi-directional patterning capability was determined as the boderline for top-down methods. All these techniques were compared in Table 1.1. which is adapted from the recent review of Biswas et al. (2012).

9

Table 1.1. Comparison of micro and nanopatterning techniques (Biswas et al., 2012).

	Methods	Resolution	Complexity	Structural Defect	Material Range
Top-down Techniques	Optical Lithography	50 nm	High	Low	Inorganic and organic
	E-beam Lithography	10 nm	High	Extremely Low	Mostly organic
	Nanoimprint Lithography	5-10 nm	High	Low	Inorganic and organic
	Scanning Probe Lithography	<5 nm	High	Extremely Low	Mostly organic
	Block Co-polymer Lithography	10 nm	Low	Low	Inorganic and organic
Bottom-up Techniques	Atomic Layer Deposition	<5 nm	High	Extremely Low	Mostly organic
	Sol-gel	50 nm	High	High	Mostly organic
	Molecular Layer-by-layer and Directed Self Assembly	<5 nm	Low	Low	Inorganic and organic
	Physical and Chemical Vapor Deposition	<5 nm	High	Low-moderately high	Inorganic and organic

The developments referred to above are openning up new possibilities in medical applications. A new field called nanobiomedicine has emerged as a result of these. It has become increasingly evident that cells are affected by textures, chemical and biological cues, and mechanical forces at the micro and nanoscale. Particularly, nanomaterials with complex surface features and well controlled physical and chemical properties constitute a rapidly developing platform that mimics the biological systems. These are becoming the prerequisites of and designing better implants. Another exciting possibility is the emergence of smaller and more sensitive diagnostic and therapeutic tools and devices.

In the following sections surface topography and their interactions with cells are covered.

1.2   Deformability of Cells and Nuclei

The study of cell biomechanics is important for understanding cell behavior in tissues, in the development of diagnostic methods for cell identification and development of the therapeutic approaches. Therefore, the measurement of the viscoelasticity and

deformability of cells started to receive much attention in the recent years (Suresh et al., 2007). In this section biomechanics of cancer and stem cells were discussed.

1.2.1   Biomechanical Tools

Cells sense and respond to chemical, topographical and mechanical signals originating from the extracellular matrix or from intercellular interactions. Cell biomechanics involves the study of the mechanics of living cells and their relations to diseases (Fitzgerald, 2006). Technological advances over the last few decades in the fields of micro and nanotechnology and in the visualization techniques have intensified the research on mechanical properties of cells. These tools allow scientists to measure forces and displacements at piconewton and nanometer scales, respectively, and these help deduce the physiological states of molecules and cells.

To date, various groups have used different techniques (Bao and Suresh, 2003, Suresh, 2007) such as magnetic beads (Mijailovich et al., 2002), optical tweezers (Guck et al., 2001, Dao et al., 2003, Mills et al., 2004), optical stretchers with microfluidics (Guck et al., 2005, Remmerbach et al., 2009), magnetic twisting and pulling cytometry (Gardel et al., 2004, Overby et al., 2005), micropipette aspiration (Ward et al., 1991, Hochmuth R.M, 2000), optical tweezers (Guck et al., 2001), magnetic tweezers (Bausch et al., 1999,) atomic/molecular force probes (Lekka et al., 1999, Park et al., 2005, Suresh, 2007) microplate manipulators (Thoumine et al., 1999). Figure 1.6. presents these biomechanical tools.
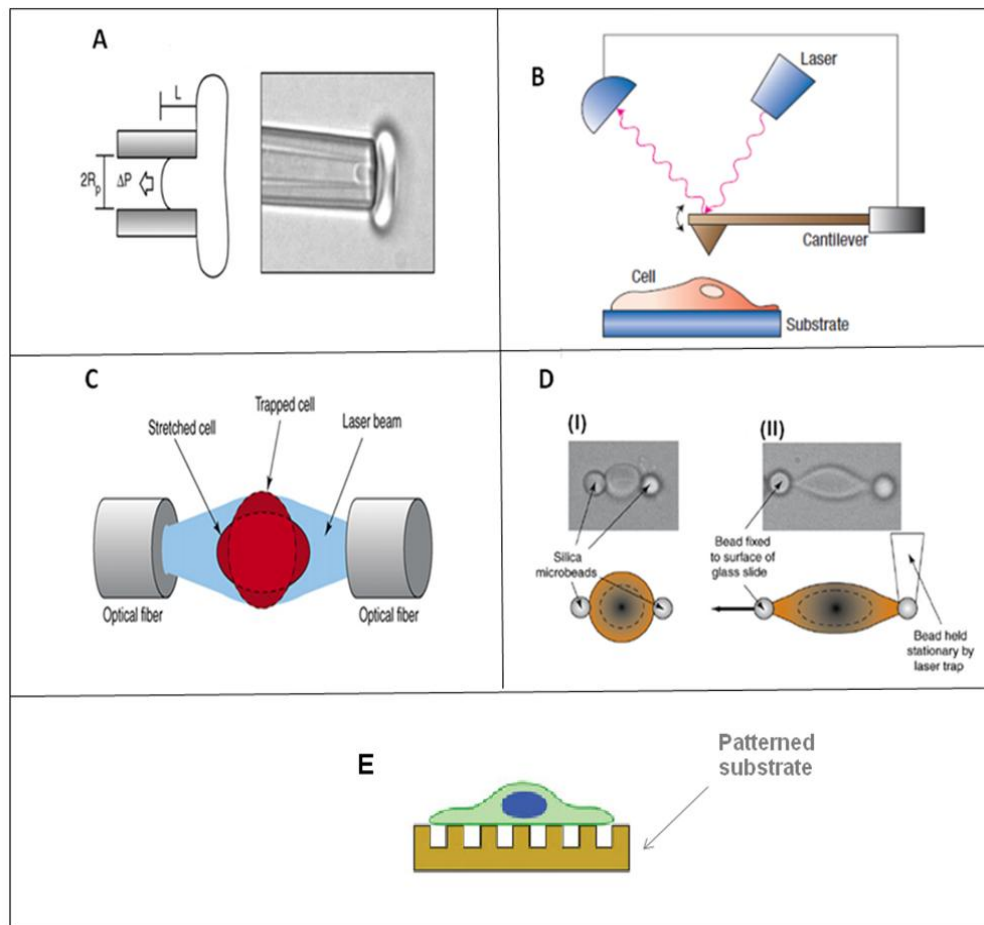
Figure 1.6. Schematic diagram of biomechanical techniques used to determine cell response (A) Micropipette aspiration, (B) Atomic/molecular force probes, (C) Optical tweezers, (D) Magnetic tweezers, (E) Micro-postarray deformation (Sureh et al., 2007, Davidson et al., 2009).

Micropipette aspiration can be applied to both adherent and non-adherent cells and it was used to study the deformabilities of red blood cells (RBCs) infected with *Plasmodium falciparum* at different stages of infection by Nash et al. (1989). They reported a decrease in stiffness of RBCs infected by the parasite-exported proteins. The rigidity of the cell membrane and cytoskeleton can be calculated from applied pressure and resultant aspiration length (Hochmuth, 2000).

AFM functions as a powerful tool due to its high-resolution topographical imaging ability and presence of a force sensor with pico newton sensitivity (Lim et al., 2006). The local stiffness of a cell is measured and stiffness is mapped by indentation with the micro-scale cantilever.

Optical tweezers (or optical stretchers) also allow the measurement of mechanical response of a single cell at pico newton forces and micrometer resolutions (Mills et al., 2004, Lim et al., 2006). In this method, a trapped cell is stretched along a laser beam axis by increasing the power of a laser on either side of the cell and deformation of the cell is measured which is then correlated with cytoskeletal rigidity. Particles can be attached to the cell membrane and manipulated laterally and the laser power required to constrain the particle is used to measure the stiffness of the cell. Recently, different groups have developed a combinatorial technique by coupling the optical stretcher system with a microfluidic flow chamber to characterize thousands of individual non-adherent cells (Lincoln et al., 2004, Guck et al., 2005, Remmerbach et al., 2009).

Post-patterned microarrays were developed by thin film lithographic technologies. Cells adhered on the surface cells sense the local elasticity of their matrix by pulling on the substrate via cytoskeleton-based contraction. These tractional forces are tuned by the cell to balance the resistance provided by the substrate. These post devices serve to measure cellular forces exerted on the posts (Tan et al., 2003, Van Vliet et al., 2003, Wong et al., 2004, Liu and Chen, 2005, Schoen et al., 2010).

1.2.2 Anatomy of the Nucleus

The nucleus is the largest organelle (~5–20 μm in diameter) in a eucaryotic cells and it is positioned by the cytoskeleton near the center. It is interconnected to ECM via integrin and cytoskeletal cross-linkers such as actin filaments, intermediate filaments, and microtubules, plectin and nesprin. Interconnected ECM receptors, cytoskeletal elements, and nuclear scaffolds is presented in Figure 1.7.
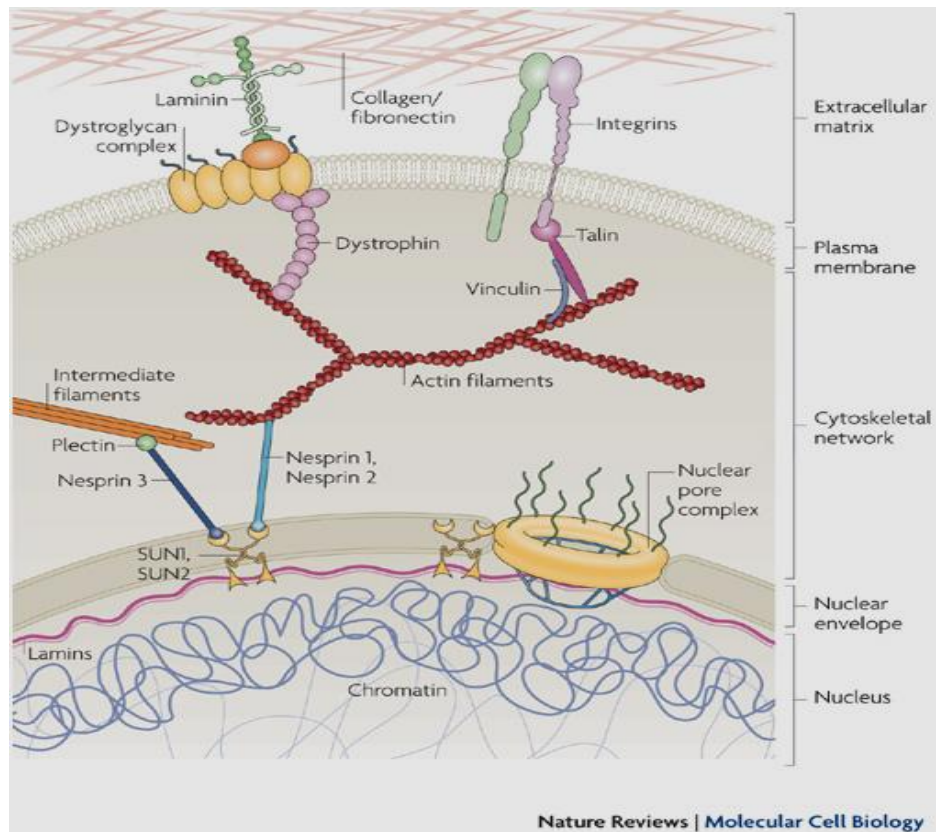
Figure 1.7. A scheme of the interconnectivity between ECM, cytoskeletal elements and nucleus. (Jaalouk and Lammerding, 2009).

ECM, consists of a variety of molecules including proteins such as collagen, laminin and fibronectin. These proteins transmit forces arising from cell-material interaction through focal adhesion complexes that are used in attachment to the ECM. This complex is comprised of integrins, talin, vinculin and other proteins and provides physical link between ECM and the cytoskeleton. External forces are transmitted through the cytoskeletal network consists of actin filaments, microtubules and intermediate filaments to the intracellular elements and the nucleus. The cytoskeleton is connected to the nucleus through nesprins and other proteins on the outer nuclear membrane such as SUN1 and SUN2. A similar contact is seen in pore complexes. The lamins bind to chromosomes and that might lead to modifications in gene expression.

The nucleus can be divided into two compartments: the nuclear envelope and the nuclear interior. The nuclear envelope is composed of the inner and the outer nuclear membranes,

and it physically separates the genetic content from the cytoplasm. The inner and outer membranes are interconnected at the sites of nuclear pores.

Underlying the the inner nuclear membrane the lamina forms a protein network (Dahl et al., 2004, Rowat et al., 2008). The lamina is a fibrous meshwork that is mainly comprised of lamins, type V intermediate filaments specific to the nucleus. Mammalian somatic cells express two lamin isoforms: A-type (mainly lamins A and C, resulting from alternative splicing of the LMNA gene) and B-type lamins (lamins B1 and B2). Nuclear lamins give the structural integrity of the nucleus. The nuclear lamina acts as a nuclear "shock-absorber", and is the main determinant of nuclear shape and stiffness (Lammerding et al., 2006, Shimi et al., 2008, Schape et al., 2009). B-type lamin is expressed ubiquitously whereas A-type lamins are expressed only in differentiated cells. Aspiration experiments of Pajerowski et al. (2007) showed significant stiffening of soft mouse embryonic stem cells after differentiation in culture. Thus, nuclear stiffening can be attributed to differential expression of A-type lamins. The lamins also differentially expressed in many cancers. Lamins A and C are over-expressed in ovarian cancers (Hudson et al., 2007), and in colorectal cancer (Willis et al., 2008); and they are silenced in leukemias and lymphomas (Agrelo et al., 2005), small cell lung cancer (Broers et al., 1993) and gastrointestinal cancer (Moss et al. 1999).

Lamins are also thought to be involved in important nuclear processes, such as regulation of transcription and chromatin organization (Dechat et al., 2008). Differentiated cells reflect highly condensed and rigid chromatin (Krauss et al., 2005, Pajerowski et al. 2007, Hampoelz and Lecuit, 2011). Chromatins are mechanically integrated with the cytoskeleton through nuclear envelope and the lamin network. Hence, bidirectional intearctions between these cellular elements affect cell function and behavior. Changes in chromatin configuration are also associated with cancer cells since these create more open chromatin (Pajerowski et al., 2007).

The coordinated alignment and interaction of structural elements through the interconnected network is explained by Ingber et al. (1997) with in the concept of tensegrity and mechanotransduction. Tensegrity explains how local stresses produce coordinated changes in cell and cytoskeleton. Mechanotransduction defines a mechanism by which cells convert mechanical stimuli into biochemical responses. These changes and biochemical responses can have important implications in cell development and function or disease states.

1.2.3 Biomechanics of Cancer Cells

It is known that when a normal cell transforms into a cancerous one, its growth, morphology and organization of the cytoskeleton structure change (Asch et al., 1981, Chakraborty and Von Stein, 1996).

With micropipette aspiration, a 50% reduction in elasticity response of malignantly transformed fibroblasts as compared to their normal counterparts was observed (Ward et al., 1991).

Lekka et al., (1999) have compared elastic properties of two normal human bladder cell lines (Hu609 and HCV29) with three cancerous ones (Hu456, T24, BC3726) by SPM and found that normal cells have a Young's modulus of about one order of magnitude higher. Findings of Darling et al (2007) also confirmed the reduction in the resistance of human chondrosarcoma cell lines to deformation.

For example, differences in elasticity and viscosity between normal and malignantly transformed fibroblasts were shown on single suspended cells (Wottawah et al., 2005). The test performed with the optical stretchers and it revealed that normal cells were 50% more rigid than the cancerous cells. In another study, primary oral cells obtained from the oral mucosa of cancer patients were compared with normal oral epithelial cells and cancer cells were shown to have higher a mean deformability (Remmerbach et al., 2009).

All this literature suggest that cancerous cells are "softer" or more deformable than healthy cells. It was also reported that metastatic cancer cells display even greater reduction in structural strength than the malignant ones (Raz and Geiger, 1982, Ward et al., 1991, Guck et al., 2005).

Darling et al. (2007) tested with AFM the viscoelastic properties of three human chondrosarcoma cell lines which had different degrees of invasiveness and malignancy. While the most malignant human chondrosarcoma cell line JJ012 showed the lowest moduli, it was followed by other two cell lines (FS090, 105KC) which are known to be less metastatic. Lincoln et al., (2004) investigated optical deformability of three types of cells by an optical stretcher combined with a microfluidic delivery system. They showed that nonmetastatic mammary epithelial cancer cells were about five times more stretchable than normal cells. Metastatically competent cells modified from a nonmetastatic cancer cell by

phorbol ester treatment were found to stretch about twice as much as the unmodified nonmetastatic cancer cells. Similarly, by using AFM, Cross et al., (2009) reported that live metastatic cancer cells taken from the lung, chest and abdomenal cavities of a patient were nearly four times less stiff than benign cells from similar cavities. In addition, they observed that metastatic cancer cells 70% softer when compared to non metastatic ones. Guck et al. (2005) used a different approach; they measured the deformability of highly metastatic breast cancer cells (MDA-MB-231) before and after treatment with all-trans retinoic acid. This drug is a chemotherapy agent which used to treat acute promyelocytic leukemia. After the treatment MDA-MB-231 cells become less aggresive (less metastatic). Correspondingly, the optical deformability decreased with loss of metastatic property. Thus, the correlation between increased cell deformability and progression of a transformed phenotype from a nontumorigenic, to malignant one can be used for mechanical phenotyping of the cells.

When a normal cell transforms into a cancerous one, its morphology and cytoskeleton changes.This causes changes in their ability for adhesion, movement and spreading on substrates. Low stiffness of cancerous cells may be a result of a partial loss of actin filaments and/or microtubules (Ben-Ze'ev, 1997). Changes in the cytoskeletal organization have been associated with tumorigenesis and the viscoelastic nature of metastatic cancer cells is consistent with their ability to squeeze through the surrounding tissue matrix, to pass through the walls of blood vessels and lymph systems and circulate through these systems and to form tumors at distant regions of the body (Shah-Yukovich and Nelson, 1988, Wyckoff et al., 2000, Lindberg et al., 2004, Buda and Pignatelli, 2004). Changes in the expression of cytoskeleton genes and their regulatory proteins can be taken as indication of the progression of cancer from early, benign stage to aggressive, metastatic stage. Creekmore et al., (2011) have shown a 78% reduction in F-actin concentration in the course of transition from early stage to late stage in progressive ovarian cancer in mice. In the same study, progressive loss and disorganization of the cytoskeleton is also reflected by the drastic changes in the expression of actin and actin binding regulating genes. Such pathophysiological alterations of the cytoskeletal architecture during the progression of cancer is further confirmed by very recent study by Ketene et al. (2012) who measured cell elasticity and viscosity of the ovarian cancer cells by AFM and found a 50% decrease in transition from early to late stages.

Abnormalities in nuclear morpologies such as indentations, undulations, polylobulations are alo linked to cancer (Zink et al., 2004). These changes can be specific for different cancer

17

types and for the stage of disease (De May, 1996). In addition, Dahl et al. (2008) proposed that the altered nuclear shape and reduced nuclear stiffness in cancer cells facilitates the formation of metastases because these could increase the penetration of the transformed cells in to the tissues. Although it is not clear how changes in nuclear morphology affect characteristics of a cell, two mutually exclusive hypothesis can be proposed: 1) Changes in nuclear shape alter the rigidity of the nucleus; this could be beneficial for cells that need to squeeze through tight spaces, 2) These changes are often accompanied by an altered nuclear lamina and spatial organization of the chromatins and altered gene expression. Thus, stiffness based assays might be useful diagnostic markers in combination with morphology based automated imaging and image analysis.

1.2.4   Biomechanics of Mesenchymal Stem Cells (MSCs)

Mesenchymal stem cells (MSCs) are one of the most promising types of adult stem cells for cell based therapies, regenerative medicine and tissue engineering. MSCs are nonhematopoietic and multipotent. They can differentiate into osteocytes, chondrocytes, adipocytes, tenocytes and stromal cells under appropriate in vitro conditions (Caplan 1991, Pittenger et al., 1999.) Figure 1.8 explains the multipotentiality of MSCs. These cells show the ability of self-renewal and differentiation mesodermally origined tissued (solid arrows). In addition, they can transdifferentiate into ectoderm and/or endoderm origined cell types (dashed arrows).
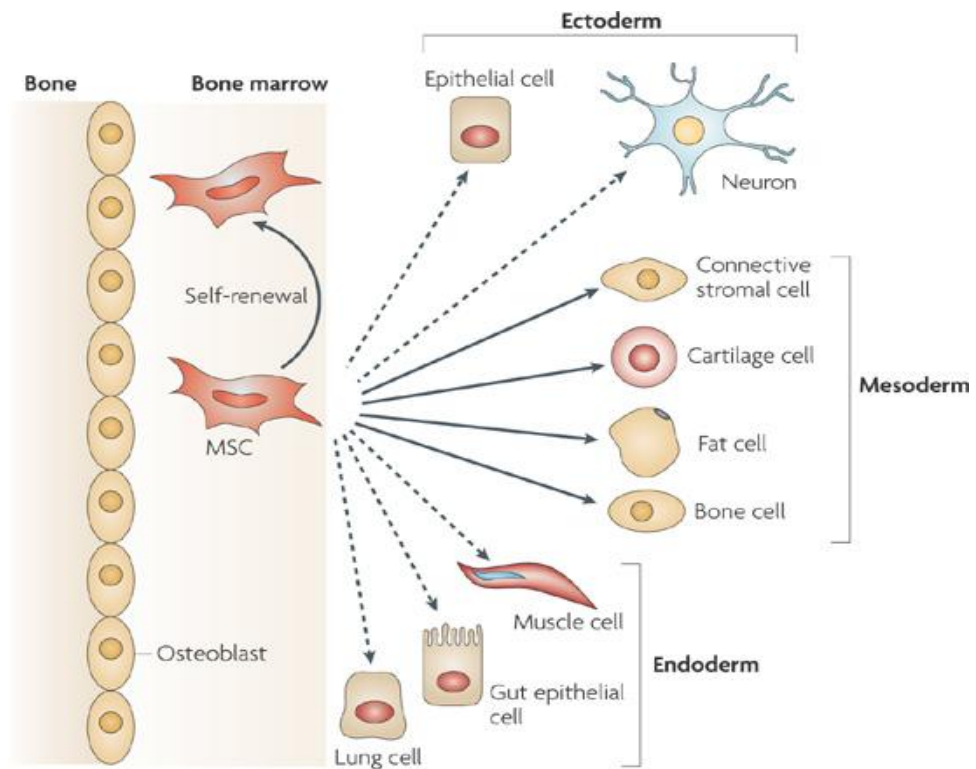
Figure 1.8. Schematic view of the multipotential characterictics of MSCs and all cell types MSCs can differentiate or transdifferentiate (Uccelli et al., 2008).

MSC was first described by Friedenstein et al. as fibroblast precursors from bone marrow in 1970. Because of that, MSCs were named as fibroblast colony-forming units (CFU-Fs) or marrow stromal cells (Phinney, 2002). There is evidence that MSCs exist not only in mesoderm origined tissues such as adipose, muscle, bone, and tendon but also in non-mesodermal tissues and organs. (Krampera et al., 2007, Prunet-Marcassus et al., 2006). Da Silva Meirelles et al., (2006) reported that they isolated plastic-adherent MSC-like colonies from the brain, spleen, liver, kidney, lung, bone marrow, muscle, thymus, and pancreas of mice.

Although there is not a complete list of markers for MSCs, their cell surface antigen profile has been well studied (Kolf et al.,2007). "The Mesenchymal and Tissue Stem Cell Committee of the International Society for Cellular Therapy" proposed that cells must be

positive for CD73, and CD90 and CD105, and negative for CD45, CD34, CD14 or CD11b, CD79a or CD19, and HLA-DR to be defined as MSC.

Stem cells are different from differentiated cells with their biochemical, structural and mechanical properties (Le Blanc et al., 2003). Cell shape, cytoskeleton organization and elasticity, deformability and adhesion strength, matrix elasticity may play an important role in cell fate (Thomas et al., 2002, Settleman J., 2004, Murphy et al., 2004, Engler et al., 2006, Fu et al., 2010). During the process of differentiation, cells undergo a number of morphological and molecular changes originating from expression of cytoskeletal proteins and their spatial distribution. Particularly actin and its downstream effectors play the major roles in ostegenic differentiation of hMSC (Mac Beath et al. 2004, Rodriguez et al., 2004, Titushkin and Cho, 2007).

Mac Beath et al. (2004) have demonstrated that when human MSCs are allowed to adhere, flatten, and spread they became osteoblasts but unspread and round cells underwent adipogenesis.

In another study, patterned cells deposited in groups of different shapes were treated with a mixture of adipogenic and osteogenic differentiation molecules to initiate the differentiation of MSCs. Patterns or shapes which promoted formation of more contractile actin cytoskeleton led to osteogenic lineage while shapes of identical area that disrupt contractility favored adipogenic differentiation. The same results were also supported by microarray analysis which suggested that increased myosin contractility enhances osteogenesis through MAP kinase and Wnt signaling pathways (Kilian et al., 2009).

Yourek et al., (2007) used Cytochalasin D (CytD) to temporarily disrupt cytoskeleton in hMSCs, hMSC derived chondrocytes and in osteoblasts to show that changes of cytoskeletal components are linked with MSC differentiation. The changes in actin cytoskeleton caused by actin disruption and repolymerization and differentiation of the cell were studied by AFM and distinct differences between the actin cytoskeletons of undifferentiated and differentiated hMSCs were observed. The actin cytoskeleton of hMSCs was thicker and more disordered with entangled actin filaments after osteogenic differentiation. In a recent study with hMSCs, Maloney et al. (2010) showed decreased mechanical compliance and differentiation potential over >15 population doublings *in vitro*. In addition AFM measurement of the mechanics of these cells showed five fold stiffening of attached hMSC.

Upon differentiation, there are also distinct changes within the structural reorganization of the nucleus, including chromatin condensation and nucleoprotein immobilization. Therefore, it can be proposed that nuclei in stem cells would be more flexible and also more deformable than nuclei of differentiated cells. Pajerowski et al. (2007) measured the degree of deformability of human embryonic cells, adult stem cells and fully differentiated cells by micropipette aspiration. Human embryonic stem cells were found to be highly deformable and stiffen 6-fold upon terminal differentiation. However, nuclei of human adult stem cells showed an intermediate stiffness and irreversible deformability.

The changes in nuclear mechanics during differentiation and development are generally associated with alterations in mechanical properties of the nuclear lamina and rearrangements in chromatin architecture. Lamins A and C are the main determinants of nuclear stiffness (Constantinescu et al., 2006, Lamemerding et al., 2006). Hematopoietic stem cells and mesenchymal stem cells were shown to lack lamins A and C which interact to stiffen the inner lining of the nucleus and are expressed in cells only after gastrulation. In order to support this idea, Pajerowski et al. (2007) knocked down Lamin A/C in human epithelial cells. These cells demonstrated nuclear deformability comparable to that measured in hematopoietic stem cells.

The malleable character of the nucleus was shown to be determined also by chromatin which is constituted by DNA and the DNA binding proteins. Pluripotent ESCs reflect high accessibility of chromatin due to significantly increased mobility of the nucleosomal proteins. In contrast, core histones form stable complexes with chromatin in turn, the extent of heterochromatinization increases in differentaiated cells (Meshorer et al., 2006, Bhattacharya et al., 2009). Thus, multiple structural proteins control nuclear shape and rigidity.

1.3   Cell Responses to the Micro and Nanotopography

1.3.1   Alignment of Cells on Patterned Surfaces

Cell alignment is very advantageous for engineering various types of tissue where controlling tissue microarchitecture and biological function is critical e.g. muscle, cardiovascular or blood vessel tissue, corneal tissue and nerve tissue.

Cells are known to be embedded in nanoscale topography *in vivo.* The basic topographical feature of ECM is composed of collagen fibers (diameter 50 to 300 nm) which could make into thicker collagen fibers around diameter 1–4 µm (Hulmes, 2002).

Recent advances in micro and nanofabrication enabled the study interactions of cells with surface features by controlling their pattern, periodicity, shape, and dimensional properties. Cell respond to the environmental topography by adjusting their cellular morphology and functions. It is well known that cells can align along micro and nanosized parallel grooves/ridges patterns (Clark et al., 1991, Curtis et al., 2001, Teixeira et al., 2003, Curtis et al., 2004, Recknor et al., 2004, Kenar et al., 2006, Tsuruma et al., 2006, Öztürk et al., 2009, Yang et al., 2009, Zorlutuna et al., 2009, Lamers et al., 2010, Beduer et al., 2012, Mattoitt et al., 2012).

The effect of topography on cell was first reported by Harrison, (1912), and later by Weiss (1945) who called the behavior as "contact guidance". According to the phenomenon of contact guidance (Clark et al., 1991, Curtis and Wilkinson, 1997) cell shape and movement follow the topographical features of the substrate, and this leads to changes in cellular cytoskeleton (Wojciak-Stothard et al., 1995). As cells spread on a surface, they extend their filopodia to explore their surroundings and in the mean time form local adhesions. Alignment behavior is related to the probability that a cell will make a successful protrusion in a given direction.

It has been reported that the cells cultured on the micro and nano structured substrates show similar behavior (oriented spreading, alignment, and morphology change). It has been suggested that the mechanism existing for the cells to sense ultrafine substrate topographies may be mediated by mechanical forces between the 3D nanoscale ridges/grooves and cell adhesions (i.e., focal adhesion points). On the other hand, Curtis and Clark (1990) propose that the aggregation of actin along the discontinuity is the first step determining cell orientation at micro scale. At the later stages of cell spreading, elongation of stress fibres and microtubules help formation of primary protrusions in a certain direction. The Curtis and Clark proposal was supported by Wojciak-Stothard et al., (1995) who showed that actin polymerization along groove-ridge boundaries is the primary driving event in determining fibroblast orientation on microgrooved substrata (5, 10, and 25 µm width and 0.5, 1, 2, and 5 µm depth). After 30 min period of cell attachment, F-actin condensations were seen close to the intersection of groove wall and ridge top. Then vinculin expression and arrangement of microtubule system was observed during early cell

spreading stage. Thus, the driving force and sequence of events responsible for the alignment phenomenon appears to be different at the microscale.

It is known that focal adhesions are associated with the tips of actin filaments and serve to adhere the cell to the ECM proteins and (Wozniak et al., 2004). Ohara and Buck, (1979) suggested that cells cannot align with surface features if focal adhesions cannot sense the grooves with an excessive pitch. In support of this, Lamers et al., (2010) demonstrated that cellular alignment decreases with very small pitches where the patterns can be recognized by the focal adhesions.

The dimensions of groove and ridge width, groove depth and pattern periodicity affect orientation of the cells. On micro grooved surfaces, groove depth is one of the most important parameters in defining cell alignment. The degree of alignment of the cells along the microscale grooves is generally proportional to groove depth and inversely proportional to groove/ridge width if the other parameters are fixed (Dunn et al., 1986, Clark et al., 1987, Clark et al., 1990, Holthaus et al., 2012). On the other hand, Glawe et al., (2005) investigated the influence of high aspect ratio (aspect ratio=groove height/groove width) microchannels with varying widths (20-60 μm) on the alignment of smooth muscle cells. It is observed that alignment is dependent on the channel width and narrow microchannels (20 μm and 30 μm) promote alignment of smooth muscle cells. On nano-grooved substrates, cell orientation is found to be also less sensitive to groove width (90 to 500 nm) for MG-63 cells and C3A cells (Tsai and Lin 2009, Yang et al., 2009). When the ridges are smaller than that of focal adhesions (0.25–0.5 μm wide and 2.0–10.0 μm long), cell alignment is inhibited. Nano grooves are too narrow for the cells to descend into the bottom of grooves. Thus, the focal adhesions and actin filaments are localized on the ridges. However, C3A orientation was proportional to groove depths of the PS nano grooved surface, but not on the silicon substrates. It implies that surface chemistry also plays a role in the formation of actin filaments. The impact of nanogrooves on C3A elongation is also less sensitive to ridge width, but strongly depends on groove depth.

Although several studies have shown that almost all types of cells can align in the direction of gratings and both the width and depth of the features can have strong effects on cell behavior, there is not an agreement on the degree of their contribution. For instance, there are conflicting reports on which property has a stronger effect on cell behavior, depth or width (Flemming et al., 1999) and nano or microstructures (Wojciak-Stothard et al., 1997, Hu et al., 2005, Eliason et al., 2007). Such inconclusive data often led to inaccurate

prediction for cell behavior against width–depth variations. One major reason for this is the use of very different types of designs, chemistries, dimensions and materials by different groups.

The lack of data on how height and groove width or in which quantitative interaction of these two parameters determine the degree of cell orientation causes to establishment of aspect ratio dependent models.

For example, Kemkemer et al. (2006) developed a model for prediction the cell orientation for cases where the cell is larger than the grooves. According to this, the square of the product of groove height and spatial frequency or the aspect ratio for symmetric grooves were found to be the important features for alignment. They verified this by culturing human melanocytes on parallel rectangular grooves with heights between 25 and 200 nm and spatial frequencies between 100 and 500 mm^{-1}.

In another study, Crouch et al. (2009) proposed a simple model to explain the relationship between aspect ratio and cell behavior on gratings with varying widths and depths. They observed a direct relationship between the alignment of human dermal fibroblasts and aspect ratios. While aspect ratios as small as 0.01 induced significant alignment (60%), 80% alignment was achieved with an aspect ratio of 0.05. The maximum aspect ratio required for 95% alignment was 0.16. This study indicates that within a certain range the aspect ratio can be used for controlling cell response to substrate topography without distinguishing the effects of width and depth. However, it is important to point out that when the grating surface is wider than cell width, the probability of lateral cell spreading is high.

Several studies indicate that alignment occurs when the periodicity and dimensions of the patterns are above a critical value. For example, Loesberg et al. (2007) have shown that groove depths around 35 nm and ridges narrower than 100 nm, the fibroblasts did not show noticeable alignment. In another study 100 nm depth was determined as a threshold for alignment of cardiomyocytes (Wang et al., 2011), osteoblast-like cells (Tsai et al., 2009, Yang et al., 2009) and hepatoblastoma cells (Tsai and Lin, 2009). Thus, obtaining cell-type-specific responses such as different contact guidance thresholds by the help of above mentioned prediction theories can be useful to develop implant surfaces.

Although cell alignment on physically patterned surfaces is widely studied, the effect chemical patterns (Kumar et al., 1994, Craighead et al., 1998, Wheeler et al., 1999, Kane et

al., 1999, James et al., 2000, Branch et al., 2000, Thakar et al., 2003, Patel et al., 2006) or synergistic effects of physical and chemical patterning (Magnani et al., 2003, Lussi et al., 2004, Recknor et al., 2006, Charest et al., 2006, Zhang et al., 2006) were also studied intensely. Generally, in order to control cell adhesion and alignment, adhesion mediated molecules such as collagen, laminin, SAM (self assembled monolayes) are patterned by soft lithography techniques. In some cases instead of synergistic effects of chemical and physical patterning one of the cues can overcome the other one. For example, when Charest et al., (2006) presented physical topography (grooves with 4 µm depth, 8 µm width) overlaid with an orthogonal chemical pattern (10 µm adhesive lanes with spacings ranged from 10 to 100 µm), physical topography determine the alignment of osteoblast-like cells.

Another approach for aligning the cells is to apply mechanical stimulus by cyclic stretching, fluid flow, and hydrostatic compressive pressure. In several studies cardiac, ligament and tendon derived fibroblasts, myoblasts, vascular smooth muscle cells and osteoblasts were subjected to mechanical forces under *in vivo* conditions. Studies have shown that when cells grown on patterned surfaces with micron sized (Park et al., 2006, Houtchens et al, 2008) or nano sized groove/ridge patterns (Prodanov et al., 2010) or on unpatterned (Kim and Mooney, 2000, Standley et al., 2002, Houtchens et al., 2008) substrates subjected to cyclic stretching orient themselves in the direction perpendicular to the applied strain. It should be noted that applied strains in these examples were parallel to the direction of the groove axis. However, there are studies showed that tendon fibroblasts and osteoblasts aligned along the direction of micro grooves regardless of the stretching direction (Wang et al., 2000 and 2004).

1.3.2 Effects of Surface Topography on Gene Expression and Differentiation

Micro and nanoscale technologies are suitable for investigation of the interactions between stem cells and their microenvironment. *In vivo,* the interactions among cells and between cells and their including surface sensing and recognition, occur at nanoscale or at a smaller dimension, the molecular level. Studies indicate that culturing stem cells on micro and nanotopographies could be a tool in determining their fate (Mahoney et al., 2005, Dalby et al., 2006, Yim et al. 2007, Lee et al., 2010, Beduer et al., 2012).

As was discussed earlier topographical features affect cell behavior such as adhesion, morphology, cytoskeletal arrangement, migration, proliferation, surface antigen display, and gene expression. During changes in cell shape forces are transferred to the nucleus through the actin-intermediate filament system (Maniotis et al., 1997). Various studies have shown that cell elongation and distortion of nucleus could result in changes of gene and protein expression. For example, it has been reported that cell elongation can induce protein expression in embryonic mesenchymal smooth muscle precursor cells (Relan et al., 1999). It was also reported that the elongation of cytoskeleton and nucleus have been correlated with changes in gene expression profile and cell differentiation in other studies (Thomas et al., 2002, Itano et al., 2003, Dalby et al., 2003). It was also shown that *in vitro* constraining nuclear shape could trigger osteoblasts to begin expressing osteocalcin (Thomas et al., 2002). Itano et al. (2003) showed that in spreading cells the shape of the nucleus changes and along with nuclear calcium level increases. Dalby et al. (2003) proposed that deformation of nucleus may alter the relative positions of the chromosomes and their accessibility for transcription, thus leading to changes in gene expression.

Cells and underlying substrates are in a dynamic contact through focal adhesion complexes. These complexes form after binding of integrin in the cell membrane to ECM components and recruitment of several effector proteins. In addition to their attachment role, integrins mediate signalling between the ECM and the cell activating signalling pathways that regulate transcription factor activity, and direct cell growth and differentiation. Although integrin molecules provide a platform for intracellular signalling, they do not show intrinsic enzymatic activity in their cytoplasmic domains (Clark and Brugge, 1995, Liu et al., 2000). Therefore, non-receptor tyrosine kinases mediate the downstream signalling following integrin binding (Schaller et al., 1992). One such pathway that may regulate the proliferation and differentiation of skeletal stem cells is the extracellular signal regulated kinase (ERK) signalling cascade, a member of the mitogen activated protein kinase (MAPK) pathway. ERK-MAPK signalling transfer physical information from the extracellular environment to the nucleus and acts to regulate the cell cycle (Ge et al., 2007). In addition to playing a role in both proliferation and apoptosis, the ERK-MAPK pathway has important functions in cellular differentiation (Jaiswal et al., 2000, Jadlowiec et al., 2004, Klees et al., 2005) and has been implicated in the differential response of bone cells to a variety of signals, including ECM-integrin binding and mechanical loading. Furthermore, it has been shown that integrin mediated activation of the ERK/MAP kinase pathway results in phosphorylation and stimulation of activity transcription factors (e.g RUNX2) critical in early osteoblast differentiation.

Alignment of bone cells and collagen matrix is closely related to the anisotropic mechanical properties of bone. For example, the natural bone ECM consists of well organized collagen type-I forms fibrils with an interfibrillar spacing of 68 nm and 35 nm depth (Weiner and Wagner, 1998). Zhu et al. (2005) reported that rabbit mesenchymal stem cell (MSC)-derived osteoblast-like cells aligned on groove-ridge patterns with depth of 60-70 nm and 300 nm periodicity. In addition to alignement of the cells and their actin filaments, collagen matrix was also the oriented along the direction of the nanogrooves.

In a recent study, response of osteoblasts in terms of alignment, morphology, calcium phosphate mineralization was examined on grooved substrates which in all dimensions were nanometric (Lamers et al., 2010). SEM and TEM studies showed that osteoblasts deposited calcium phosphate along quite small (500 nm in width and 153 nmin depth) or even much smaller (50 nm width and 17 nm depth) grooves depth. Real time PCR revealed on nanogrooves a higher increase in osteoblast-specific genes (ALP, OCN, BSP, Col-I, Cbfa1) than on smooth controls.

Dalby et al. (2006) tested human osteoprogenitor cells by using a range of nanometric scale shallow pits and grooves. Cytoskeletal organization, growth and production of the osteoblastic markers osteocalcin and osteopontin (without use of media supplements such as dextramethasone or ascorbic acid) increased by day 4 of culture on all the topographies examined. An increase in osteocalcin and osteopontin production was observed on surfaces with pits of 300 nm depth and 30 µm width. In agreement with these studies, Lamers et al., (2010) observe that the nanogrooved substrates were specifically effective in the very first days of osteoblast-specific gene expression, which suggests that nanotextures can stimuli initial osteoblast differentiation. Gene expression of osteoblast specific markers (ALP, OCN, BSP, ColI and Cbfa1) was shown to be upregulated by nanogrooves.

In another study, surface features which are similar in scale to osteoclast resorption pits, were used to study *in vitro* bone formation in basal medium (Wilkinson et al., 2011). Here, the pit dimensions were: 330 nm depth, and diameters: 20, 30 and 40 µm, and centre–centre spacings: 50, 60 and 90 µm. Osteopontin expression was relatively high in the human osteoblasts grown on the larger diameter (30 and 40 µm) pits. In addition to expression of osteogenic markers mature calcium depositions were shown by alizarin red staining of these substrates.

Biological tissues are hierarchically organized from nano-to-micron scales. For instance, the average roughness of a bone tissue is 32 nm (Palin et al., 2005). During bone mineralization, the hydroxyapatite crystals form micro and nanocomposites with collagen fibers (Weiner and Wagner, 1998). Thus, designing biomimetic surfaces which present synergistic effects of micro and nanostructures is expected to provide additional advantages. Two separate studies have examined the behavior of bone stromal cells derived osteoblasts on micropit and nanonodule hybrid topography of TiO_2 (Ogawa et al., 2008, Kubo et al., 2009). They created nanonodules with diameters of 100 nm, 300 nm and 500 nm by self-assembly technique and demonstrated that 300 nm nanonodule containing substrates created the most promising environment for osteoblast differentiation and bone–titanium integration. Osteoblast differentiation on TiO_2 micro-nanohybrid surfaces was investigated by ALP assay and ALP activity was found to be the heighest on 300-nm nanonodules. RT-PCR confirmed that these surfaces promoted osteoblastic differentiation by the 3- to 4-fold increase in early (Collagen I) and late (osteocalcin) markers on the surfaces with nanonodules. Bone and implant integration was tested mechanically. These results are in agreement with more recent studies (Mendonca et al., 2010, Gittens et al., 2011), which have indicated presenting the micron and submicron-scale surface roughness on the same surface accelerate bone differentiation.

In addition to hierarchical complexity of bone, mimicing the dynamic mechanical environment (cyclic stretch or compression) is also considered in designing functional bone implants in several studies. These tudies pointed out that osteoblasts change their morphology, gene expression and matrix mineralization by either introducing surface topography on biomaterials or by mechanical stimulation (Song et al., 2007, Chau et al., 2009, Dumas et al., 2009). However, Prodanov et al. (2010) tested the simultaneous effects of nanotextured surface (300 nm wide and 60 nm deep grooves) and mechanical stretching in terms of cell attachment, ECM formation and osteoblast differentiation. It was shown that dual stimulation (nanogrooved surface and 8% of strain) the expression of fibronectin and Cfba synergistically increased 2 fold in comparison to nanotextured surface alone. Such combined effects of topography and mechanical stimulation were also observed by other groups (Wang et al., 2004, Loesberg et al., 2005, Ahmed et al., 2010, Wilkinson et al., 2011).

Although micro-nanogrooved substrates are extensively used to promote differentiation, topographies such as pillar/post (Sjostrom et al. 2009, Lovmand et al., 2009, Kim et al., 2010, Brammer et al., 2011, McNamara et al. 2011) and pits (Kantawong et al., 2009, Biggs

2009) were also studied by different groups. For example Kim et al. (2010) investigated the effects of microposts (10 μm in diameter, 6 μm in height and with 10 μm seperation) on osteogenic differentiation of connective tissue progenitor cells by days 9, 30 and 60. They observed that gene expression of collagen I and osteocalcin is doubled on microposts relative to smooth surfaces at three time points. In a recent study, Brammer et al. (2011) tested differentaition ability of MSCs into bone, chondrocyte and adipocytes by quantifying the extractable amount of alizarin red, alcian blue, and oil red respectively. Compared to other lineages, ostegenic differentiation seemed to be promoted by nanoposts. Alizarin red staining indicated 3 fold increse in osteogenic mineralization of MSCS grown on nanoposts with respect to smooth control. Similar to post, nanopits also were used for the induction osteoprogenitor differentiation. Kantawaong et al. (2009) achieved osteoconversion of human bone marrow osteoprogenitors on nanopits. By whole proteome analysis osteospecific differentiation was linked to focal adhesion formation and FAK mediated activation of the ERK/MAPK signalling pathway.

Mesenchymal stem cells are multipotent stromal cells which can differentiate into mesenchyme origined tissues like bone, tendon or adipose. However, Woodbury et al. (2000) demonstrated the differentiation of rat and human bone marrow stromal cells into neurons. A number of biomaterials have been designed for neural tissue engineering application. Synthetic materials such as fiber or hydrogels have been used to reconstruct neural network (Silva et al., 2004, Yang et al., 2005, Christopherson et al. 2009, Xie et al., 2009, Yücel et al., 2010). In the last decade, several studies reported that micro and nanopatterned surfaces can be valuable tool for directed growth (Rajnicek et al., 1997, Miller et al., 2002, Mahoney et al., 2005, Tsuruma et al., 2006, Yao et al., 2009) and differentiation (Recknor et al., 2006, Yim et al., 2007, Sorensen et al., 2007, Mattotti et al., 2012) of neurites. In one of the recent studies Yao et al. (2009) compared guided growth of neurons on small (5 μm) and larger grooves (10 μm). While the average alignment angle of neurites grown on smaller microgroves micropatterned PLGA films was $5.8^0 \pm 1.5$, this value became $10.7^0 \pm 2.3$ on the larger grooves. Mattotti et al. (2012) have achieved differentiation of radial glia-like progenitors into astrocytes by using microgrooved substrates. Both Western Blots and immunoassays showed upregulation of two astroglial markers (GFAP and BLBP).

Micro and nanostructures, especially groove-ridge type topographies, were shown to induce neuronal differentiation of stem cells and directed growth of terminally differentiated neurons. However, Migliorini et al. (2011) analyzed the effect of nanopillars on

differentiation of embryonic stem cell derived progenitors in the absence of biochemical factors and observed an increase in the neuronal yield with increasing pillar height from 35 to 400 nm. Similarly, it was found that PC12 cells on nanopillars (229 ± 28 nm diameter, 69 ± 32 nm spacing and 2123 ± 84 nm height) developed higher density and shorter neurite extension than cells on smooth substrates (Haq et al., 2007).

Recently, the shape of the MSC is started to be considered as a new parameter to control differentiation (Graziano et al., 2007, McBride et al., 2008, Kilian et al., 2010, Peng et al., 2011). In fact, Ingber and collegaues performed a "starter" work in this field 15 years ago (Ingber et al., 1997). They investigated the influence of geometrical patterns not on the stem cell fate but on the decision of cells to initiate apoptosis. They found that endothelial cells switched from growth to apoptosis on extracellular matrix-coated adhesive islands with decreasing area in the range of 40x40 μm^2 to 5x5 μm^2.

The first studies in the context of cell shape and differentiation were conducted by two different groups. Chen and coworkers (2004) demonstrated the important role of cell shape and spreading in deciding the fate of MSCs. They used microcontact printed, self-assembled monolayers on thin gold layers in the form of star and flower shapes. While the cells culturing on star shapes was shown to be higher in osteogenic transcripts, adipogenic transcripts were higher in the cells grown on flower shapes. The possible reason of this shape-dependent differential expression was found to be the expression of noncanonical Wnt/Fzd signaling molecules previously shown to be involved in osteogenesis (McBeath et al., 2004, Arnsdorf et al., 2009). In a recent study micropatterns of arginin glycine aspartic acid (RGD) on poly(ethylene glycol) (PEG) hydrogels were fabricated by keeping the same adhesive area but in different shapes (circular, square, triangular, and star) (Peng et al., 2011). Mechanical factors affect degree of cytoskeletal tension and and gene expression. The adhesive border (i.e. shape/perimeter) determines spatial distribution of tension. Peng et al. (2011) showed that the high tension of multi angular shapes (square, triangle and star) is optimal for osteogenic differentiation. On the other hand, adipogenic differentiation was shown to be happened in the circular cells having evenly distributed tension.

1.3.2.1   Cell Mechanics and Differentiation: Matrix Rigidity and Tractional Force

In the last decade the influence of the matrix rigidity of the substrate on the cell function of cells that are attached on them. Cell contraction (Discher et al., 2005), migration (Lo et al., 2000, Hadjipanayi et al., 2009a), proliferation (Hadjipanayi et al., 2009b, Winer et al., 2009), organization (Krieg et al., 2008) and cell death (Wang et al., 2000) were shown to be modulated by matrix rigidity.

ECM presents physical cues to the cells. As a cell interacts with matrix and actively probes, it senses the local elastic resistance of the ECM through mechanotransduction, that is, by translation of mechanical forces and deformations into biochemical signals such as activation of diverse signalling pathways and gene expression.

Although signalling initiated by integrin receptor has been well studied, the physical properties of the matrix, such as its elasticity or stiffness, are also important (Discher et al., 2005, Vogel and Sheetz, 2006).

Differentiation of stem cells is controlled by their unique local microenvironments which are composed of chemical factors and the extracellular matrix (Nakagawa et al., 1989, Fuchs et al., 2004). Although there are large number of studies on the effects of chemical inducers, the effects of matrix stiffness on stem are not studied as much.

Engler et al (2006) showed that they can change hMSC fate by using substrates based on polyacrylamide gels coated with collagen. The rigidity of the materials ranged from that of soft brain and fat to the intermediate stiffness of muscle and to that of relatively rigid cartilage and osteoid (Figure 1.9).
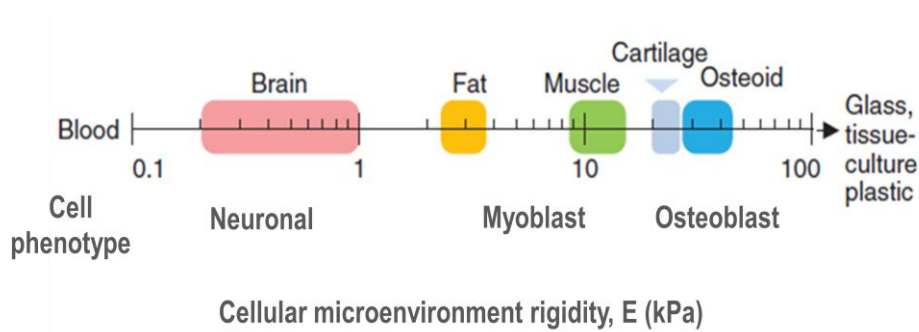
Figure 1.9. The influence of substrate rigidity on the hMSC fate (adapted from Buxboim et al., 2010).

On soft substrates resembling the brain tissue hMSCs stem cells started to show a neuronal phenotype, on substrates of intermediate stiffness similar to that of muscle they differentiated into the myoblast; and on stiffer substrates the same cells became osteoblasts (Figure 1.9). In a recent study Buxboim et al. (2010) tested differentiation of MSCs on substrates showing different elasticities. When the elasticity of substrate is 11 kPa cells differentiate into myoblast. On the other hand, stiffer substrate (34 kPa) initiates osteogenesis. 4 to 6 fold increase in respective cell markers was quantified by microarray analyses.

However, whether cells sense the rigidity difference between adhesion sites and transduce it at the microscopic scale, or do they recognize local alterations in receptor-ligand binding characteristics at nanoscopic scale remains an open question (Houseman and Mrksich, 2001, Keselowsky et al., 2005).

Studies have also begun on cellular traction force on cells seeded onto elastomeric micropost arrays (Beningo and Wang, 2002, Tan et al, 2003, Vogel and Sheetz, 2006, Yang et al., 2007, Ghibaudo et al., 2008, Schoen et al., 2010, Fu et al., 2010) using finite element method.

Fu et al. (2010) prepared a series of micropost arrays with rigidity varying between 1.31 nN μm^{-1} and 1556 nN μm^{-1} and with different post heights (0.97 μm, 6.1 μm, 12.9 μm) to investigate the regulatory role of micropost rigidity on stem cell lineage commitment (Figure 1.10A). They plated hMSCs on micropost arrays and incubated them in either growth

medium or in bipotential differentiation medium which can promote both osteogenic and adipogenic differentiation. After a two week induction, osteogenic differentiation was observed on rigid micropost arrays whereas adipogenic differentiation took place on soft ones. On the other hand, stem cells cultured in growth medium did not differentiate either bone or adipose tissues. Micropost rigidity was characterized by displacement of the center node on the top surface due to applied horizontal traction force and wereable to construct a force-displacement curve (Figure 1.10B). Vogel and co-workers also quantified the cellular force by using the same method with an additional parameter: contribution of substrate warping to pillar deflection (2010).
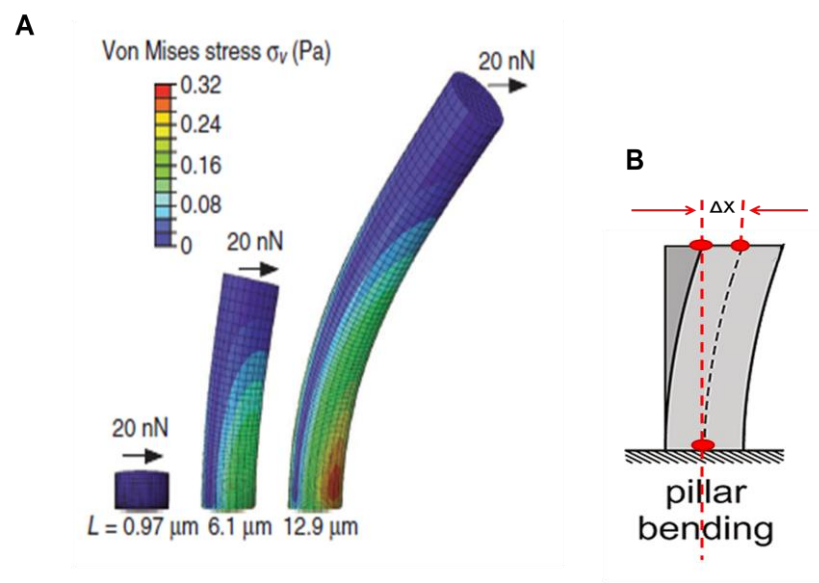
Figure 1.10. Graphical presentation of elastomeric posts. (A) Graphics of finite-element method (FEM) analysis of microposts bent due to h bending in of 20 nN force, (B) Total displacement of center node on the top of the pillar (Fu el al, 2010, Schoen et al., 2010).

These findings tell us that although the signalling between receptors and presence soluble factors are crucial to control cells, the physical parameters of the microenvironment also play key roles in stem cell differentiation.

1.4 Aim and Novelty of the Study

The aim of this study was to investigate the possibility that whether micro and nanopatterned polymeric substrates placed in the form of matrix with variable distance, substrates would influence population of these areas by cells and whether cell type and substrate stiffness would influence this response. The cell types were specially selected to include cancer cells which are known to be soft and are able to metastase. The frequency and extent of nuclei deformation of the nucleus of four cell types (human osteosarcoma cell line (Saos-2), a healthy human bone cell line (hFOB 1.19), a stem cell (rat bone marrow stem cell (BMSC)) and one fibroblastic cell line L929) was also studied. Deformability of the cells was investigated morphological changes of nucleus and the cell body caused by physical restrictions created by micropillars. Tugging force applied by Saos-2 and L929 (observed as bent micropillars) were investigated. The design of the test surface were consisted of nanopillar covered fields where the distance between the pillars are varied systematically to create an array. Difference in the adhesion behavior of two types of cells, Saos-2 cells and BMSCs were studied. The effects of chemical and mechanical cues on cell adhesion were investigated.

CHAPTER 2

MATERIALS AND METHODS

2.1   Materials

Poly(dimethylsiloxane) (PDMS) and its curing agent was purchased from Dow Corning (Sylgard 184 Elastomer Kit, USA). Poly(L-D,L-lactic acid) P(L-D,L)LA (70:30, inherent viscosity: 5.5–6.5 dL/g), and and Triton X-100 were purchased from by Applichem GmbH (Germany). Fetal bovine serum and Dulbecco's Modified Eagle Medium (DMEM), (High and Low Glucose), RPMI 1640, penicillin/streptomycin (10000 units), trypsin-EDTA (0.25%) were purchased from Hyclone, Thermo Scientific (USA). DMEM-F12 mixture was obtained from Gibco Invitrogen Co. (USA). Poly(D,L-lactide-co-glycolide) (50:50) (PLGA (Mol. wt. 30.000-60.000), paraformaldehyde (37%), 6-diamidino-2-phenylindole (DAPI), FITC-labelled Phalloidin, cacodylic acid (sodium salt), ascorbic acid, glutaraldehyde (Grade I, 25 % aqueous solution), dimethyl sulfoxide (DMSO), dexamethasone, β-glycerophosphate, L-ascorbic acid, Anti-Lamin A (C-terminal), produced in rabbit, Anti-Rabbit IgG (whole molecule), F(ab')2 fragment-FITC produced in goat, were supplied by Sigma Chem. Co. (USA). Osteopontin (OPN), goat anti-mouse IgG-FITC were from Santa Cruz Biotechnology (USA). Saos-2 and L929 cells were purchased from ATCC.

2.2   Methods

2.2.1   Design and Production of Micro and Nanopatterned Silicon Wafers

Photolithography was used to produce three types of micron sized pillars. The Type 1 and Type 2 silicon masters which consist of rectangular prism shaped micropillars were kindly produced by Prof. A. Aydinli (Bilkent University, Ankara, Turkey). Briefly, a photoresist is coated in 500 nm thickness on a silicon wafer (2 cm^2), exposed to a laser of λ=325 nm for

10 min and developed revealing patterns in the form of pillars. Later, these patterns were transferred to silicon by using an epoxy replica of the original template. The Type 1 master had symmetrically patterned pillars 4 µm tall, and seperated 7 µm by in x and y directions, Type 2 was asymmetrically patterned and had pillars same height as Type 1 except that their interpillar distances were 12 in the x and 24 µm in the y directions. Type 3 template was kindly provided by Dr. Celestino Padeste (PSI, The Paul Scherrer Institute, Villigen, Switzerland). Asymmetrically distributed pillars were columnar in shape with 5 µm in height and 1 µm width. While the shorter pillar to pillar distance ~4.2 µm, the longer distance was ~9.2 µm (Figure 2.1).
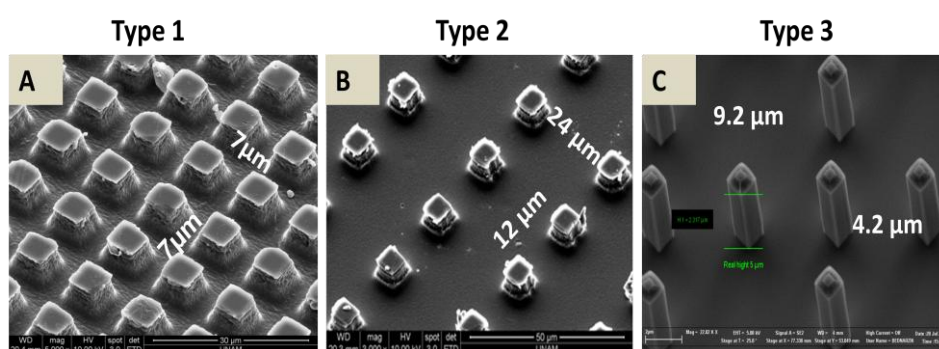
Figure 2.1. SEM micrographs of polymeric replicates of the original silicon wafer (A) Type 1 pillars, (B) Type 2 pillars, (C) Type 3 pillars (original silicon wafer).

Graded series of nanopillar patterns were produced by Dr. Celestino Padeste. The test surface design based on nanopillar covered fields where the distance between the pillars (ca. 900 nm tall, 200 nm wide) was varied from 1 to 10 µm. Each test array consisted of 25 fields of 2 x 2 mm^2 size and had different interpillar distance than the neighboring fields (Figure 2.2). Whole arrays produced by e-beam lithography, on a 320 nm PMMA resist (Mr= 600,000) spin coated onto a silicon wafer were produced using an EBL system operated at 100 keV. Thermal evaporation of 30 nm of chromium and lift-off was used to produce a hard mask for the subsequent silicon etching step, which was performed on a reactive ion plasma etcher (Oxford Plasmalab System ICP 180) using SF6 and C4F8 etching chemistry. A fluorosilane based antisticking layer was applied to the silicon master according to published procedures (Schift et al., 2005).
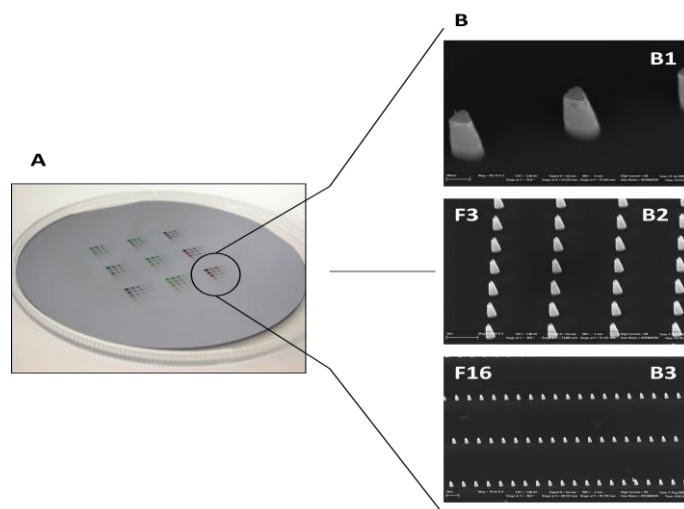
Figure 2.2. Nanopillar array on the silicon wafer. (A) 9 copies of 25 nanopillar covered fields produced by EBL and RIE, (B1, B2, B3) SEM images of different fields (F stands for the field).

2.2.2 Preparation of Patterned Polymeric Films

A negative replica of the silicon master was made of polydimethylsiloxane (PDMS). This was prepared by pouring a prepolymer–catalyst mixture (10:1 (w/w)) onto the patterned silicon templates, and cured at 70°C for 3 h. PDMS replicas served as the templates to prepare patterned polymeric films by solvent casting. A poly(L-D,L-lactic acid) P(L-D,L)LA solution (3%, w/v) and P(L-D,L)LA-PLGA (50:50) blend 60:40 (M) in chloroform were prepared. Polymeric solutions were poured on the PDMS template and after evaporation of the solvent at room temperature in 6 h the films were dried under vacuum at room temperature for a further 24 h (Figure 2.3). Unpatterned P(L-D,L)LA films were made by solvent casting a chloroform solution of polymers on PDMS templates which is obtained by replicating unpatterned (smooth) silicon templates.
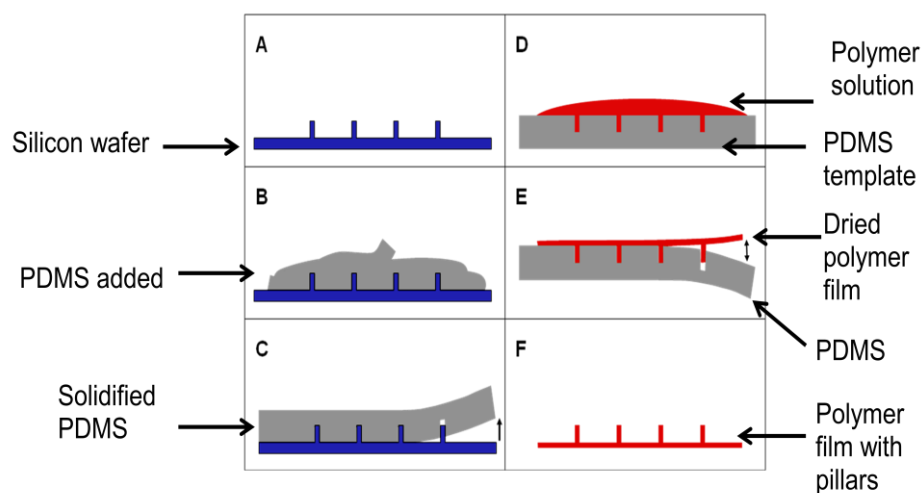
Figure 2.3. Two step replication process of micropillars on polymeric films.

2.2.3 Surface Characterization of the Polymeric Films with AFM

The surfaces of silicon templates and patterned polymeric films were characterized with Atomic Force Microscopy (Universal SPM, Quesant, Ambios Inc., USA and Nanoscope DI 3100 Scanning Solution, CH) in non contact mode with silicon tips (at 1 Hz, 40 x 40 mm^2 maximum scan area) (Figure 2.4).
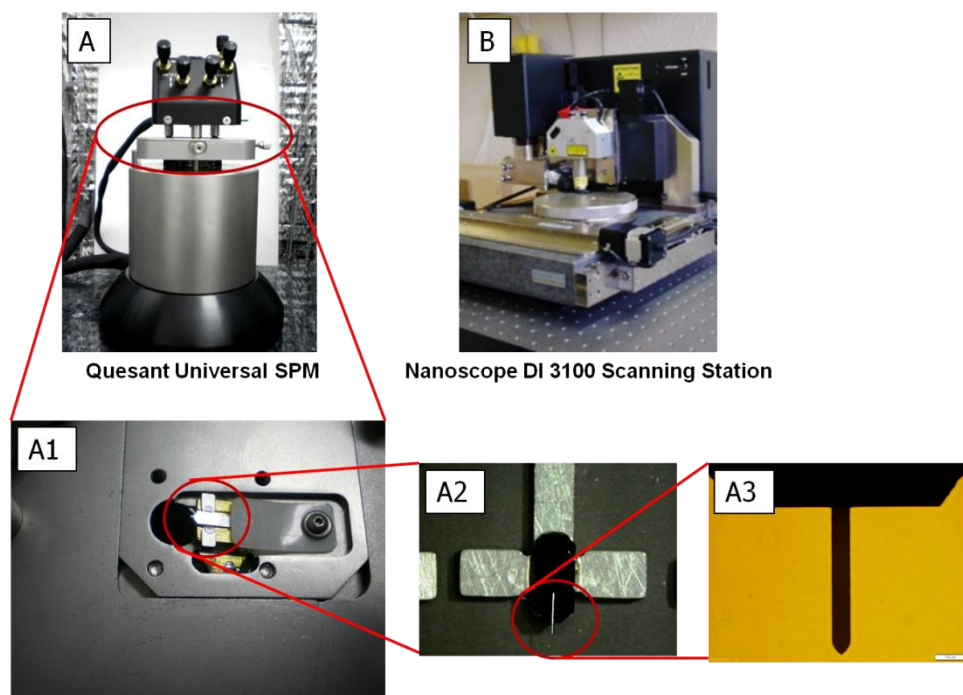
Figure 2.4. AFMs used in surface surface charcterization of silicon templates and patterned polmeric films. (A and B) Atomic Force Microscoped used in surface characterization (A1, A2 and A3). A closer view of a cantilever with a very fine probe. Scale bar is 100 μm.

2.2.4   Surface Characterization of the Polymeric Films with SEM

Dry polymeric films were coated with 10-12 nm gold-palladium under vacuum and studied with a scanning electron microscope (FEI Quanta 200F, USA).

2.2.5   Wettability of the Polymeric Films

Dynamic contact angle measurements were performed to determine the wettability of the films by using an automated goniometer (Attension-Theta, Optical Tensiometer, Finland). Contact angle values were recorded for up to and 10 s to obtain an average water contact angle for each measurement. At least six parallel measurements were made for each sample material, and the average was calculated.

2.2.6   Mechanical Characterization of the Polymeric Films

A mechanical testing system (Lloyd LRX 5K, Lloyd Instruments Limited, UK) with a load cell of 100 N was used by applying tension (Figure 2.5). Uniaxial tensile test was performed on unpatterned and P(L-D,L)LA-PLGA lend films at a rate of 10 mm/min.

Rectangular films (thickness of P(L-D,L)LA and blends were of 0.114 ± 0.003 mm and 0.173 ± 0.005 mm respectively), were prepared in a shape (40 mm long, 10 mm wide) by solvent casting from 5% chloroform solution. Tensile strength (MPa) and Young's modulus (MPa) were calculated using the load-displacement graphs obtained.

Figure 2.5. The mechanical tester used to study the tensile behavior of and P(L-D,L)LA and P(L-D,L)LA:PLGA (60:40) films.

2.2.7   *In Vitro* Studies

The types of cells used in this study were listed in Table 2.1.

Table 2.1. List of cells used in the *in vitro* studies.

Cell Types			
Designation	**Source**	**Code**	**Description**
Saos-2	Human	ATCC, HTB-85	Osteosarcoma cell line
MCF7	Human	ATCC, HTB-22	Adenosarcoma cell line
hFOB 1.19	Human	ATCC, CRL11372	Osteoblast cell line
L929	Mouse	ATCC, CCL-1	Fibroblast cell line
BMSC	Rat	Primary isolate	Bone marrow cell isolate

2.2.7.1   Cell Culture and Cell Seeding on Films

Saos-2 human osteosarcoma cells were cultivated in RPMI 1640 medium with 10% fetal bovine serum (FBS) and penicillin/streptomycin (100 U/mL). They were preserved in culture medium, 95% and DMSO, 5% at 37°C. They were subcultured from passage 6 to passage 16.

MCF7 human adenosarcoma cells were cultured in Dulbecco's Modified Eagle Medium with low glucose 10% FBS and penicillin/streptomycin (100U/mL). They were stored frozen in their medium and 10% DMSO in a liquid nitrogen tank at -196°C.

hFOB 1.19 human osteoblast cells were grown in 1:1 mixture of Ham's F12 Medium and Dulbecco's Modified Eagle's Medium, with 2.5 mM L-glutamine (without phenol red). To make the growth medium complete 0.3 mg/mL G418 and 10% FBS were added. Their growth temperature is reported as 34°C by ATCC ((American Type of Culture Collection). The composition of freezing medium of hFOB 1.19 was: Culture medium, 72%; additional fetal bovine serum, 20%; DMSO, 8%. Storage was at -196°C.

L929 mouse fibroblast cells were propagated in Dulbecco's Modified Eagle Medium high glucose supplemented with 10% FBS, penicillin/streptomycin (100 U/mL). L929 cells were propagated until passgae 13. The standard medium was used in freezing the cells with 10% DMSO. Storage was at -196°C.

Rat bone marrow stem cells (BMSCs) were isolated from 6 week old, 150 g male Sprague-Dawley rats. This process was carried out according to Kenar et al., 2006 and Yılgör et al., 2010. Marrow was flushed out of the femurs and tibia, centrifuged at 8 g for 5 min, transferred into T-75 flasks. The cultures were left undisturbed for 3 days in a CO_2 incubator (5% CO_2, MCO-17AIC, Sanyo Electric Co. Ltd., Japan) at 37°C. Rat bone marrow stem cells (BMSCs) were cultured in Dulbecco's Modified Eagle Medium, high glucose, supplemented with 10% (v/v) FBS, penicillin/streptomycin (100 U/mL). The cells were passaged when they were confluent. Experiments were performed on cells at passages 1-2 for BMSCs. At subconfluency, cells were passaged until passage 3 and frozen at -196°C for future use. The standard medium was used in freezing the cells in 10% DMSO. For differentiation of BMSCs into bone cells, the induction medium containing 10 nM dexamethasone, 50 mM L-ascorbic acid, and 20 mM b-glycerophosphate was used.

Before cell seeding, P(L-D,L)LA films (1 and 2 cm^2) were placed into 12 or 24 well plates with patterned side up and sterilized by incubating in EtOH (70%) for 2 h, washed 3 times with 1x PBS (10 mM, pH 7.4). They were dried under sterile conditions in a laminar flow cabin (Lamin Air Safe 2000, Holten A/S, Denmark).

For cell seeding, medium was removed and the cells were detached with Trypsin-EDTA solution (0.25%, Sigma, U.S.A.) for 5 min at 37°C. After detachment, the cell suspension was centrifuged at 3000 rpm 5 min, the supernatant discarded and the pellet was resuspended in 3 mL fresh medium. The cells were stained with Trypan blue and counted with hemocytometer. After determining the number of live cells, 50 µL of the cell suspension was seeded onto polymeric films at a cell density of $2x10^4$ cells/cm^2. The films

were incubated in the CO_2 incubator for 2 h to allow the cells to attach. According to type of multiwell plate used (12 well or 24 well), 1 or 2 mL of medium was added into each well, the medium was changed daily.

2.2.7.2 Fluorescence Microscopy

Fluorescence microscope (Olympus IX 70, Japan and Leica DM2500, Germany) was used to study orientation of cells on micro and nanopatterned surfaces. More specifically, cell and nucleus morphology and cytoskeleton organization were investigated. In addition, expression of Lamin A and vinculin proteins and osteogenic differentiation marker, osteopontin, was observed after immunostaining.

2.2.7.2.1 Staining Actins and the Nucles with FITC-Phalloidin and DAPI

Staining of the cells with FITC-Phalloidin was performed to observe the organization of cytoskeletal actin filaments while DAPI was used as nuclear counterstain to determine the orientation of nuclei of the cells. Before staining, samples were fixed with formaldehyde (4%, 10 min). Cell membranes were permeabilized with 0.1% Triton X-100 for 5 min at room temperature. Following washing with PBS, samples were incubated at $37^{o}C$ for 30 min in 1% bovine serum albumin (BSA) containing PBS solution to block nonspecific binding sites. Then, FITC labelled Phalloidin (0.5 μg/mL, 1:100 dilution in 0.1% PBS-BSA, excitation and emission wavelengths 490 and 520 nm) was added and samples were incubated for 1h. The films were washed with PBS and the nuclei were stained by incubating the samples in 4',6-diamidino-2-phenylindole (DAPI) prepared in 0.1% PBS-BSA solution at 1:3000 dilution for 10 min. Finally, the samples were washed with PBS and observed under the fluorescence or a confocal microscope (Olympus IX 70, Japan and Leica DM2500, Germany).

2.2.7.2.2 Lamin A staining with Anti-LaminA Ig G and Anti Rabbit IgG FITC

The cells were fixed in of 4% paraformaldehyde for 20 min. After permeabilizing with 0.1% Triton X in PBS for 15 min, they were blocked with BSA for 30 min. Each step was followed by washing in PBS. Then, anti-lamin A Ig G produced in rabbit (1:300) was added to the samples for 1 h at room temperature. After washing with PBS, the samples were incubated in anti-rabbit IgG-FITC (1:300) for 1 h at room temperature. In order to observe the

presence of potential non-specific binding or artifacts, anti-rabbit IgG-FITC stained samples were used as negative controls. The samples were observed with fluorescence or confocal microscope (Olympus IX 70, Japan or Leica DM2500, Germany).

2.2.7.2.3 FAC staining with Anti-Vinculin and Anti Mouse IgG FITC

To mark FAC, Anti-Vinculin antibody was used. The samples were fixed in 4% paraformaldehyde for 20 min. The cells were permeated with 1% Triton X in PBS for 15 min and blocked with bovine serum albumin (1%) in PBS for 30 min. Each step was followed by three rinses in PBS. FACs were stained by incubating cells in diluted primary anti-vinculin antibody, in blocking solution (1:200) for 1 h and subsequently labeled with diluted secondary antibody (1:200) (anti-mouse FITC conjugate) (Sigma– Aldrich Chemie GmbH, Munich, Germany) for 45 min. Samples labeled with DAPI at were incubated in a solution prepared in PBS (100 ng mL^{-1}) for 10 min, followed by rinsing with PBS and observed with fluorescence microscope. In order to eliminate the possibility of non-specific binding or presence artifacts anti-mouseFITC stained samples were used as the negative control. The samples were then observed under a fluorescence microscope or a confocal microscope (Olympus IX 70, Japan or Leica DM2500, Germany).

2.2.7.2.4 Osteopontin staining

Once fixed, the cells were washed twice with wash buffer (1x PBS containing 0.05% Tween-20). To permeabilize the cells 0.1% Triton X-100 in PBS solution was added for 10 min. Then incubated for 1 h at room temperature in 1% BSA containing PBS followed by the addition of antiosteopontin (OPN) antibody (1:100) and incubated overnight at 4°C. After incubation, cells were washed three times for 5 min each wash with wash buffer (1x PBS containing 0.05% Tween-20). Goat anti-mouse IgG-FITC (1:100) in PBS was added and the cells were incubated again for 1 h at room temperature. The cells were washed three times with wash buffer for 5 min each wash. The samples were then observed under a fluorescence microscope or a confocal microscope (Olympus IX 70, Japan or Leica DM2500, Germany). Goat anti-mouse IgG-FITC stained samples were used as the negative controls.

2.2.7.3   SEM Examination

Cell seeded films were fixed in 2.5% glutaraldehyde in 0.1 M, pH 7.4 sodium cacodylate buffer for 2 h and. Samples were washed three times with cacodylate buffer and distilled water 3 times for 5 min each wash. After lyophilization, the films were coated under vacuum with 10-12 nm gold-palladium and observed with a scanning electron microscope (FEI Quanta 200F, USA).

2.2.7.4   Image analysis

Microscopy images were analyzed by using the software of Image J (http://rsbweb.nih.gov/ij/). The frequency and extent of nuclei deformation was quantified. The extent of nucleus deformation was calculated by measuring the circularity. The ratio of nucleus area to cell area was determined by the help of Image J. Displacement of Type 3 pillars due to the force applied by the cells was assed by analysis of SEM micrographs. Preferential adhesion of the cells on nanopillar array was measured by using the "color histogram" tool of the same software.

CHAPTER 3

RESULTS AND DISCUSSION

3.1 Preparation of Patterned Polymeric Films by Two Step Replication Process

Here a two step casting replication process was used, aiming at producing patterned surfaces for studying cell material interactions. The first replication step is to create a PDMS copy of a master template carrying micro and nano level features. The second replication step is carried out on the PDMS to create a biodegredable film to study interactions with cells (Figure 3.1).
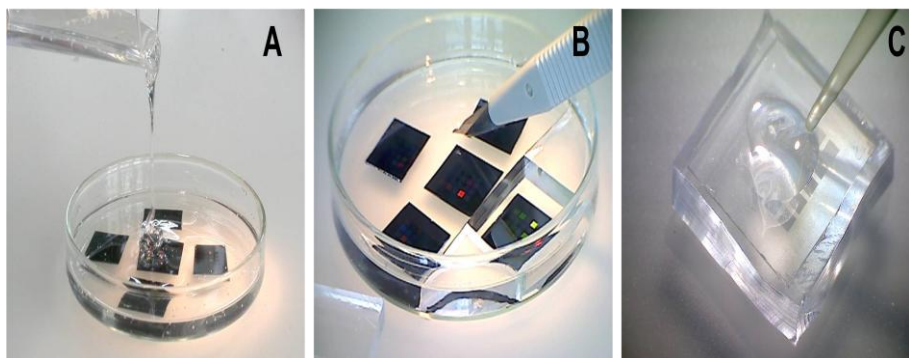
Figure 3.1. Sequence of the replication process. (A) PDMS template formation, (B) Removal of PDMS replicates, (C) P(L-D,L)LA film formation on PDMS template.

3.2 Surface Characterization of the Polymeric Films

3.2.1 Microscopic Evaluation

After the two-step replication process, the films were examined by different microscopic methods. Optical microscopy was used to screen the defect containing areas in the replicated structures. Figures 3.2A, 3.2B and 3.2C present defect and artifact free Type 1, Type 2 and Type 3 micropillar patterned films. The quality of the replication of micron sized pillars was assessed by SEM are observed very good (Figures 3.2D - 3.2F).
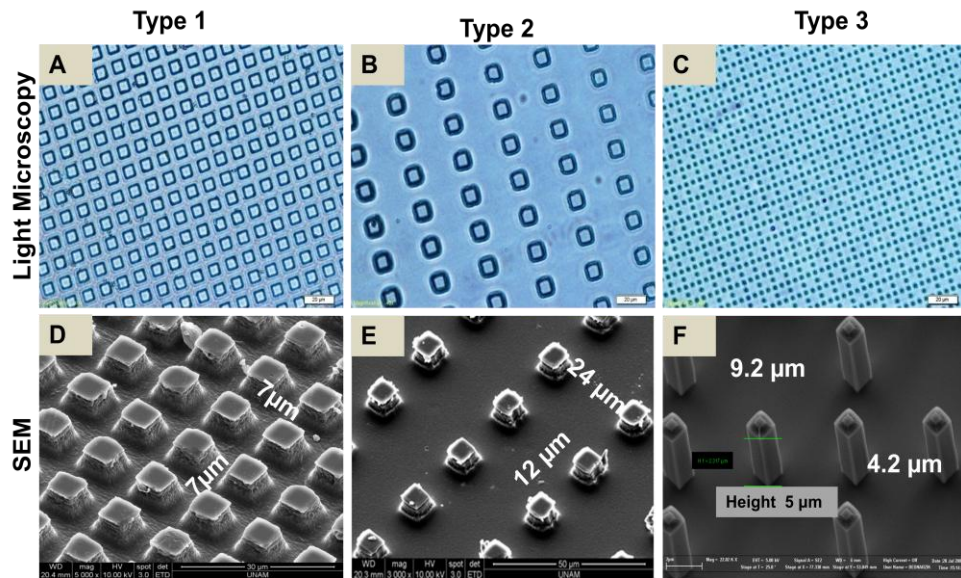
Figure 3.2. Light (A, B, C) and SEM (D, E, F) micrographs of polymeric replicates of the original silicon wafer (A and D), Type 1 pillars, (B and D), Type 2 pillars, (C and F) Type 3 pillars. Scale bars: A, B, C: 20 µm.

Nanopillars were examined by SEM, optical microscopy and AFM. Figure 3.3 shows master silicon wafer (Figures 3.3A and 3.3B). Exemplary SEM micrographs show the 3D appearance of the nanopillars (Figure 3.3C1). In addition, images of nanopillars of Fields 3 and 16 are presented to show how pillar-to-pillar distances change systematically along x and y directions throughout the surface (Figures 3.3C2 and 3.3C3).
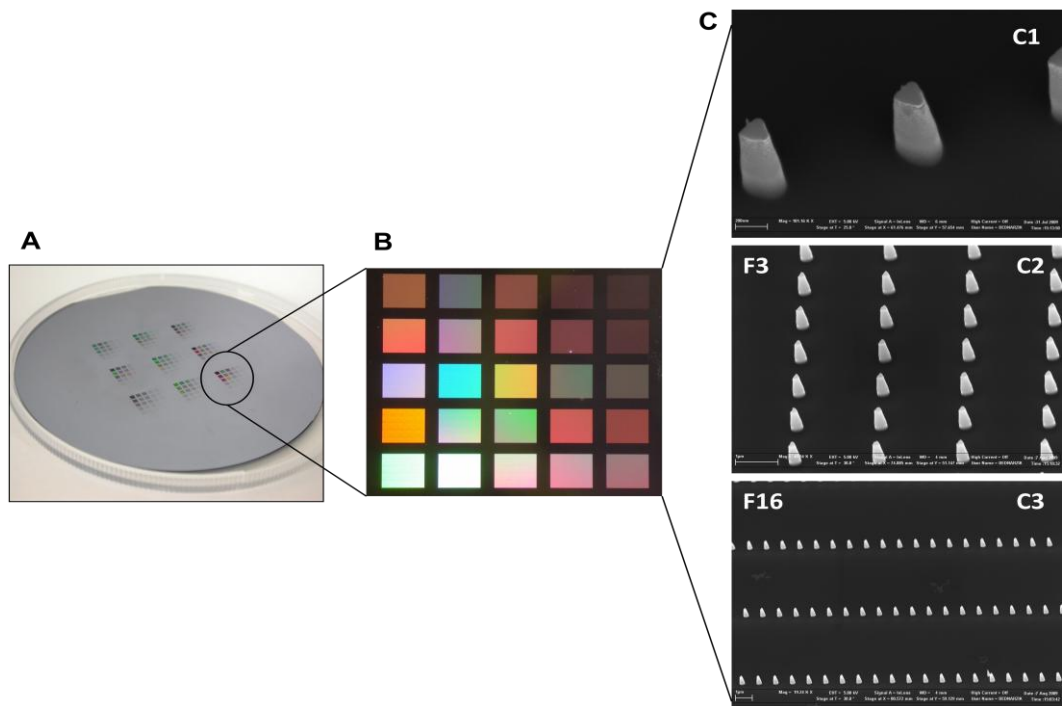
Figure 3.3. Silicon wafer containing the nanopillar array. (A) 9 copies of 25 nanopillar covered fields produced by EBL and RIE, (B) Test arrays consist of 25 fields which are 2 x 2 mm^2 in size and have a different interpillar distance than the neighboring fields, (C1, C2, C3) SEM images of different fields (F stands for the field).

The general appearance of the topography of various fields on the final replicates is shown by optical microscopy to be almost defect free (Figure 3.4A). The size and heights were found to be very close to that of the master structures, as confirmed by AFM measurements (Figure 3.4B). The height of the pillars was shown by section analysis with AFM to be very close to 900 nm, as was originally planned (Figure 3.4B).
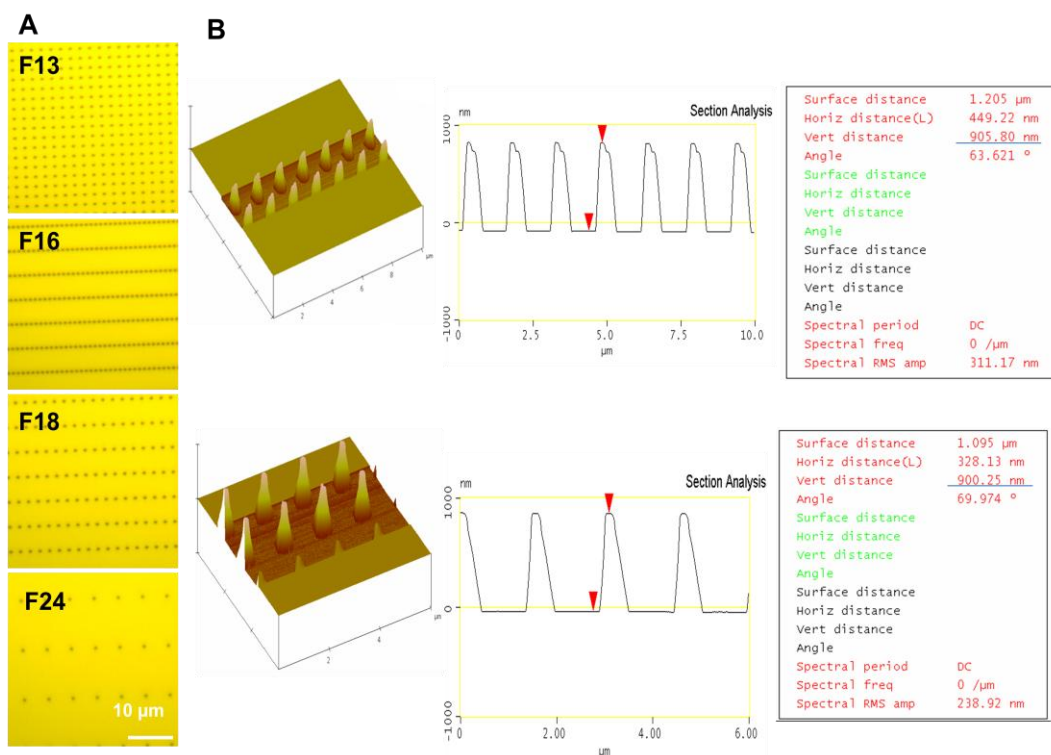
Figure 3.4. Microscopy of the P(L-D,L)LA the test samples made from a nanopillar template. (A) Optical micrographs of nanopillars replicated nanopillars on P(L-D,L)LA films as visualized in 2D (top view) showing pillar organization on the films. (F stands for the field) (B) AFM of the original template (master silicon wafer) in 3D and in cross section showing the pillar dimensions and spacing.
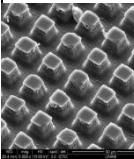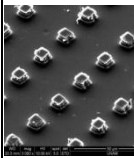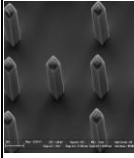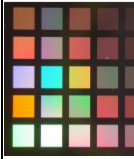
PDMS replication of features is a suitable method to transfer surface topographies to another substrate. Due to the elasticity of PDMS and the low surface energy the detachment from structured surfaces is relatively simple and works with a resolution down to the nanometer scale (Ye et al., 2009, Zorlutuna et al., 2009, Padeste et al., 2011). However, due to the chemical properties, PDMS casts are of little interest for *in vitro* studies, but they are well suited as intermediate templates. For example, casting of liquid polymers into a PDMS mold followed by UV-induced curing was used to replicate high aspect ratio microstructures produced with deep X-ray lithography (Perennes et al., 2006). Furthermore, P(L-D,L)LA maintained above its glass transition temperature of 180°C was pressed into a PDMS to form microstructured surfaces for cell growth experiments (Davidson et al., 2009).

In this study, two-step replication process was used for the production of micro and nano level features on biocompatible and biodegredable polymers to study cell material interactions. In particular, structured surfaces of polymers of the P(L-D,L)LA and PLGA family were reproduced in large quantities from re-usable high-quality masters. The presented replication method is simple and can be performed without the need of specific microfabrication facilities to produce well defined micro and nanostructures.

3.3 *In Vitro* Studies on Type 1 and Type 2 Micropillars

In this study cell and nucleus deformation of five cell types, namely hFOB 1.19, L929, Saos-2, BMSCs and MCF7, were examined on Type 1 and Type 2 structures consiting of rectangular prism shape micropillar features. To study the deformation of pillars on Type 3 substrates due to tugging force applied by the cells only L929 and Saos-2 cells were used. BMSCs and Saos-2 cells were chosen to study differential adhesion behavior on the nanopillar arrays (Table 3.1).

Table 3.1. Summary of *in vitro* studies.

Cellular Response	Pattern Type		Height	Length x Width	Spacing	Cells
Cellular and nuclear deformation	Type1		4 µm	7x7 µm^2	7x7 µm	Saos-2 MCF7 hFOB 1.19 L929 BMSC
	Type 2		4 µm	8x8 µm^2	12x24 µm	Saos-2 MCF7 hFOB 1.19 L929 BMSC
Pillar bending-tugging force	Type 3		5 µm	1 µm (Diameter)	4.2x9.2 µm	Saos-2 L929
Differential cell adhesion and alignment	Nanopillar Array		900 nm	200 nm (Diameter)	1 to 10 µm	Saos-2 BMSC

3.3.1 Study of Deformation of Cell Morphology and Nucleus and Adhesion

In this section the influence of microscale rectangular prism shaped pillars on adhesion, cytoskeletal organization and nuclear deformation of human osteosarcoma cells (Saos-2) cells, human breast adenocarcinoma cells (MCF7), rat bone marrow stem cells (BMSC) and mouse fibroblast cells (L929) were investigated using Type 1 and Type 2 surfaces. Deformation was used to describe the temporary or permanent changes that occurred in shape due to physical restrictions caused by micropillars. It does not correspond to any functional or biological deformity.

Although several earlier studies had been performed with cells on surfaces with features of micron size, less attention was paid to the subsequent effects of mechanoresponsiveness of the cell and its organelles except for elongation of the cell and nuclei in the grooves of micropatterned surfaces (Dalby et al., 2003, Grechet et al., 2007).

3.3.1.1 Deformation of the Nucleus on Type 1 Pillars

These cells were chosen with the expectation that cancer cells and non-cancerous cells (at the cellular and organelle level) have different mechaniresponsiveness and also to study the physical effects of micro and nanotopography on the stem cell. Mouse and rat cells were included because of their being adult and stem cells, and also because their use as standard cells in biocompatibility (L929) and frequent use in bone tissue engineering (Saos-2) applications, respectively.

The reorganization of the internal cellular structure and deformation of the nucleus in response to the surface topography of the material in contact with the cell was evidenced by fluorescence microscopy. The P(L-D,L)LA films were also examined with SEM to determine the orientation of the cells grown on the micropillars.

All five types of cells attached and spread on Type 1's, symmetrically distributed pillars. The deformation of the nucleus and cytoskeleton are shown in Figures 3.5 and 3.6. The cells were presented in two groups for ease of visualization. Cancerous cells, Saos-2 and MCF7, and healthy counterpart of Saos-2 which is hFOB1.19 were presented as the human cells group (Figure 3.5). Rat bone marrow mesenchymal stem cells (BMSCs) and L929 fibroblasts

which are the least specialized cells in connective tissue family were presented as the second set which is rat and mouse origined respectively (Figure 3.6).
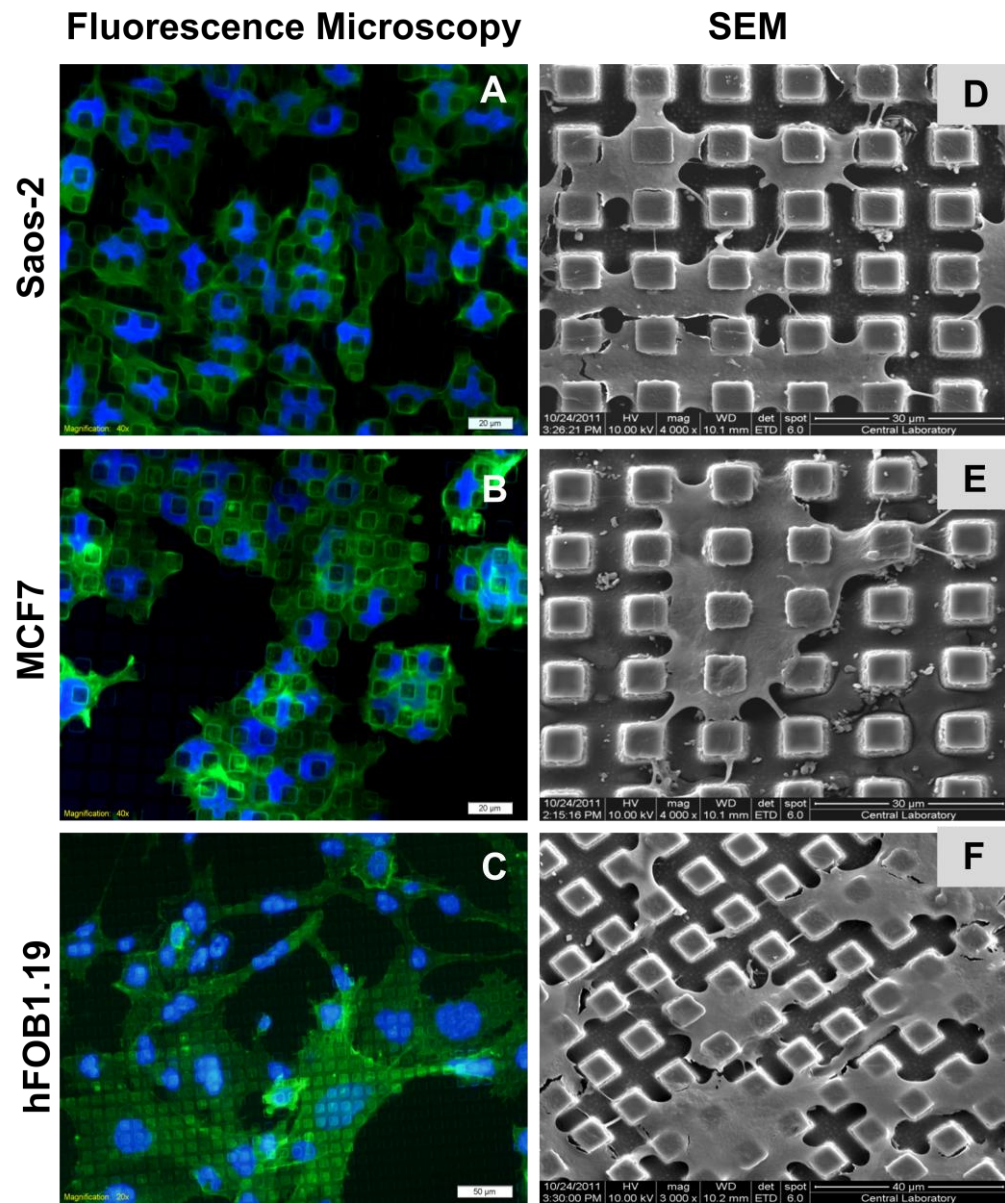
Figure 3.5. Interactions of Saos-2, MCF7 and hFOB 1.19 cells with Type1 substrates as studied by microscopy. Fluorescence (Left panel: 3.5A, 3.5B, 3.5C) and SEM micrographs (Right panel: 3.5D, 3.5E, 3.5F) of two cancerous cell lines (Saos-2 and MCF7) and healthy bone cell hFOB 1.19 on Type 1 pillars. Scale bars: A and B: 20 µm, C: 50 µm.

It was observed that Type 1 micropillars lead to extensive deformation of the nuclei of Saos-2 and MCF7 cells (Figures 3.5A and 3.5B). Their nuclei showed a deformation matching the underlying topography. The pillars under the cells are visible as dark squares. The nuclei of these cells were found to be localized in between the pillars (Figures 3.5A and 3.5B). This altered appearance is probably due to a mechanical deformation, which caused the bulk of the mass of the nucleus to be hanging in between the pillars. This deformation can be interpreted as the nucleus being stretched across the pillars or alternatively, by the nucleus being inserted in the spaces between the pillars. Consequently, the nuclei continued to deform and rearrange.

Cancerous cells such as Saos-2 and MCF7 are known to be more deformable than normal cells. Saos-2 cells are known to be metastatic. MCF-7 cells are nonmotile, lowly metastatic epithelial cancer cells. Metastatic cancer cells have been found to be to be much more flexible (Raz and Geiger, 1982, Ochalek et al., 1988, Ward et al., 1991). This appears logical because, in accordance with their need to move through tissues to invade other organs need to squeeze through the surrounding tissue matrix as they move towards circulatory system (Wyckoff et al., 2000).

An additional cell line was tested to verify whether nucleus deformation is limited to cancerous cells. Human osteoblast cells (hFOB 1.19) were selected for comparison with Saos-2 cancerous cells as they are healthy cells from the bone. When seeded on micropillared surfaces, the hFOB 1.19 cells showed very little deformation, much less than the cancerous cells Saos-2 and MCF7 (Figure 3.5C). It is well known that cancerous cells have mechanical properties that are different from healthy cells and produce less cytoskeletal filaments (Ben-Ze'ev 1985). They have been shown to be more deformable than healthy cells. Thus, this result supports that non-cancerous cells are affected by structured surfaces in a different manner than cancerous cells.

These interactions were also examined with SEM to view the whole cells more distinctly on the fields patterned with micropillars (Figures 3.5D–3.5F). It was observed that Saos-2 cells attached to the pillars and spread over the tops of number of them. In addition, cytoskeleton of both, Saos-2 and MCF7 were observed to cover the pillar tops and sag down in between the pillars (Figure 3.5D and 3.5E). The edges of square shaped pillars could be observed through the cell body. However, non-cancerous bone cells hFOB 1.19 stretched over the pillars with no sign of sagging implying that cytoskeleton is more rigid or strong (Figure 3.5F). Our data supports the findings of Bhadriraju and Hansen (2002), Bao and Suresh,

(2003) and Suresh et al., (2005) that when normal cells transform to cancerous cells, they become less stiff and this brings about their increased ability to spread.

Interestingly, a significant level of nucleus deformation was observed with the L929 mouse fibroblast cell line (Figure 3.6A). On the other hand, BMSCs were found to be the least deformable one of the five types of cells (Figure 3.6B).
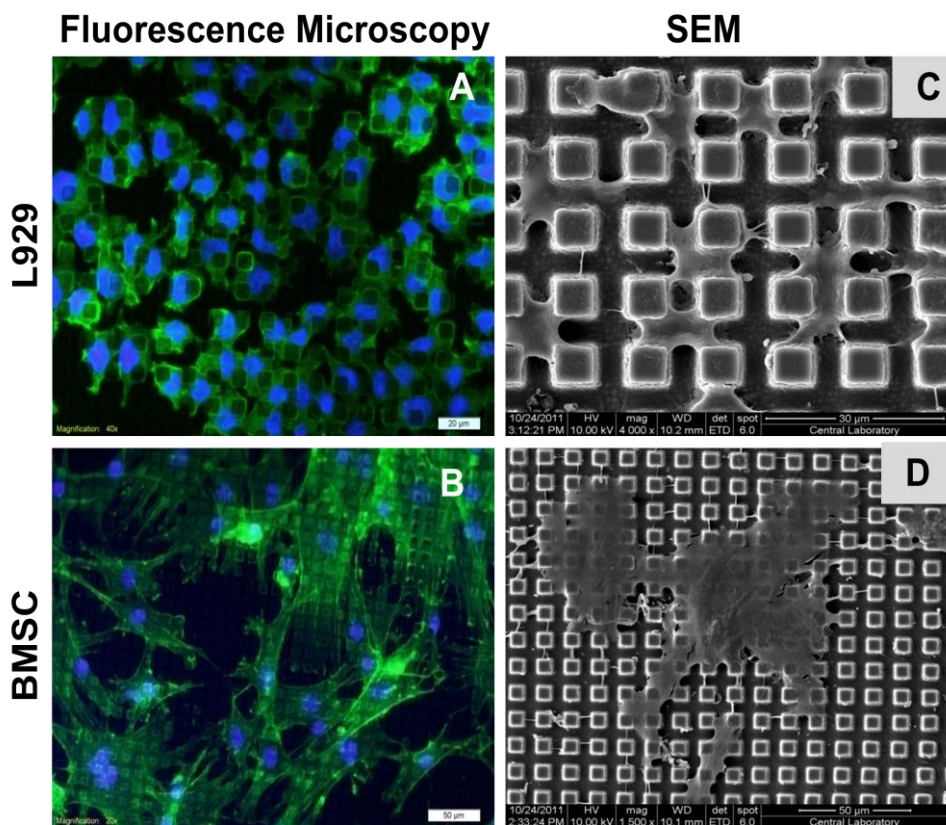
Figure 3.6. Interactions of L929 cells and BMSCs with Type1 substrates as studied by microscopy. Fluorescence (Left panel: 3.6A, 3.6B) and SEM micrographs (Right panel: 3.6C, 3.6D) of L929 cells and BMSCs on Type 1 pillars. Scale bars A: 50 µm, B: 20 µm.

These findings presented in Figures 3.6A and 3.6B may be regarded as a sign of high mechanical plasticity of fibroblasts. These cells have been widely used to explore the influence of micro and nanoscale surface topography on cellular response (Alves et al., 2010). The fibroblasts seem to be the least specialized cells in the connective tissue family,

found dispersed in connective tissue throughout the body, where they secrete a non-rigid ECM which is rich in type I and/or type II collagen. Fibroblasts also seem to be the most versatile of connective tissue cells, displaying a remarkable capacity to differentiate into other members of the family. Thus, deformation of their nuclei by micropillars is not surprising.

The stromal cells of bone marrow can be regarded as a kind of fibroblast and are isolated from bone marrow and propagated in culture. They are multipotent and are reported to differentiate into various anchorage-dependent cell types, including bone, cartilage, adipose, tendon, muscle, neural cells.

Discher and coworkers (2007) showed that nuclei in human embryonic stem cells are the most deformable, followed by hematopoietic stem cells, HSCs, that generate a wide range of blood and tissue cells. This is because both types of stem cells lack lamins A and C, the two filamentous proteins that interact to stabilize the inner lining of the nucleus of most tissue cells. Lamins A and C stiffen the cell nuclei and are expressed in cells only after gastrulation. In this perspective, occurence of high frequency of nuclei deformation in BMSCs was expected in this study. However, BMSCs showed the lowest degree of nuclei deformation among the five types of cells that were tested (Figure 3.6B). Pajerowski et al., (2007) have discovered that the nuclei of human stem cells are particularly soft and flexible, rather than hard, making it easier for stem cells to migrate through the body and to adopt different shapes, but ultimately to put human genes in the correct "nuclear sector" for proper access and expression. Thus, least deformability of BMSCs was unexpected. In contrast to the low nucleus deformation, cytoskeletal response of the BMSCs was the most prominent in all five types of cells. In the cytoskeleton of BMSCs, distinct actin fibers were observed in the form of a highly organized network.

The SEM micrographs of L929 cells and BMSc also support the distinct reactions of the cytoskeletons (Figures 3.6C and 3.6D). While the more deformable L929 cells coated the pillar tops and bodies partially, BMSCs did only spread over the tops. However, one must be cautious as size effects cannot be discredited: the difference in size of the studied cells may also contribute to the observed difference in deformation behavior.

Figure 3.7 brings together the nuclear and cytoplasmic deformation micrographs of the deformable cancerous cells (Saos-2 and MCF7) and mouse fibroblasts (L929). Varying degrees of nucleus deformation were observed. The regions where the nuclei sags down

the pillars (partially or totally) were indicated by yellow circles (Figures 3.7A, 3.7B and 3.7C). These microgrpahs show the ability of the nucleus to stretch and deform in response to the microstructured surface. In addition to nuclei deformation, these cell types showed extensive cytoplasmic or cell body deformation, as shown in the SEM images. In the example shown (Figures 3.7D, 3.7E and 3.7F), the cytoplasm seems to cover the top and then sag a few microns to the base of the pillars.

In general, the difference in the extent of deformation is most probably linked to the viscoelastic properties of the nuclei and much less to the deformability of the cytoskeleton of cell types. The deformation is most likely the result of a balance between the rigidity of the nucleus and the force that the cytoskeleton exerts on it.
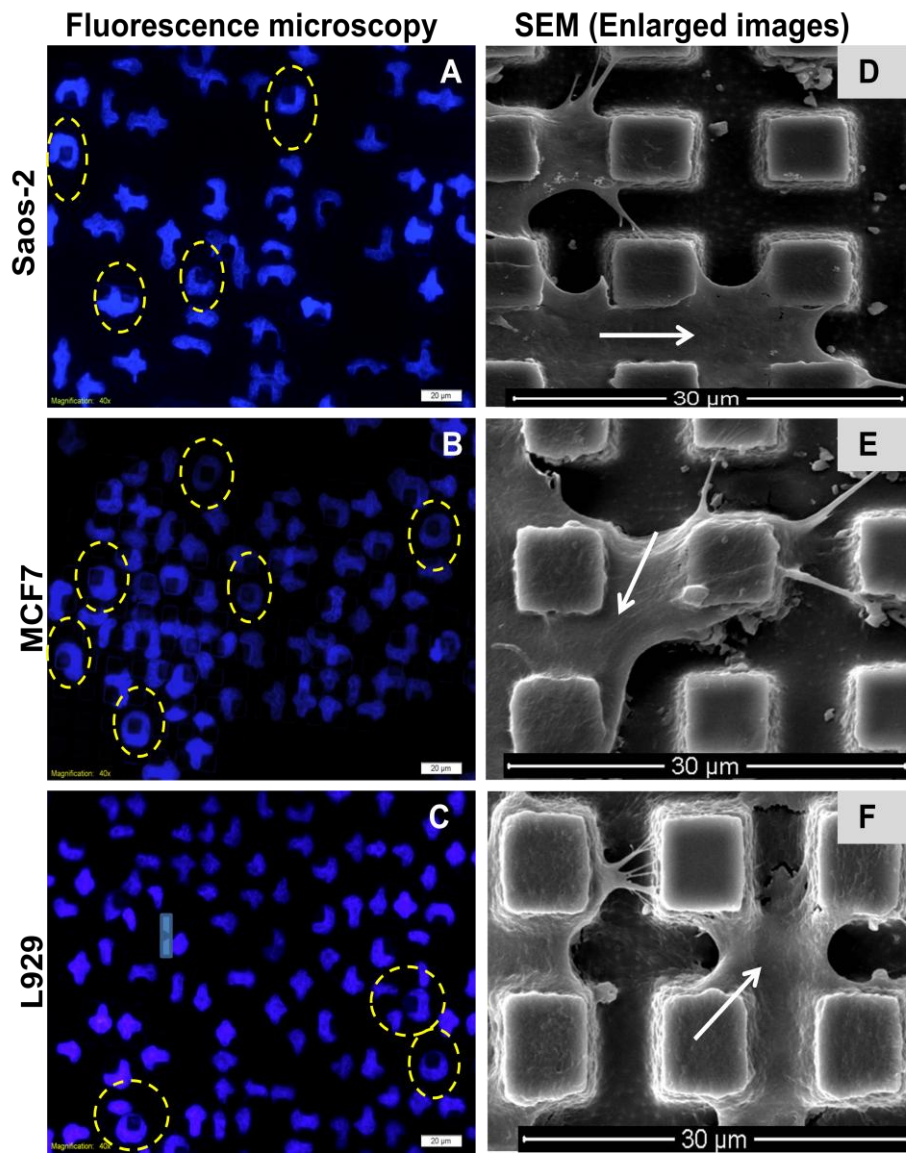
Figure 3.7. Micrographs of three cell types whose nuclei deformed on the pillars of Type 1 surface. Fluorescence micrographs of DAPI stained nuclei of (A) Saos-2, (B) MCF7 and (C) L929 cells on Type 1 pillars. Scale bars: A-C: 20 μm. SEM micrographs of the same cells (D) Saos-2, (E) MCF7 and (F) L929 cells.

3.3.1.2 Deformation of the Cell and Nucleus on Type 2 Pillars

It must be considered that there are a multitude of factors that affect the behavior of cells on surfaces with featured topography. These include the height, width, shape, and the organization of these features, the chemistry and rigidity of the material and the type of the cell used. In this study some parameters such as the chemistry, shape and height were kept constant while the position of the pillars with respect to each other was changed. In Type 1, square pillars (7x7 μm^2) were used, spaced by 7 μm. In the Type 2 surface the pillar-to-pillar distance was increased to 12 and 24 μm along the x and y axes. This means that the distribution became asymmetric (Figure 3.2).

All five types of cells were also tested on Type 2 micropillars. In Figure 3.8 the cancerous human cells and healthy human cell type are presented on Type 2 surface. Nuclei of two cancerous cells showed distinct deformation on Type 2 patterned films as they did on Type 1 (Figures 3.8A and 3.8B). Since the pillars were more distant to each other on this template, the nuclei of the cells either wrapped the pillars or were positioned between two closest pillars instead of hanging down and spreading between them. Still, a few hFOB 1.19 cells displayed deformed nuclei motifs on the asymmetrically distributed pillars indicating a nucleus contorted by pillars (Figure 3.8C).
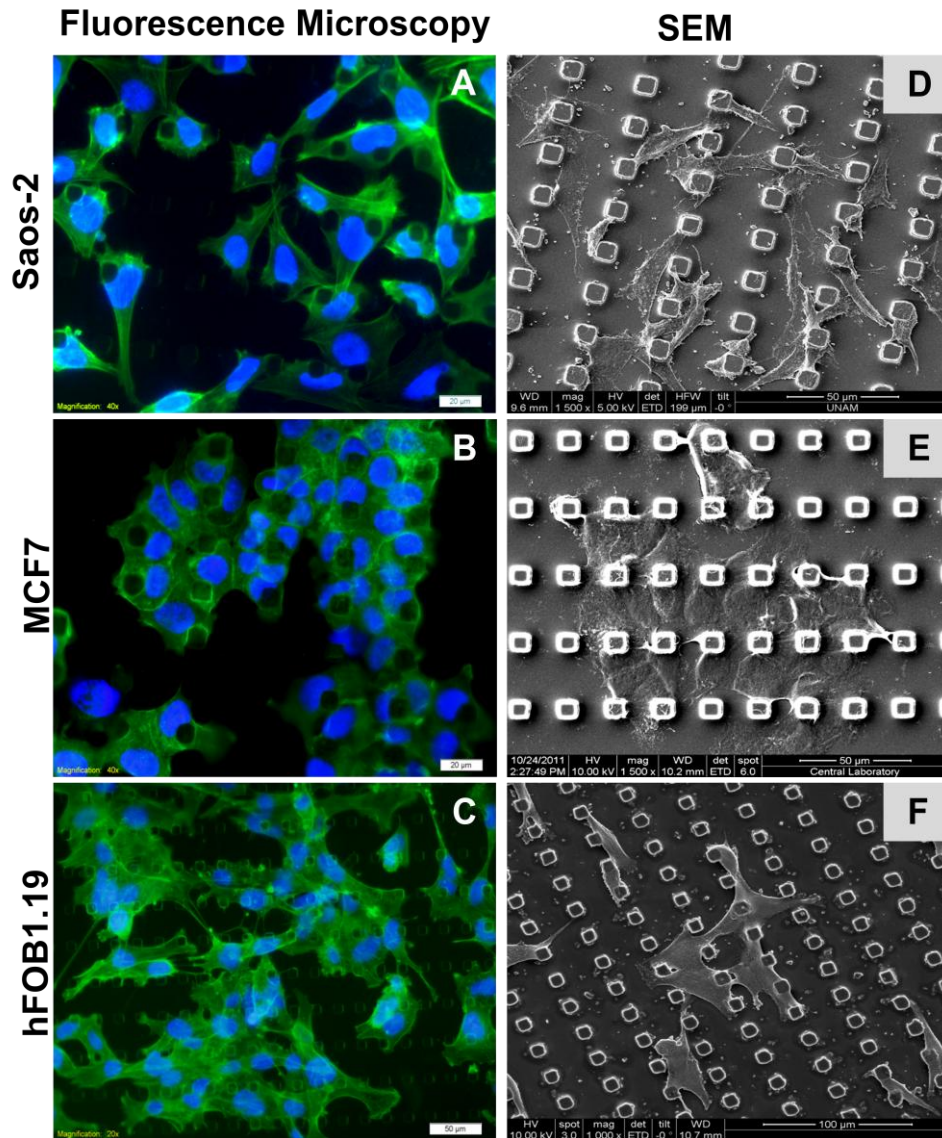
Figure 3.8. Interactions of Saos-2, MCF7 and hFOB 1.19 cells with Type 2 substrates as studied by microscopy. Fluorescence (Left pannel: 3.8A, 3.8B, 3.8C) and SEM micrographs (Right pannel: 3.8D, 3.8E, 3.8F) of two cancerous cell lines (Saos-2 and MCF7) and healthy bone cell hFOB 1.19 on Type 2 pillars. Scale bars: A and B: 20 µm, C: 50 µm.

In order to study the orientation of cells on Type 2 pillars more distinctly SEM analysis was performed. Saos-2 cells which were grown on these asymmetrically distributed pillars appeared to be spread. The longer distance between the pillars (24 μm) exceeded their size/length and this allowed them to spread on the surface between the pillars (Figure 3.8D). The main difference in the behavior of MCF7 cells on Type 2 surfaces was their cell morphology. MCF7 cells grown on Type 2 pillars showed distinct cubodial morphology. Even the nuclei of the individual cells could be seen clearly (Figure 3.8E). Very similar to Saos-2 cells, healthy bone cells (hFOB 1.19) also spread well on the surface between the pillars (Figure 3.8F).

Deformation behavior of two fibroblast like cells, L929 and BMSCs was tested on Type 2 pillars (Figure 3.9). In Figure 3.9A it is seen that the L929 cells and their nuclei are localized around the pillars. Due to their smaller size they were able to fit in the gaps occupied the gaps between the pillars with no distinct alignment or orientation. With BMSCs finely branched cytoskeletal extensions were observed (Figure 3.9B). Such cytoskeletal responses of BMSCs to pillars also were consistent with the extremely high elongation and spreading ability of the stem cells (Engler et al., 2006). However, their nuclei appeared to be the least deformable among the five types of cells grown on Type 2 pillars.

The above observations on L929 and BMSCs with fluorescence microscopy were confirmed by SEM. The cytoskeletal response of both cell types was more evident on Type 2 pillars where cell-to-pillar and cell-to-cell intearctions are seen better. Their size difference is remarkable. While three L929 cells were attched and spread between any four pillars, there was only one BMSC observed to spread on the same area (Figures 3.9C and 3.9D).
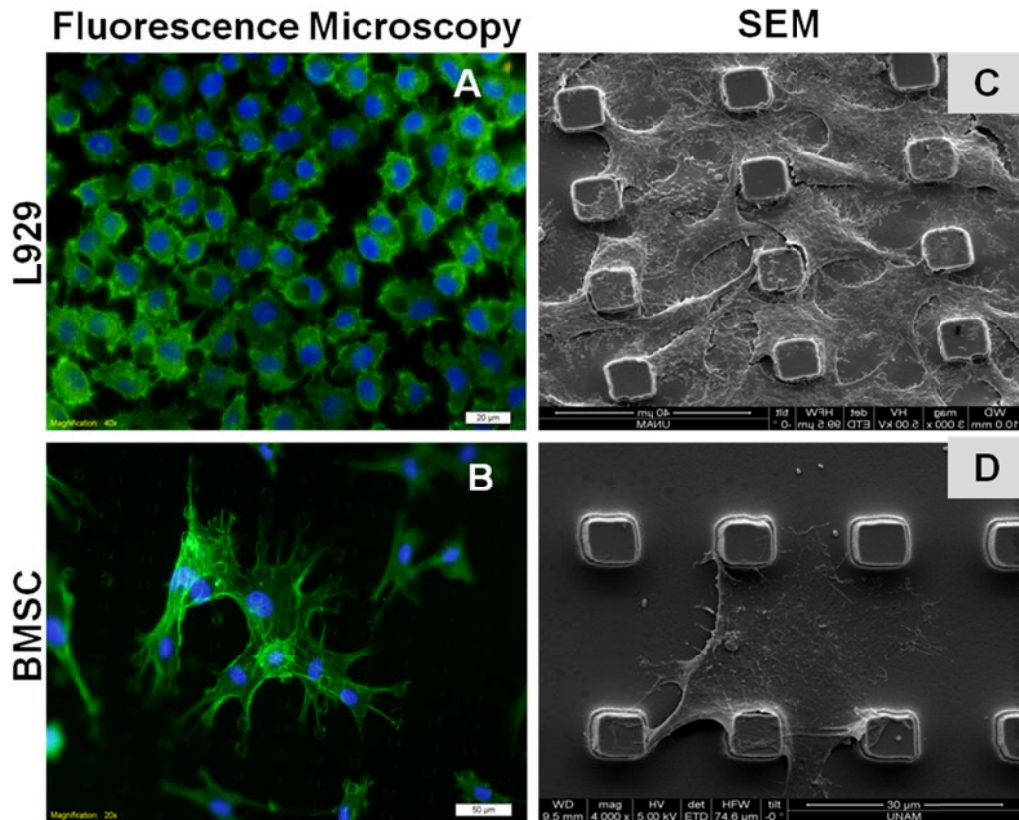
Figure 3.9. Interactions of L929 cells and BMSCs with Type 2 substrates as studied by microscopy. Cell-substrate Type 2 interactions as studied by microscopy. Fluorescence (Left panel: 3.9A, 3.9B) and SEM micrographs (Right panel: 3.9C, 3.9D) of L929 cells and BMSCs on Type 2 pillars. Scale bars: A: 20 μm, B: 50 μm.

In Figure 3.10, the highly organized cytoskeleton of four types of cells (Figures 3.10A - 3.10D) and their fine cytoplasmic projections (Figures 3.10E – 3.10H) on Type 2 pillar surfaces presented in more detail. MCF7 was excluded due to its "cluster" type growth characteristics.
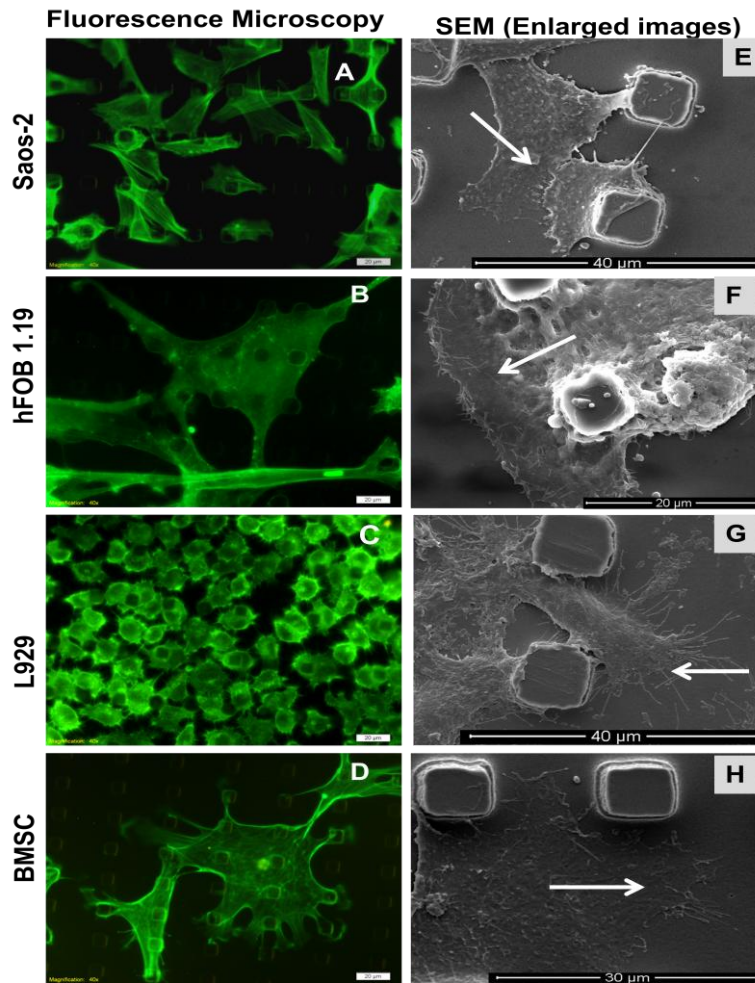
Figure 3.10. Fluorescence micrographs of FITC-Phalloidin stained cytoskeleton for (A) Saos-2, (B) hFOB 1.19 (C) L929 and (D) BMSC cells. SEM micrographs of the same cells (E) Saos-2 (F) hFOB 1.19 (G) L929 and (H) BMSC cells showing fine filopodial extension on Type 2 pillars and basal surface (see white arrows). Scale bars: A-D: 20 μm.

Cytoskeletons were wrapped around the pillars in Saos-2, hFOB1.19 and BMSC cell (Figures 3.10A, 3.10B, and 3.10D respectively). The exception was L929 cells (Figure 3.10C probably due to their small cell size, their spreading, hence their extension was not distinct. In the magnified SEM images, many finely branched filopodia, shown by white arrows, were visible especially on surface of the film and on the pillar tops for all four types of the cells (Figure 3.10E–3.10H). Although all types of the cells spread at the surface of the film, the 4-5 μm height of the pillars was short enough for the cells to climb them. Figures 3.10E and G present the cells that partially covered the surface of the pillars. In

addition, the shorter distance between the pillars seemed to be suitable for the elongation of fillopodial extensions (Figure 3.10E).

3.3.2 Quantification of Nucleus Deformation by Image Analysis

3.3.2.1 Measuring the Frequency of Nucleus Deformation

The extent and frequency of nucleus deformation was analyzed by using the images with NIH Image J software.

Figures 3.11A and 3.11B present the nucleus deformation observed on Type 1 and Type 2 pillars schematically. For the determination of frequency of nucleus deformation on micropillars, "cross" and "horseshoe" shaped nuclei were considered.
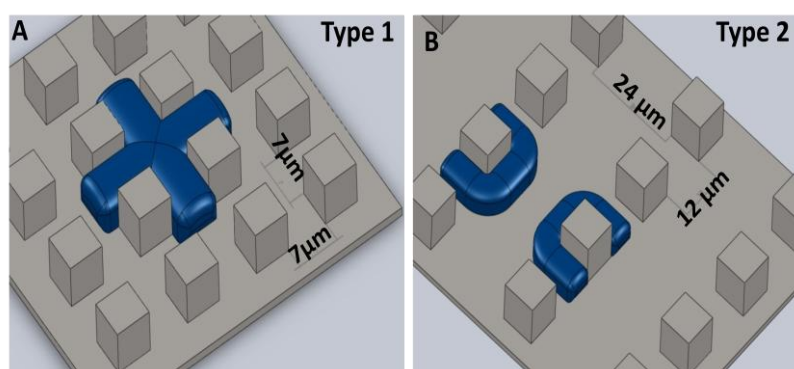
Figure 3.11. Schematic presentation of typical nucleus deformation on Type 1 and Type 2 patterns.

To calculate the extent of nucleus deformation for each cell type, 15 images were counted on Type1 and Type 2 pillars. All of the images were have the same magnification, 40X. Then, the frequency of deformed nuclei in each image was calculated [% Frequency of deformed nuclei= (No. of deformed nuclei / No. of cells) x 100)].

Figure 3.12 shows the frequency of deformation of nuclei on Type 1 and Type 2 pillars. On Type 1 pillars BMSC and hFOB 1.19 cells showed as much as 28% and 8% deformed nulcei respectively, while cancer cells MCF7 and Saos-2, and fibroblasts L929 were almost

fully deformed. This result is consistent with expectations that cancerous cells are "softer" or more deformable. Deformation of nuclei of L929 cells (97%) was not surprising since they are the most versatile of connective tissue cells, displaying high mechanical plasticity. High frequency of nucleus deformation was expected the stem cells, but for BMSCs the lowest nuclei deformation of all was observed (Figure 3.12).
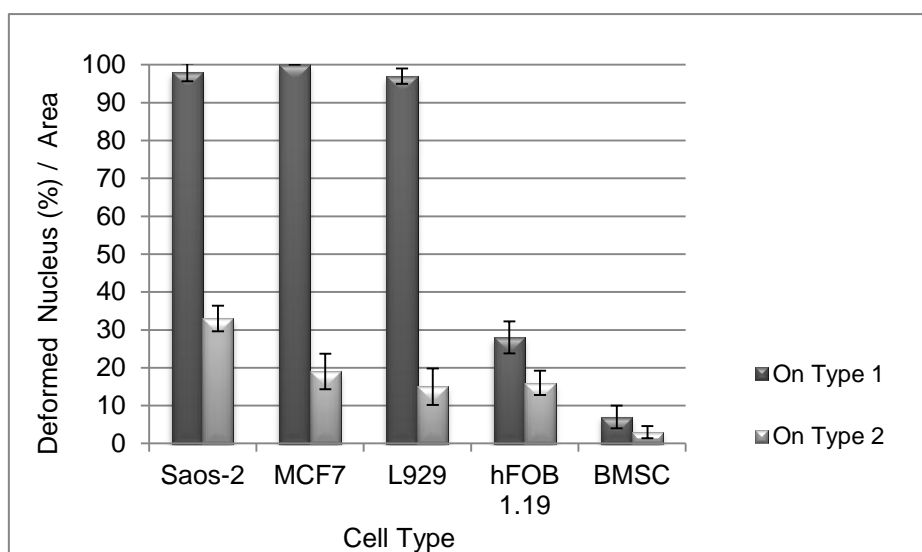
Figure 3.12. Frequency of deformation of nuclei (%) of the four cell types cultured on Type 1 and Type 2 pillars.

On Type 2 pillars, the maximum extent of deformation decreased to one third when compared to results obtained from Type 1 pillars. The highest deformation was still observed in two cancerous cells. The values were 33% (Saos-2) and 19 % (MCF7). In contrast to L929 cells grown on Type 1 pillars, Type 2 pillars triggered deformation of only 15% of the cells. The frequency of nuclei deformation in healthy bone cells was 16%. The least deformable nuclei were observed in BMSCs again (Figure 3.12). In summary we can conclude that, the derived quantitative data on the extent of nucleus deformation are in good accordance with microscopic studies.

3.3.2.2   Quantification of Extent of Nucleus Deformation

In order to quantify the intensity of nuclei deformation, circularity was calculated by Image J (Figure 3.13). The program has the tools to calculate various shape descriptors. It calculates the circularity of seleceted object by using the formula of

$$\text{Circularity} = 4\pi \times \frac{(\text{Area})}{(\text{Perimeter})^2}$$

The value of 1.0 indicates a perfect circle. As the value approaches 0.0, it indicates an increasingly elongated shape. Thus, the circularity of the nuclei of five types of cells was measured to show the extent of deformation/irregularity due to micropillars (Figure 3.13). On Type 1 pillars, while the nuclei of the least deformable cells had a value close to perfect circle (1.00). While the circularity of hFOB1.19 was calculated as 0.87, it was the heighest for BMSCs (0.90). The circularity of the most deformable cancer cells was much lower (0.43). These findings suggest that cellular elasticity may be used as a cell marker and a diagnostic parameter together with biochemical tests for underlying disease (Figure 3.13).
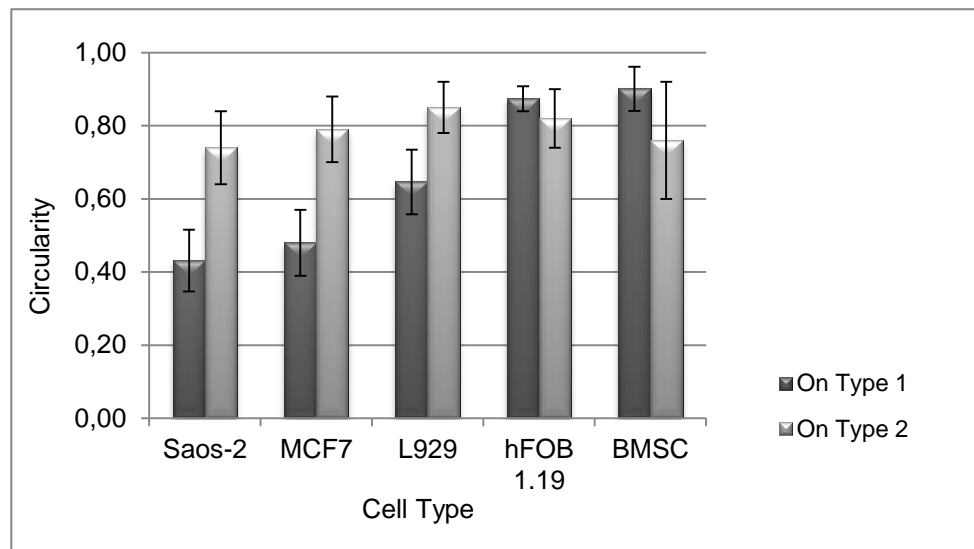
Figure 3.13. Cell type and nucleus circularity relation obtained with the five cell types grown on Type 1 and Type 2.

The same shape descriptors were calculated for the cells grown on Type 2 pillars. As the fluorescence micrographs revealed these pillars could only trigger cell bending. So, for example no typical cross-shaped nuclei were observed on this surface. Because the inter pillar distances are too long for spreading of one cell on top of 3-4 pillars, most of the cells could locate themselves at the basal surface which does not contain any barrier for their nuclei. So, no significant difference was detected between the cell types in terms of the circularity of their nuclei. The circularity of five types of cells grown on Type 2 pillars was around 0.8 (Figure 3.13). Thus, we may conclude that the distribution of pillars on Type 2 substrate does not provide high selection capability, as Type1 does, to distinguish deformable cancer cells from nondeformable ones.

3.3.3   Immunohistochemical Studies

3.3.3.1   Labelling Nuclear Membrane with Lamin A

In all studies performed up to now, while Saos-2 was determined as the most deformable cell, BMSC was appeared to be the least deformable one. In order to better visualize the nuclear deformation in these two cell types it was decided to stain the nuclear membrane to make the nuclear membrane's inner protein network of lamins (Figures 3.14 and 3.15).

Lamin A is a structural protein of the nuclear lamina. The nuclear lamina is a meshwork of intermediate filaments that underlie the inner face of the nuclear envelope. In Figure 3.14 DAPI and LaminA staining of Saos-2 on Type 1 and Type 2 are presented. Saos-2 nucleus stained with DAPI (blue) grown on Type 1, Type 2 and smooth control respectively. In Figures 3.14D, 3.14E and 3.14F, the same area of the nuclear membrane labelled with Lamin A antibody (green) is seen. Note that the nucleus or DNA and nuclear membrane images coincide with each other in most instances. In enlarged images (Figures 3.14A1 and 3.14D1) anti Lamin A stained nuclei on Type 1 (indicated by arrows), sagged down the top of the pillars; the green stain is still visible across the top of the pillar, information which is not clearly visible with the blue nuclear DNA stain. This indicates that the nucleus is stretched across the top of the pillars. On Type 2 pillars, the Saos-2 cells were observed to be located around the pillars and bent (Figures 3.14B1 and 3.14E1). Figures 3.14C and 3.14F and their enlarged versions present undeformed, round, nuclei on the smooth control samples. Anti-rabbit IgG-FITC and DAPI stained samples were used as the negative

controls of this experimental set. Although DAPI verified the existence of nuclei, no staining was observed when use of primary antibody was omitted (data not shown).
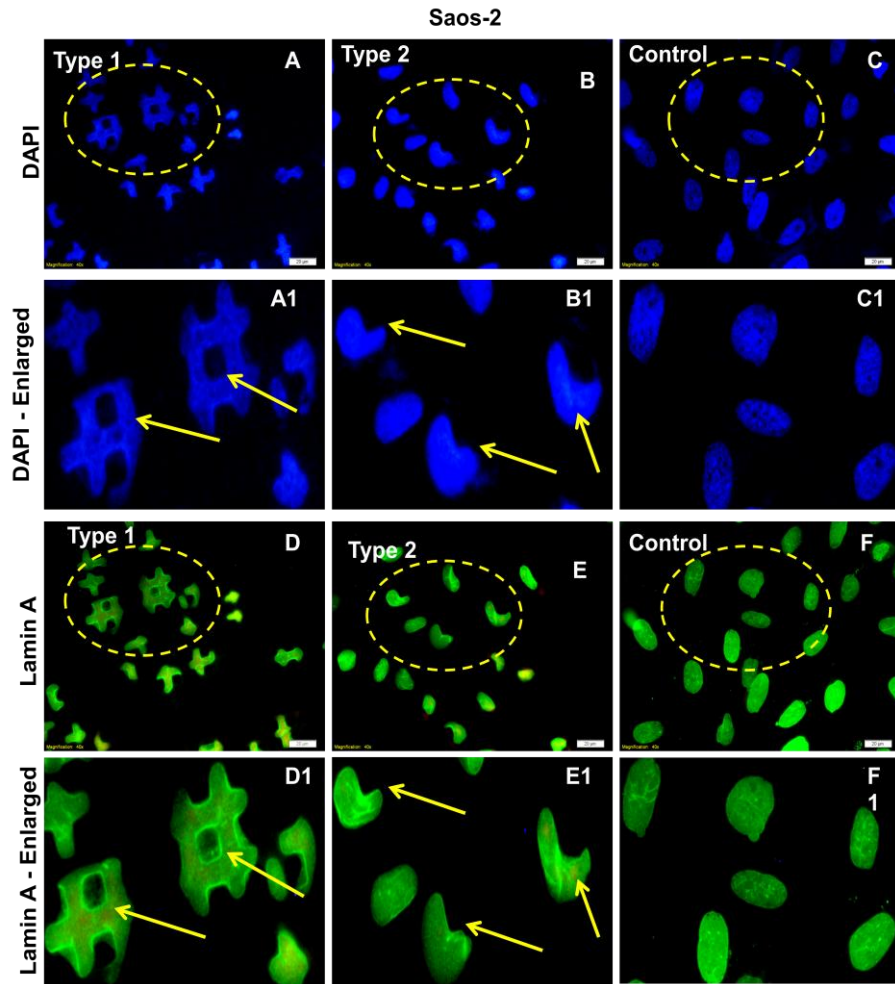
Figure 3.14. Fluorescence micrographs of (A, B, C) DAPI and (D, E, F) anti-Lamin A stained nuclei of Saos-2 cells, on Type 1, Type 2 pillars and on control samples. Enlarged images present the areas labelled with dashed circles. (A1-F1). Arrows indicate the Saos-2 nuclei sagged down on the pillars. Scale bars: A-F: 20 µm.

BMSCs were shown to have the least deformable nuclei among the 5 cell types. In Figure 3.15 DAPI and Anti-Lamin A labelled nuclei were presented for two types of micropillars and control sample. BMSCs preserved their typical round or oval morphology on all of the

samples. SEM micrographs and cytoskeletal labelling with FITC-Phallodin shown that they spread on the pillars (if the pillars are to close too squeeze between them as in the case of Type 1) or between the pillars (if the pillars are seperated enough as in the case of Type 2). Nucleus/DNA and nuclear membrane labelling confirmed these results. For example, Figures 3.14A1 and 3.14D1 indicated that BMSC nuclei spread on Type 1 pillars. The pillars are still visible under the Anti-Lamin A stained nuclei. On Type 2 pillars, BMSCs seem to localize themselves in the gaps between the pillars. Because, it was not observed any pillar underneath the visualized nuclei (Figures 3.15B1 and 3.15E1). Figures 3.15C and 3.15F and their enlarged versions present undeformed, round, nuclei of BMSCs grown on the smooth control samples. Non-specific staining was tested by using the samples treated with only the secondary antibody. No signal was detected (data not shown).
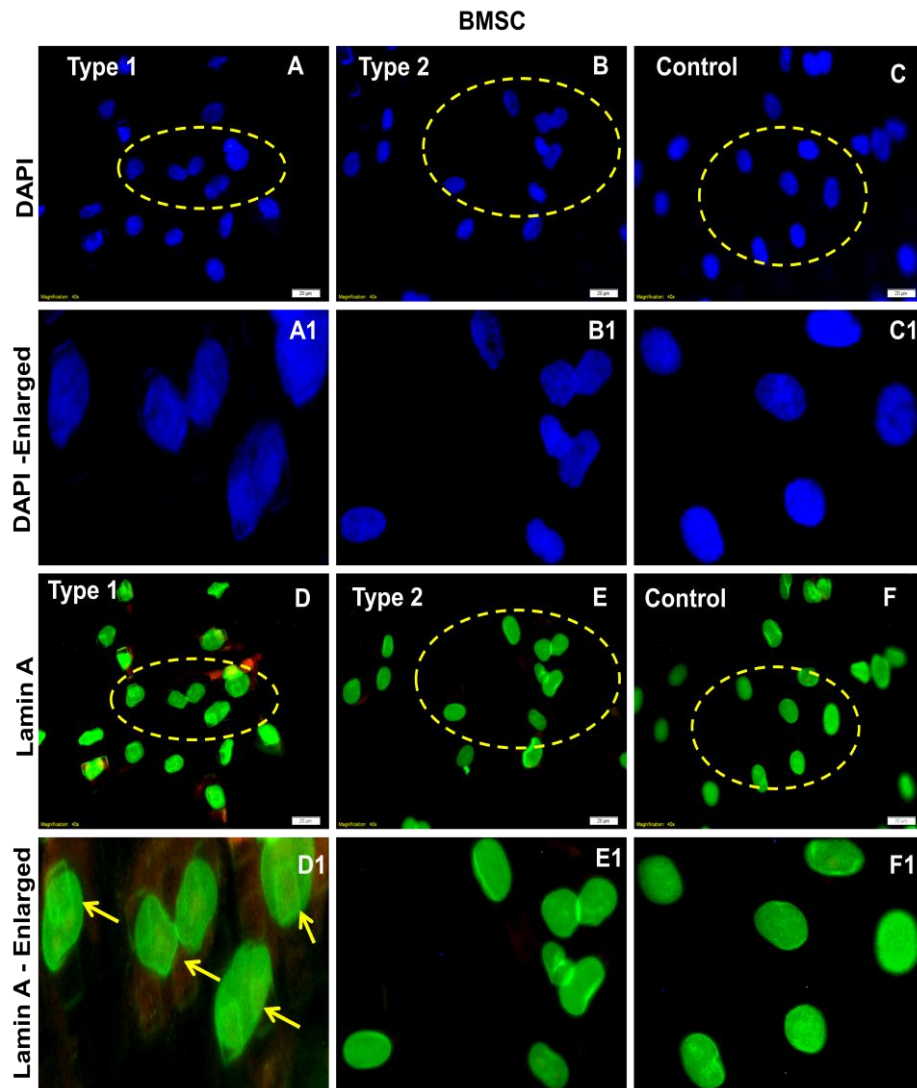
Figure 3.15. Fluorescence micrographs of (A, B, C) DAPI and (D, E, F) anti-Lamin A stained nuclei of BMSCs on Type 1, Type 2 pillars and control samples. Enlarged images present the areas labelled with dashed circles (A1-F1). Arrows indicate BMSC nuclei spread on Type 1 pillars. Scale bars: A-F: 20 μm.

3.3.3.2   Labelling Focal Adhesion Points With Anti Vinculin Staining

In this study focal adhesion complexes (FACs) in the most and least deformable cell types vinculin were labelled with Anti-vinculin antibody. Vinculin is a cytoskeletal protein which is a part of FAC and functions as one of several proteins involved in anchoring F-actin to the cell membrane. In the assembly of adhesion complex, the b-subunit of integrin binds to talin, talin binds to vinculin that interacts with α-actinin forming a complex structure. Spreading of the cells is known to involve complex reorganization of the cytoskeleton that can be related to changes in physical cues. Recently, Dalby (2005) proposed a 'self-induced mechanotransduction' mechanism correlated with the 'direct mechanotransduction mechanism' proposed in the tensegrity model by Ingber (1991). According to this model forces encountered by cells during cell adhesion are directly transmitted to the nucleus via their cytoskeleton. The altered cytoskeletal tension then is fed back to induce local changes in focal adhesion assembly.

As in the case of anti-Lamin A staining, Saos-2 cells and BMSCs were selected for this assay. In Figure 3.16, FACs of Saos-2 and BMSCs can be seen as bright green regions due to vinculin staining. The location of FACs was shown in Figures 3.16A-3.16D. Negative controls (secondary antibody treated samples) did not show any signal (data not shown).
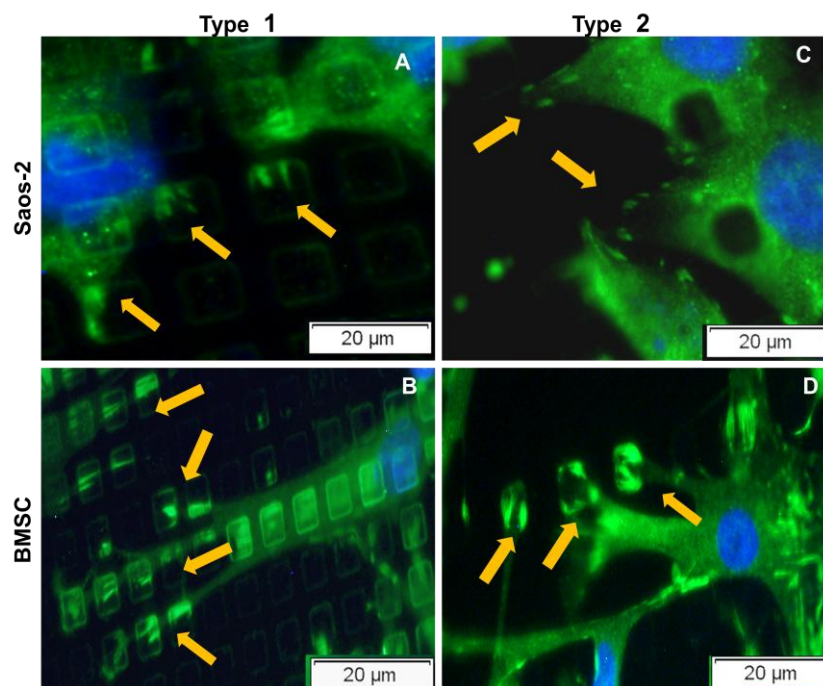
Figure 3.16. Anti-vinculin stained Saos-2 cells and BMSCs grown on Type 1 (A and B) and Type 2 pillars (C and D). Arrows indicate FAC formations. Scale bars: A-D: 20 µm.

In Saos-2 cells grown on Type 1 micropillars focal adhesion complexes were observed to be located on the pillars (Figure 3.16A). While the formation of FACs of BMSCs can be seen as "green tracks" on successive Type 1 pillars (Figure 3.16B). Since the distance between pillars exceeded the size/length of Saos-2 cells, they partially climbed up Type 2 pillars, but, mostly adhered to basal surface of the film (Figure 3.16 C). On the other hand, adhesion points of BMSCs were observed to have formed mainly on the pillars. They can be seen at the tops of Type 2 pillars were dense in FACs (Figure 3.16D). SEM micrographs and cytoskeletal labelling with FITC-Phallodin showed the prominent effects of micropillars on the spreading of BMSCs. Thus, formation of FACs on the pillars was an expected result.

3.3.4 Wettability of the Polymeric Films

A relation between cell orientation and spreading and may also surface wettability exist. In order to examine the effects of surface topography on the wettability of the films contact angle measurements were performed for Type 1, Type 2 and unpatterned control samples.

For each surface type 10 measurements were recorded. The average value of contact angle for the corresponding surfaces was plotted (Figure 3.17). It is observed (Figure 3.17) that the unpatterned films have a contact angle of 88° and this increases to 98° and 118° on Type 2 and Type 1 surfaces, respectively. Thus, as the patterns become denser (Type 1) the surface acts as a very hydrophobic surface. Hydrophobic interaction is one of the parameters that contribute to the control of protein adsorption (Arima and Iwata 2007) and in turn, wettability determines cell behavior due to dynamic biomolecule adsorption onto surfaces (Wilson et al. 2005). It is known that changes in surface roughness affect wettability (Paital and Dahotre 2009). Controlled surface structuring can be one of the way of modulation of the wettability of the surface. Ranella et al., (2010) have shown that the number of attached cells per unit area decreased as the roughness ratio and wetting angle increased.
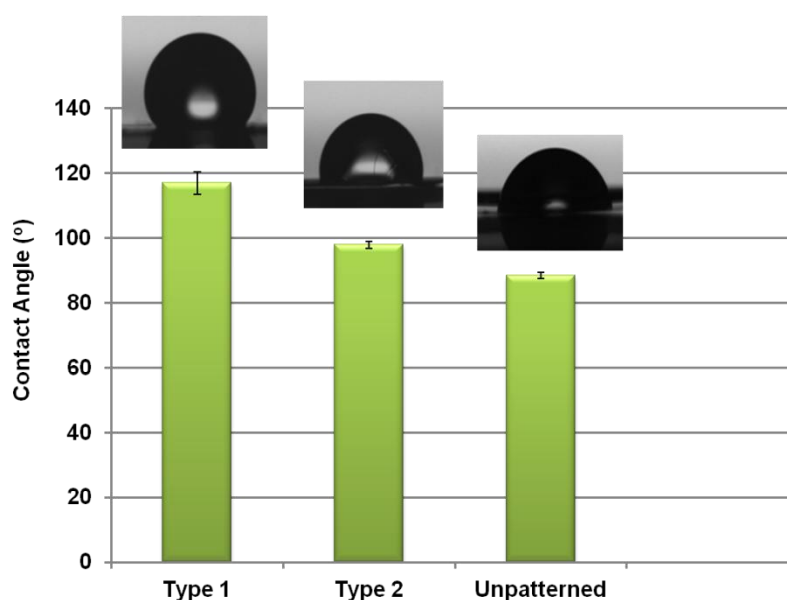
Figure 3.17. Wettability analysis of Type 1, Type 2 pillars and smooth control samples.

In the literature Cassie and Baxter, (1944) stated that water droplets can be in contact with only the peaks of a rugged surface and in addition air might be trapped in the surface grooves. On the other hand, Wenzel states that (1936) water droplets are in full contact with the rugged surface and therefore have a lower contact angle as in Type 2. Like water droplets the cells were mostly spread at the top of the Type 1 pillars and the number of cells spread on the substrate surface were much higher on Type 2 patterned films.

3.3.5   Cell and Nucleus Area and Surface Topography

Cell and nucleus areas of four types of cells were determined after 2 days of cell culture using fluorescence micrographs by the help of Image J software. Cell and nucleus area were determined for each cell type by measuring 100 cells per surface type (Figures 3.18 and 3.19). MCF7 cells were excluded since their cluster type growth characteristics made the measurement of areas of individual cells impossible.
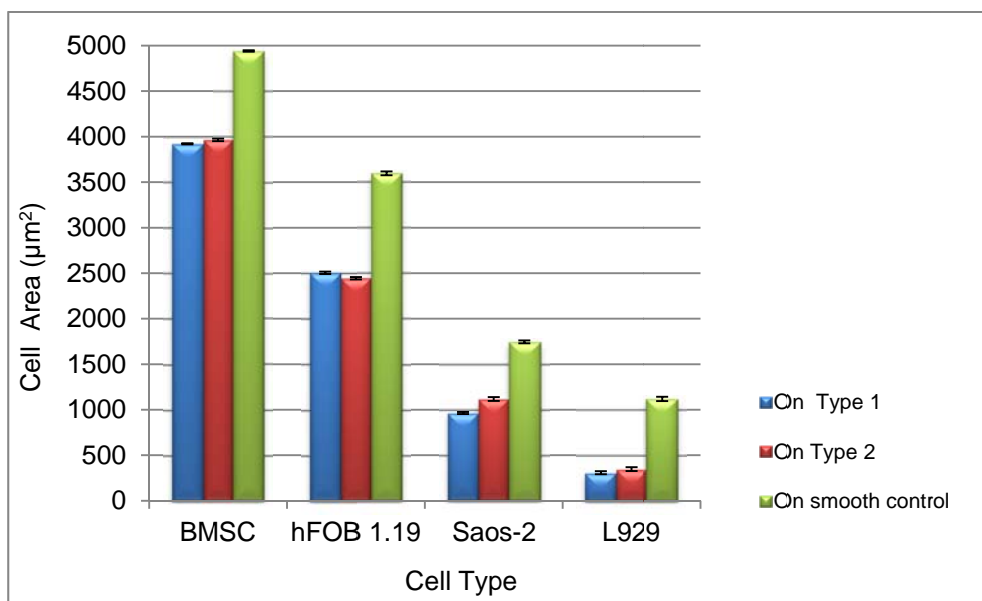
Figure 3.18. Cell area of four cell types grown on Type 1, Type 2 pillars and and smooth controls.

In the present study BMSC covered the largest area and L929 covered the smallest area regardless the surface type. These value as were around 4000 and 400 μm^2 respectively. The avarage cell area was also found to be higher on the smooth control than on either of the micropillar covered surfaces for all cell types. However, there was practically no difference between Type 1 and Type 2. The general reason for the decrease in going from smooth to pillared surfaces may be a stress situation formed in the cell induced by the pillars. In an effort to reach the surface at the feet of pillars the cell membrane invaginates many places. A possible response to decrease this stress could be to minimize the contact

area with the surface. Another explanation may be movement of the cell to find a location that provides more easily accessible attachment sites (Figure 3.18).

In addition to cell area, average nucleus area of individual cell was measured (Figure 3.19). The average nucleus area on micropillars and smooth controls was observed to be conserved in BMSCs and L929 cells. On the other hand, there is a significant decrease in the average nucleus area in Saos-2 cells grown on Type 1 and Type 2 pillared surfaces with respect to smooth controls. This difference is also the indication of deformability of cancerous Saos-2 cells which extensively hangs down between the pillars. Since the measurement based on the top view of the cells, unmeasurable volume (hence the area) between the pillars can be the reason of such a decrease of nucleus area of Saos-2 cells.
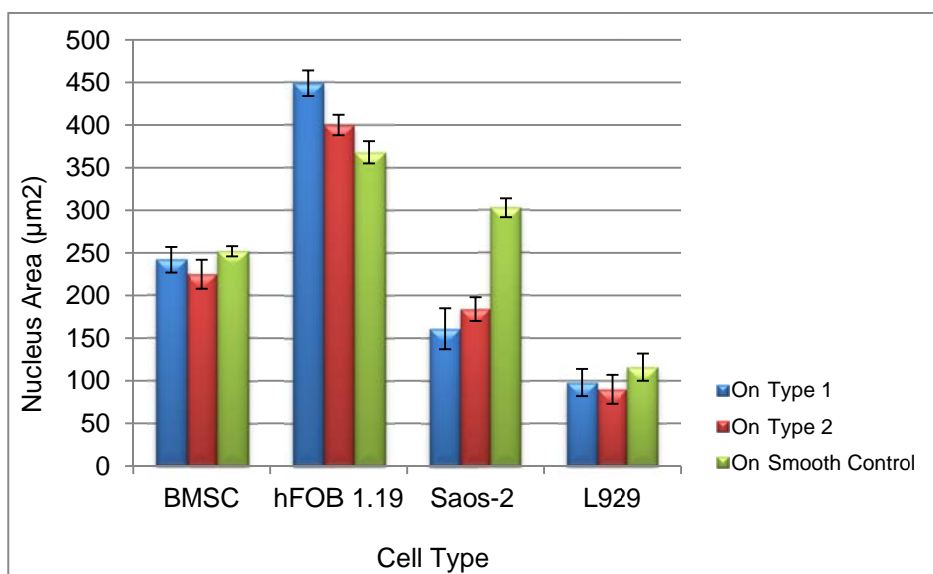
Figure 3.19. Nucleus area of four cell types grown on micropillar covered films and smooth controls.

In Figure 3.19 it is observed that in all cell types the nucleus occupies equal or more area on smooth surfaces excepting hFOB 1.19. In addition to formation of "giant" nucleus, discontinuties and severe fragmentation in nucleus was observed on Type 1 pillars (Figure 3.20). DAPI stain alone show the nucleus fragmentation more distinctly (Figures 3.20C and 3.20D). In fact, such morphologies are generally main signs of late apoptotic nucleus. The topography is known to have effects on cell behavior, including cell adhesion, differentiation

and apoptosis (Clark et al., 1987, 1990, Chen et al., 1997, Ito Y, 1999, Dalby et al., 2004, Hasirci and Kenar, 2006, Biggs et al., 2007, Spatz and Geiger, 2007, Martinez et al., 2009, McNamara et al., 2010). In addition, modifications in morphology of cells and their nuclei cultured on synthetic substrates have also been suggested to control cell growth, differentiation, and apoptosis (Huang and Ingber, 2000). Chen et al. (1997) studied the effect of spreading on cell growth and apoptosis for human and bovine capillary endothelial cells by using adhesive islands. It is found that when the cells were prevented from spreading, they shifted from growth to apoptosis. In a recent study, it was found that insufficient adhesion in the presence of fine nanoneedles on hydroxyapatite substrates lead to apoptosis of osteoblast-like cells (Okada et al., 2010).
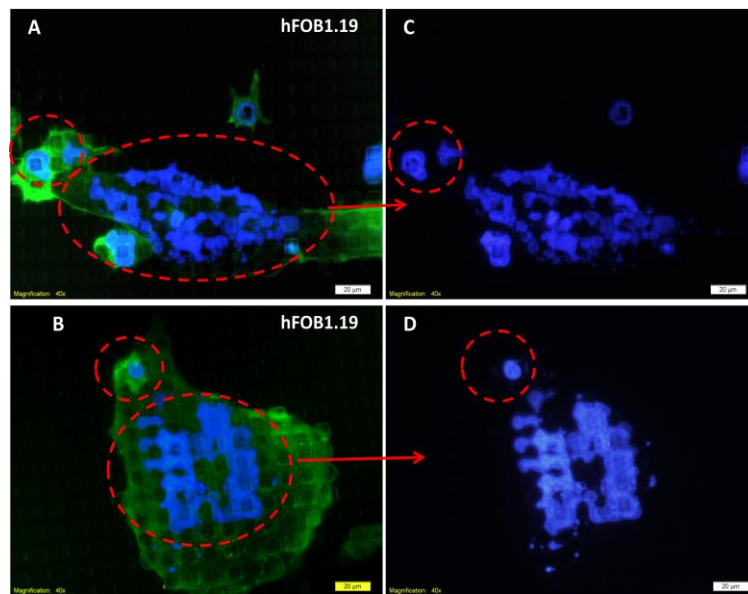
Figure 3.20. Fluorescence micrographs of hFOB1.19 cells on Type1 substrates. (A) and (B) Double stained (DAPI and Phallodin-FITC) cells showing discontinuous nuclei (Dashed circles). (C) and (D) Only DAPI stained is shown.

Finally, in order to study change of cell area to the nucleus area ratio on various surfaces Figure 3.21 was plotted.
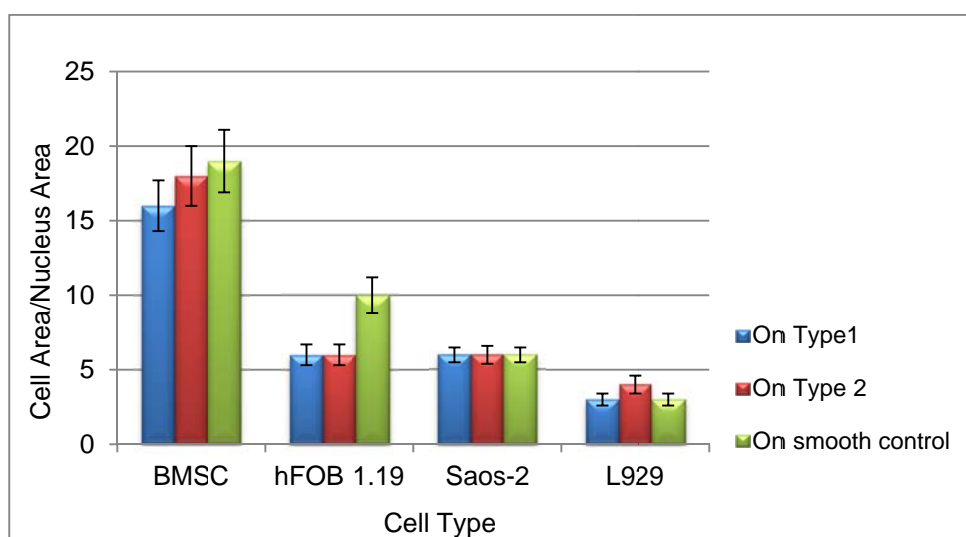
Figure 3.21. Cell Area to Nucleus Area ratio of four cell types grown on micropillar covered films and smooth controls.

Although, the ratios plotted in Figure 3.21 are not volume based, one may speculate that BMSCs, Saos-2 and L929 cells have maintained their cell to nucleus ratio on smooth controls and on micropillars. In other words surface topography did not change the nucleus to cell ratio. Of the cells used the smallest nucleus was that of in BMSC. Among the four cell types, only hFOB 1.19 cells showed a difference; their cell to nucleus area increased on the smooth surface. Thus, the apoptotic nuclei observed on Type 1 micropillars can be considered as the natural outcome of that difference.

3.4   Deformation of Type 3 Micropillars by the Cellular Tugging Force

3.4.1   In Vitro Studies on Type 3 Pillars

Mechanical forces constitute an important portion of interactions between the cells and ECM. In this section, tugging force applied by two different cells on the underlying substrate covered with pillars arranged in Type 3 organization (asymmetrically patterned) were compared. In Type 3 pattern the pillars (5 µm height, 1 µm width) (Figures 3.22A and 3.22B) have the longer interpillar spacing as 9.2 µm and the shorter as 4.2 µm.
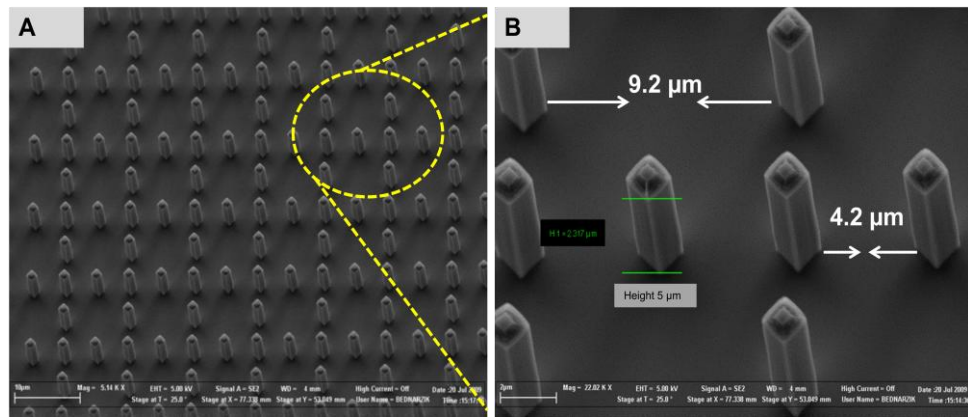
Figure 3.22. SEM micrographs of Type 3 silicon wafer to produce polyester films from.

Micropillars of P(L-D,L)LA and its blend with PLGA [P(L-D,L)LA:PLGA (60:40)] were used. P(L-D,L)LA is a very stiff material (Young's Modulus 4.8 GPa, Domb et al., 2011) while PLGA 50:50 is softer (Young's Modulus 1.3 GPa, Leung et al., 2008). Thus, when a blend of the two is made then the blend's stiffness would be somewhere between the two. Thus, two Type 3 films with different stiffness were prepared. Saos-2 and L929 cells were used as the test cells to study their behavior on the films.

In the fluorescence micrographs (Figure 3.23A) on the stiff substrate the nuclei of Saos-2 cells can be seen to conform to the pillars. When the pillars are beneath the cell cytoplasm, the region over the tip of the pillars is seen as bright green dots. When the pillar tips are under the nuclei, these regions appear black. On the other hand, the nuclei of the L929 cells did not deform, but responded by becoming lobular (Figure 3.23B). The tips of the pillars led to yellow colored points in the micrograph.
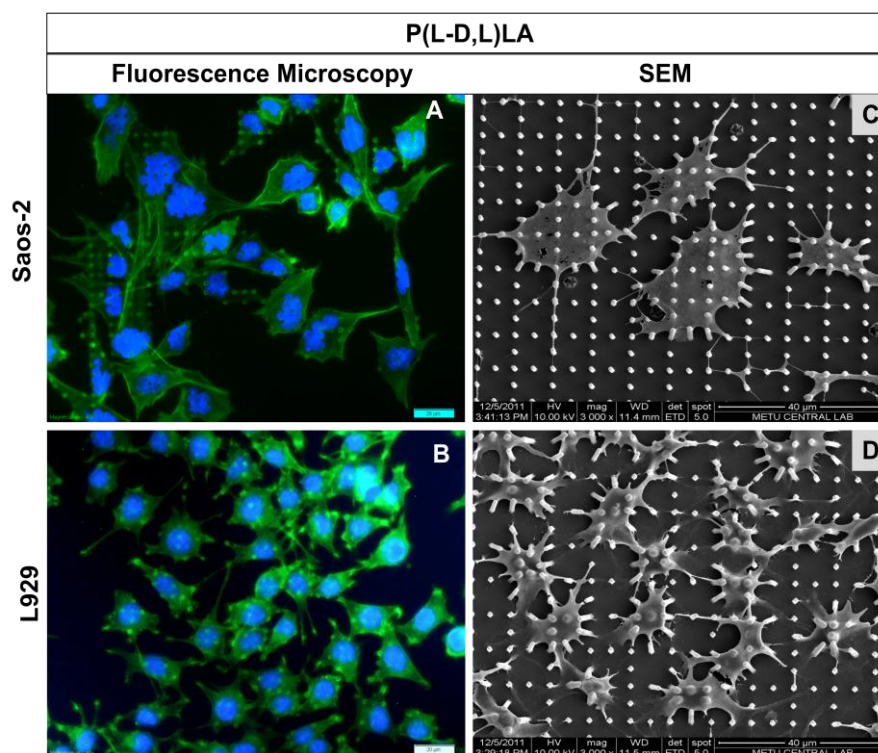
Figure 3.23. Fluorescence (3.23.A and 3.23B) and SEM micrographs (3.23C and 3.23D) of Saos-2 and L929 cells on Type 3 pillar covered P(L-D,L)LA film. Scale bars: 20 μm.

The SEM micrographs reveal that Saos-2 cells stay on the top of the pillars and only the pillars located under the cell were bent towards the cell (Figure 3.23C). In contrast, the micropillars over which L929 cells adhered/spread were bent significantly. Also, the cytoplasm of L929 cells sagged towards the substrate surface (Figure 3.23D). In brief, Saos-2 and L929 behaved distinctly different in terms of nuclear deformation and extent of bending of the pillars on the stiff P(L-D,L)LA film covered with micropillars.

Figure 3.24 shows a similar test on the less stiff substrate (the blend of the two polyesters). Nuclei of Saos-2 showed indented borders around the pillar. Here, the borders of the nuclei were again perforated. With L929, this time the nucleus was also seen to be deformed (Figure 3.24B). SEM micrographs of Saos-2 cells grown on these medium pillars showed significant bending not seen on stiffer substrate. L929 behaved as before and all the pillars contacting the cell were bent.
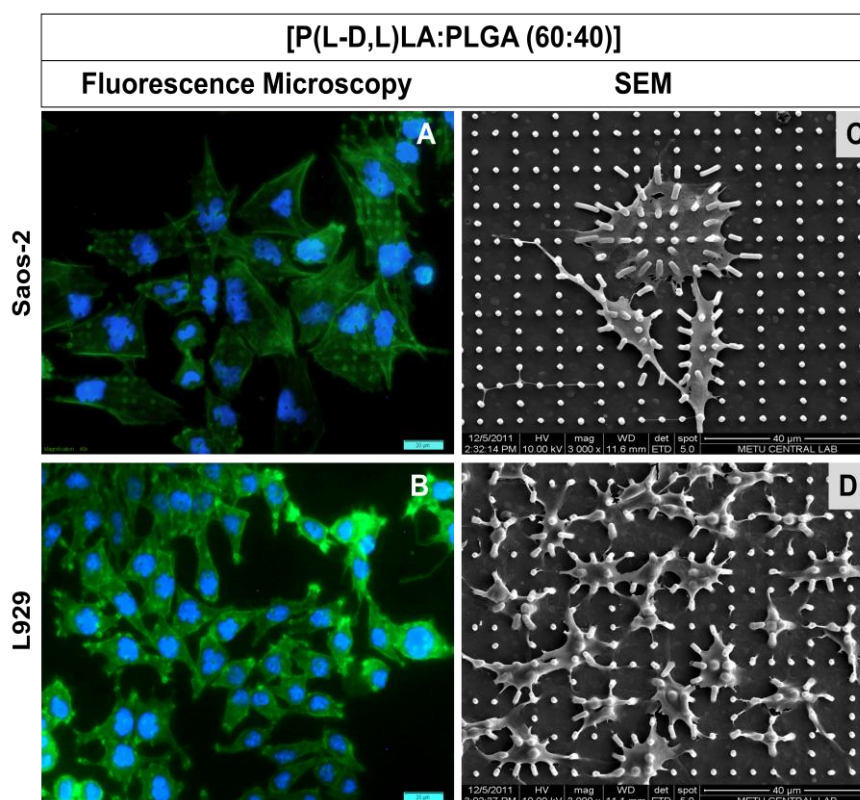
Figure 3.24. Fluorescence (3.24A and 3.24B) and SEM micrographs (3.24C and 3.24D) of Saos-2 and L929 cells on Type 3 pillar covered film of [P(L-D,L)LA:PLGA (60:40)]. Scale bars: 20 μm.

3.4.2 Determination of Bending Extent by Image Analysis

By using the SEM micrographs the bending or displacement of the micropillars were determined by using NIH Image J (USA) software. Displacement of the center of the top of the pillar (a circle) (ΔX) due to applied horizontal traction force was measured on the x-y plane as shown in Figure 3.25.
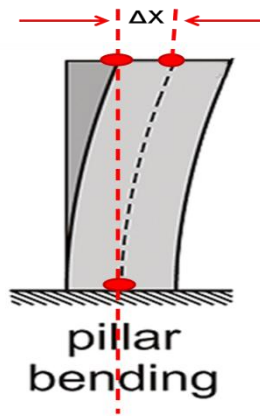
Figure 3.25. Schematic presentation of displacement of the center of the top of the pillar. Dark rectangle: before bending by tugging by the cells. Lighter gray is the bent rectangle.

Table 3.2 presents the maximum displacements imposed by the cells by tugging on the micropillars. These values were obtained by measuring the displacement of center point of (circle) on the top of the pillar (as shown in Figure 3.25). 250 measurements were made by using Image J software.

Table 3.2. Maximum displacement of the pillars caused by Saos-2 and L929 cells grown on P(L-D,L)LA and [P(L-D,L)LA:PLGA (60:40)] film.

Substrate	Cell Type	
	Saos-2	L929
	Displacement (µm)	
(P(L-D,L)LA)	3.43 ± 0.21	3.45 ± 0.31
[P(L-D,L)LA:PLGA (60:40)]	4.10 ± 0.24	3.38 ± 0.34

When the response (displacement) of the pillars on P(L-D,L)LA films to tugging by the two cell types were compared, no significant difference could be observed. On the stiff surface

the two cells could bend the pillars to the same extent. On the other hand, on softer substrate (blends), maximum displacements observed with Saos-2 cells were higher than it caused on the stiffer substrate. Its effect was also higher than that of the L929 cells. P(L-D,L)LA is a highly crystalline and stiff polyester (ca. 37 % crystallinity) whereas its glycolide containing copolymers (eg. PLGA) are of much lower crystallinity (ca. 21%) and stiffness. Thus, high degree of displacement was expected on the softer material (blend). When the extent of Saos-2 origined displacements compared, the cells grown on softer blends were observed to cause a 20% higher displacement than the cells grown on P(L-D,L)LA. This may be the result of combinatorial effects of mechanical property of substrate and metastatic nature of osteosarcoma cells. Similar results were not observed with L929 cells; the amount of deflection did not change at all with substrate type. This may be due to its smaller size and hence the lower influence of their cytoskeleton.

3.4.3   Osteogenic Differentiation of BMSCs on P(L-D,L)LA and [P(L-D,L)LA:PLGA (60:40)] Blends

Cell tugging forces play an important role in determination of cell morphology and motility (Tan et al., 2003, Li et al., 2007). In addition, rigidity of the smooth substrates or substrated decorated with micropillars have previously been shown to regulate differentiation route of the mesenchymal stem cells (McBeath et al., 2004, Engler et al., 2006, Vogel and Sheetz, 2006, Fu et al., 2010). Thus, to investigate whether rigidity of the films and micropillars could regulate stem cell differentiation, BMSCs were used and they were induced for osteogenic differentiation by using an induction medium.

Osteogenic differentiation extent was evaluated qualitatively by immunodetection of osteopontin (OPN) which is a major product of osteoblasts and osteocytes, thus, their presence indicates differentiation of BMSC into osteoblast (Figure 3.26).
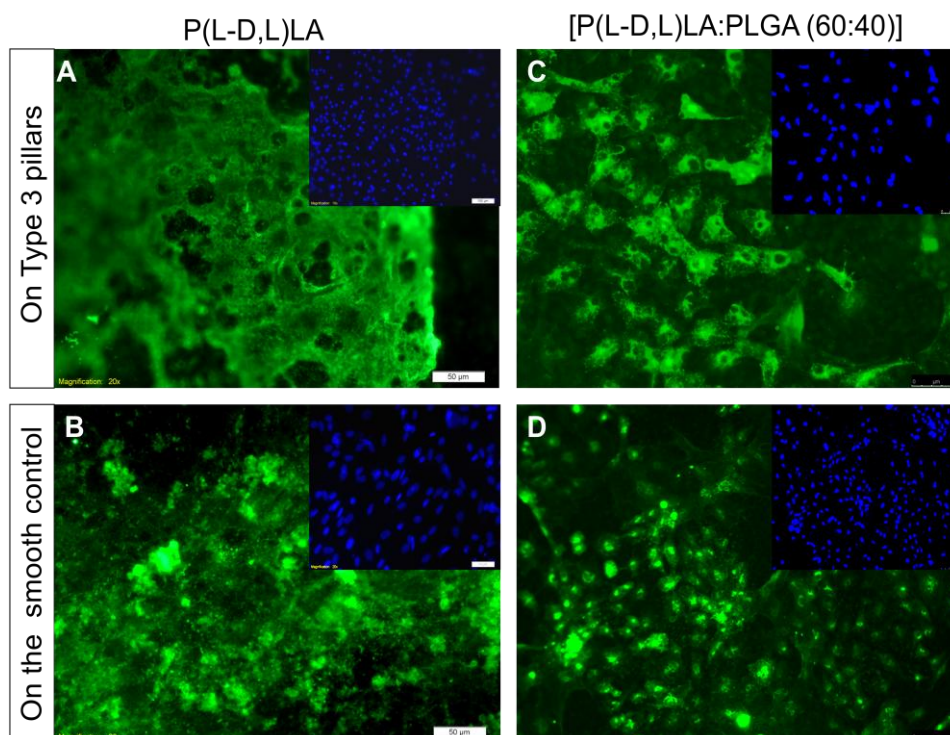
Figure 3.26. Fluorescence micrographs of anti-OPN stained BMSC on Type 3 pillars and on smooth controls made from P(L-D,L)LA) and [P(L-D,L)LA:PLGA (60:40)] blend (3.26A and 3.26B). P(L-D,L)LA patterned and smooth surfaces, (C and D) [P(L-D,L)LA:PLGA (60:40)] patterned and smooth surfaces. Insets present samples stained with DAPI for visualization of the nuclei. Scale bars: 50 µm.

In Figure 3.26 one can observe that osteogenic differentiation of BMSCs could be induced on the two films with different stiffness. However, there were distinct differences in terms of localization of the protein OPN. OPN deposition on P(L-D,L)LA was completely extracellular (Figures 3.26A and 3.26B) while the OPN signal obtained from [P(L-D,L)LA:PLGA (60:40)] blend was intracellular. Negative control samples were stained with goat anti-mouse IgG-FITC and no non-specific binding was observed (data not shown). Since OPN is a major component of the mineralized extracellular matrices of bones, this difference seems to indicate a delay in the biosynthesis of OPN on the softer substrates.This results are in good agreement with a recent study of Buxboim et al. (2010) which showed differential lineage comitment of MSCs into myoblast or osteoblast depending on substrate elasticity. They

reported 4 to 6 fold increase in osteogenic markers when MSCs grown on stiffer substrate. Thus, one may propose that differentiation of BMSCs is enhanced on stiff substrates.

3.5 Differential Adhesion Behavior of BMSCs and Saos-2 Cells on Nanopillar Array

3.5.1 Influence of Nanopillar Spacing on Patterned Surfaces on Adhesion of Rat Bone Marrow Mesenchymal Stem Cells and Saos-2 Cells

In this set of experiments the material was maintained but the surface design features were changed to nano level. Figure 3.27, presents the systematically designed nanopillar array where the pillars were ca. 900 nm in height and 200 nm in diameter and the pillar-to-pillar distances were varied in the range from 1 to 10 µm. Templates were produced on silicon wafers by e-beam lithography and reactive ion etching (RIE). The array had 25 fields each 2 x 2 mm^2 in size. Exemplary SEM images of nanopillars on Fields 1, 3 and 16 are presented to show how pillar-to-pillar distances change systematically along the x and y directions throughout the surface. Micrograph 1 represents the field with most densely packed pillars (Field 1) in which pillar-to-pillar distance is 1 µm in both x and y directions. The pillar-to-pillar distance varies along y axis and is 5 µm in Field 16 and 10 µm in Field 25. The same organization was applied along the x direction. The largest spacings in both directions is with Field 25. Thus, the whole array allows one to study a graded series of pillar placements to study the influence of interpillar distance on cell attachment.
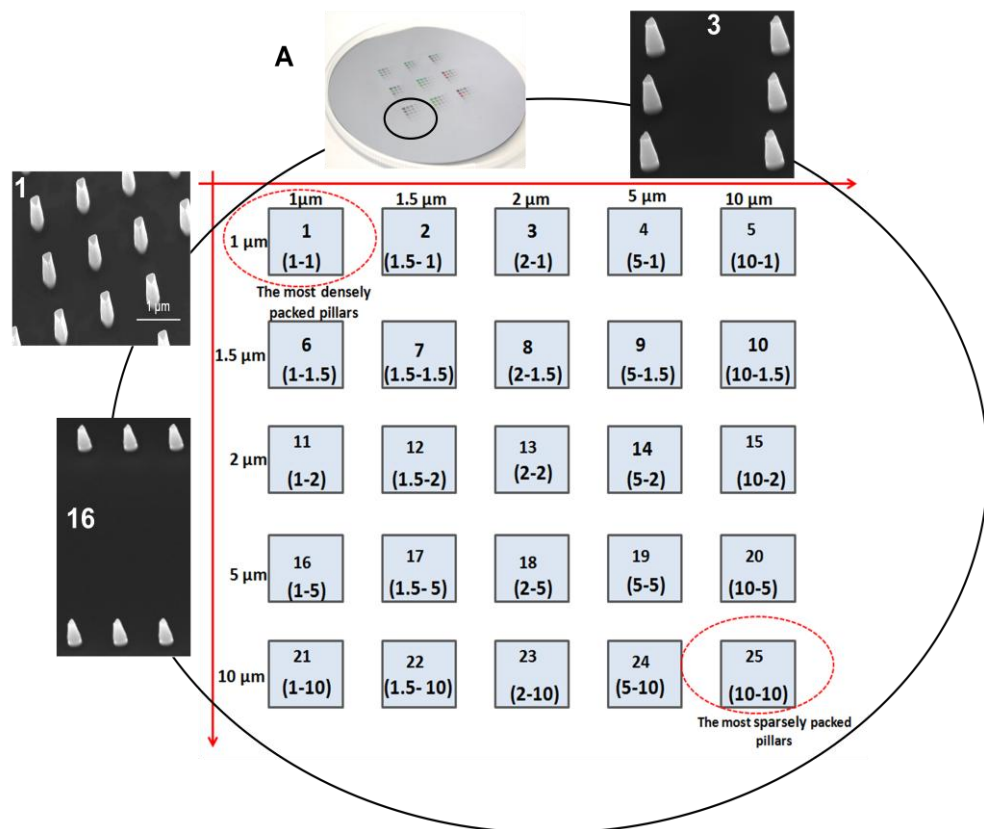
Figure 3.27. Schematic presentation of the array of patterned fields with gradually changing interpillar distances (x-y). The master silicon wafer (A) consisted of 9 identical copies carrying 25 fields of 2x2 mm^2 nanopillar-covered fields presented as 5x5 matrices. Produced by EBL and RIE.

The pillar-to-pillar spacing (in micrometers) is shown in the parenthesis for each separate field (as (1-2) indicating 1 μm in x and 2 μm in y direction). SEM micrographs show the the nanopillars.

The master silicon wafer prepared with EBL and RIE was then used as template to transfer the patterns to polydimethylsiloxane (PDMS) and this in return was used as a secondary template to prepare the test sample by solvent casting poly(L-D,L-lactic acid) P(L-D,L)LA.

3.5.1.1 *In Vitro* Studies on Nanopillar Array

3.5.1.1.1 Microscopic Investigation of Adhesion Behavior of Saos-2 cells and BMSCs

P(L-D,L)LA films seeded with BMSCs and Saos-2 cells were studied using fluorescence microscopy and scanning electron microscopy (SEM) to obtain information on cell adhesion and orientation related with interactions with substrate surfaces.
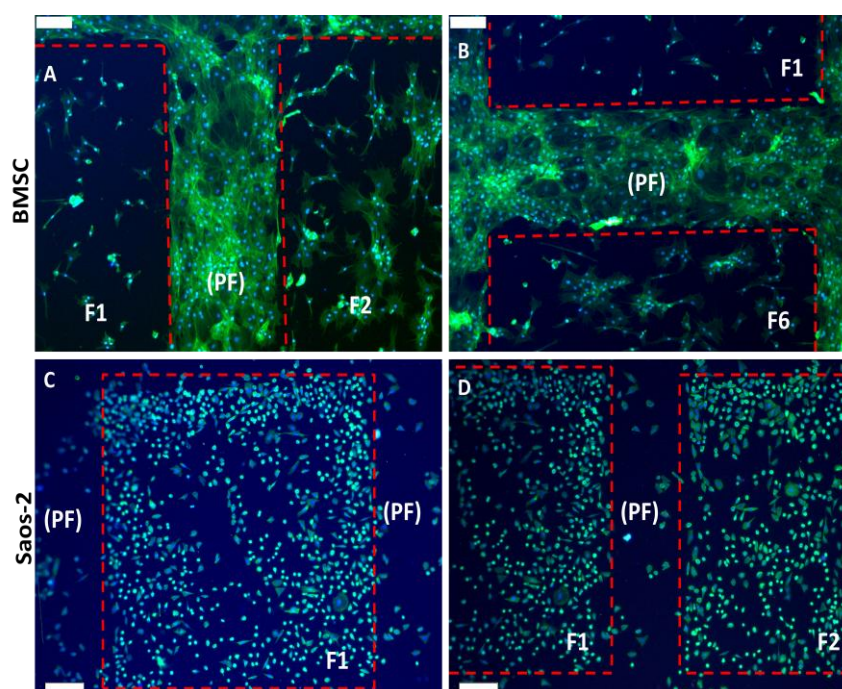
Figure 3.28. Fluorescence micrographs of BMSCs and Saos-2 cells grown on P(L-D,L)LA film for 2 days. Each image shows pattern free (PF) areas and fields (F). (A and B) BMSCs on fields F1 and F2 and F1 and F6, respectively (C and D) Saos-2 cells on fields F1 and F2. (PF) pattern free regions in between the fields F1 and F2. Stains: FITC-Phalloidin (green) for the cytoskeleton. DAPI (blue) for the nucleus. Scale bars: A, B: 250 µm; C, D: 200 µm.

When cultured on the pillar arrays the two cell types showed distinct differences (Figure 3.28). The BMSCs avoided the pillar covered fields F1, F2 and F6 (in Figures 3.28A and 3.28B) occupied the smooth, pillar-free regions. The attached BMSCs were highly spread. The Saos-2 when seeded on F1 and F2 fields, on the other hand, behaved in the exactly opposite manner (F2 and F6 are identical in design but with exchanged x and y axes).

It appears obvious that pillar presence and distances are the main reasons of the different behavior. The spacing is very critical for the interaction between integrins especially for cross-phosphorylation and maturation of the focal contacts (Burridge et al., 1996). On the other hand, Saos-2 cells were located in the F1 and F2 fields and left the PF (smooth) regions nearly empty. Thus, BMSC avoided the most densely pillar packed fields (F1, F2, F6) while Saos-2 cells avoided the pillar free gaps between the fields and occupied only the pillar featured fields. However, spreading of these attached Saos-2 cells could not spread on the F1 and F2 pillars (Figures 3.28C and 3.28D). They were round even 2 days after adhesion. Cell adhesion and focal adhesion site formation is followed by polymerization of actin filaments (Burridge and Charanowska-Wodnick, 1996, Carraghe and Frame, 2004, Patla et al., 2010) so one may speculate that formation of the cytoskeletal network by the Saos-2 cells was adversely affected.

Because the micrographs have shown the adhesion preference of two cell types clearly, the cell density difference between the patterned fields and pattern free regions was quantified by the help of Image J. By using the "color histogram" tool, the green signals which represent FITC-Phalloidin stained cytoskeleton of adhered cells were collected automatically for the respective regions, in the form pixel counts (Figure 3.29).

88
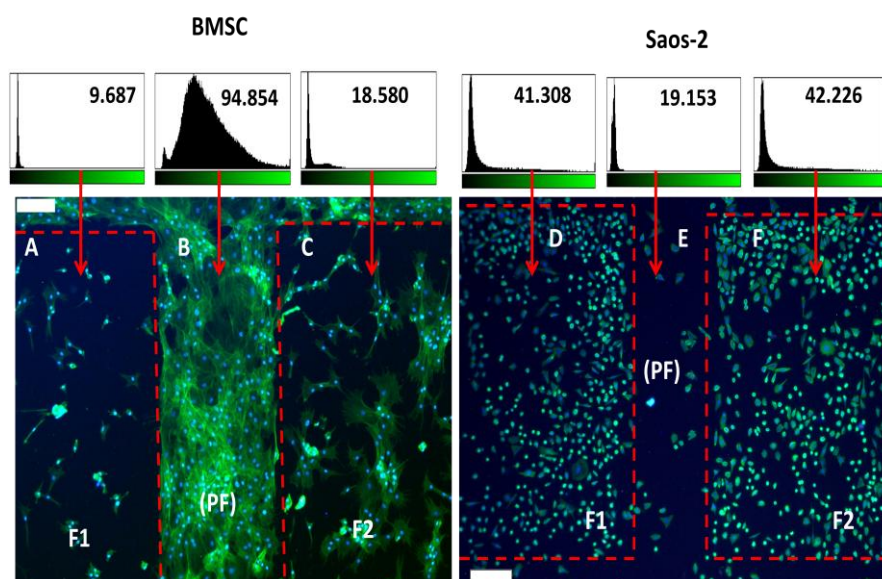
Figure 3.29. Color histograms along the six lanes which correspond to patterned and pattern free (PF) regions for each cell type BMSC (Lanes A, B and C), Saos-2 (Lanes D, E and F). Dashed lines mark the borders of the respective fields.

As can be seen from the histogram data, PF regions were observed to be occupied by BMSCs 5-10 times more densely than F1 or F2 fields (Figure 3.29B). On the other hand, Saos-2 cells were observed to grow on patterned fields (F1 and F2). When the number of pixels counted, a 2 fold difference obtained between the density of Saos-2 cells grown on patterned fields (F1 and F2) and PF regions. In addition, histogram data pointed out that Saos-2 cells attached to patterned fields (Lanes D and F) spread less with respect to BMSCs attached to (PF) region (Lane B).

In addition to preventing or promoting adhesion, the nanopillar arrays appeared to trigger alignment of both cell types. Figure 3.30 shows the two cell types in Fields 3 and 11 (identical fields) where the spacing of the pillars are 2-to-1 or 1-to-2 (in microns) in x and y directions. They appear to be aligned along the direction of shorter distance between the pillars. In Figures 3.30A and 3.30B, it can be seen that BMSCs still mostly avoided the field but not as much as they did in highest density fields (F1, F2, F6 in Figure 3.28). Besides, the cells which could attach on these fields aligned in the channels (the 2 μm interpillar distance appear to look like as channels) created by the pillars.
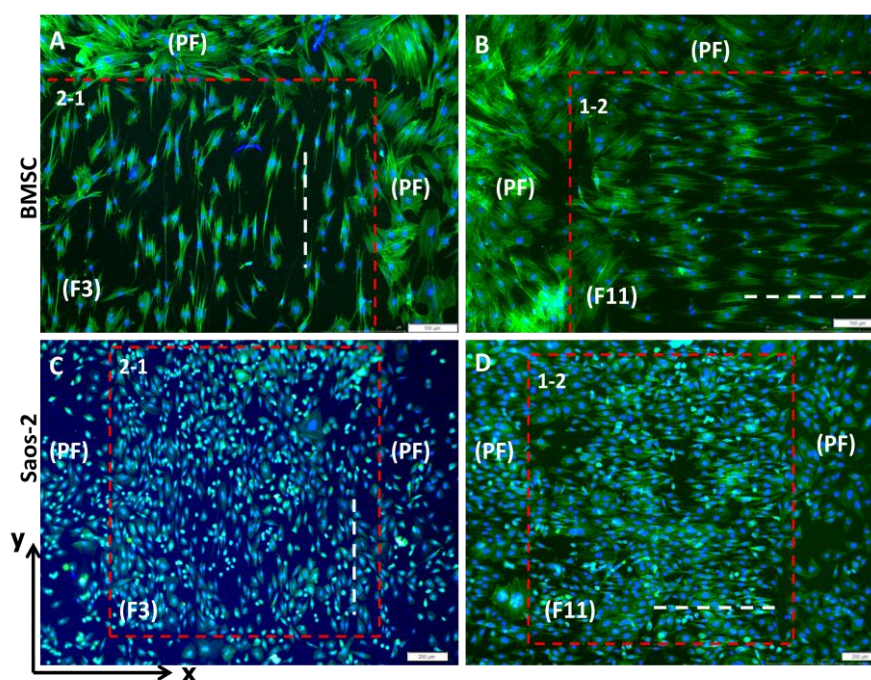
Figure 3.30. Fluorescence micrographs of aligned BMSCs and Saos-2 cells on P(L-D,L)LA films after 2 days of incubation. (A and B) BMSCs in Field 3 (F3) and Field 11 (F11), (C and D) Saos-2 in the same fields, F3 and F11. The pillar-to-pillar spacing (in micrometers) is shown in the top left corner of each separate image (as 1-2 means, 1 μm in x and 2 μm in y direction). White dashed lines indicate the direction of of the nanopillars. Stains: FITC-Phalloidin (green) for the cytoskeleton and DAPI (blue) for the nucleus. Scale bars of the main micrographs: A, B: 100 μm, C, D: 200 μm.

In contrast to BMSCs Saos-2 cells showed a different behavior, again; they adhered almost equally to pillar covered and PF regions. Another unexpected observation was that they were also aligned in Field 11 (Figure 3.30D) as the BMSCs did.

Examination of BMSCs and Saos-2 cells cultured on the various regions of the film displayed a strong alignment tendency dictated by the difference in the interpillar distances, in the x and y directions. Cells were aligned mainly in the direction of the shorter distance between the pillars or, in other words, in the channels formed by the closer pillars. Both BMSCs and Saos-2 cells started to align on the pillars if the distance in one direction was >1.5 μm (Figure 3.30). BMSCs were able to populate pillar regions on Field 3 and F11 and Saos-2 started to fill the PF regions of the same. BMSCs were highly aligned on Fields 3 (2

μm vs 1 μm) and 11 (1 μm vs 2 μm)   in which one of the pillar-to-pillar distances were 2 μm, either along the x and y directions. The alignment on F3 was in y direction and on F11 in x direction. Saos-2 cells seemed to be much less elongated and aligned than BMSCs. Preference of BMSCs for PF regions over P regions was still distinct.

Similar observations have been reported earlier. Anisotropic topographies have been shown to induce many cell types to align along the direction of the anisotropy via a phenomenon called contact guidance (Flemming et al., 1999). It is well known that various cell types can respond to contact guidance when cultured on groove and ridge patterns with lateral dimensions in the low micrometer range (Clark et al., 1990, Wojciak-Stothard et al., 1996, Matsuzaka et al., 2000, Yim et al., 2005, Kenar et al., 2006, Zorlutuna et al, 2009). However, Padeste et al., (2011) showed that mouse neural stem cells (NSCs) sense other features such as nano-sized pillars, and are aligned by them. NSCs attempted to locate between the nanopillars when the distances in any direction were ≥5 μm. In the present study, it was found that BMSCs and Saos-2 cells were aligned not by adhering in between the pillars but on them when the interpillar distances were larger than 1.5 μm.

Cell and nanopattern interactions reported until now were also studied by scanning electron microscopy (Figure 3.31). SEM micrographs clearly demonstrated that BMSCs make contact with the tops of the pillars and sag down into the spaces between pillars if the interpillar gap is 1.5 μm or more (Figure 3.31A).

Cell and cytoskeletal alignment has generally been found to be more pronounced on patterns with ridge widths between 1 and 5 μm than on grooves and ridges with larger lateral dimensions (den Braber et al., 1998, Matsuzaka et al., 2000, Meyle et al., 1994). Thus, the threshold of pillar-to-pillar spacing that caused the alignment of the cells (>1.5 μm) was found to be in this range.
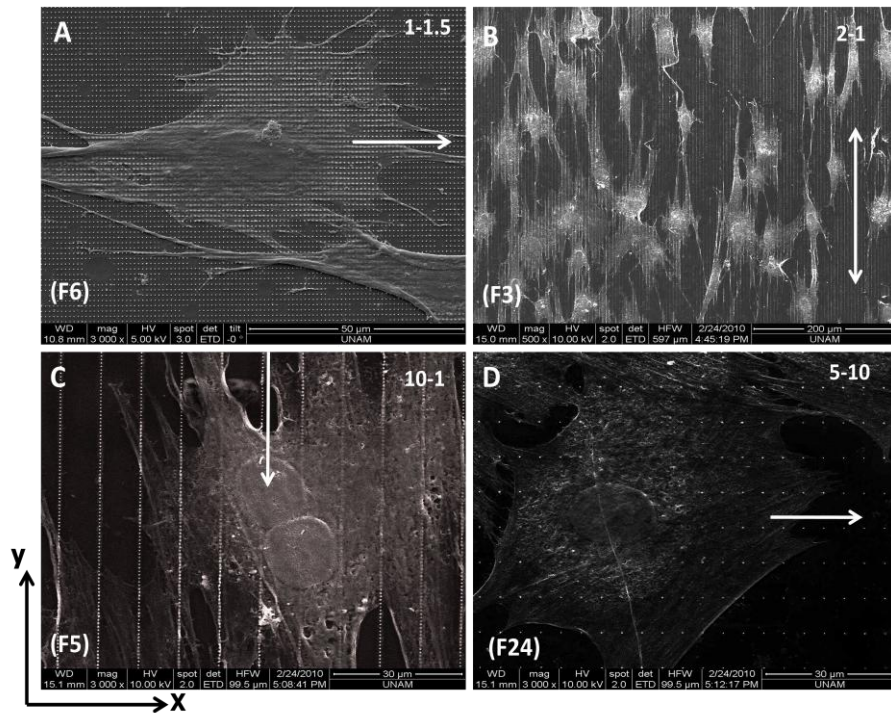
Figure 3.31. SEM images of BMSCs in different patterned fields. (A) Filopodial extensions in the direction of anisotropy (x), (B) BMSCs aligned on F3 (C and D) Fields F5 and F24 are seen.

BMSCs can be as large as >50 µm in diameter when fully spread, so they could not squeeze in the gaps of even the largest pillar-to-pillar distances (10 µm) used in this study. The nuclei which are clearly seen in SEM images can be used to estimate the size of BMSC cells compared to the largest interpillar spacing (Figures 3.31C and 3.31D). Although the cell size is incomparably larger than the interpillar spacings between the nanopillars, anisotropy still seems to guide and align the cells (Figures 3.31C and 3.31D). Similarly, Teixeira et al., (2003) tested the effects of small topographic features that are ~100 times smaller than the width of a single cell. The range of the ridge with of topographic features they have tested was between 70 nm and 1900 nm. The width of grooves were from mid-nano to low micro range (330 nm to 2100 nm). While the smallest pitch was 400 nm, the highest one was 4000 nm. They found that human corneal epithelial cells could even align along the substrate patterned with 70 nm wide ridge width and 400 nm pitch.

In order to show the focal adhesion complexes vinculin was selected as the target protein present in FAC. Labelled vinculin appeared as short strips in bright green in the fluorescence images. Absence of signals in the negative controls stained with anti-mouse FITC showed that the specificity of anti vinculin staining was very high. Staining withVinculin expression, hence indicating focal adhesion points, is found to occur at the leading edge of BMSCs (Figure 3.32).
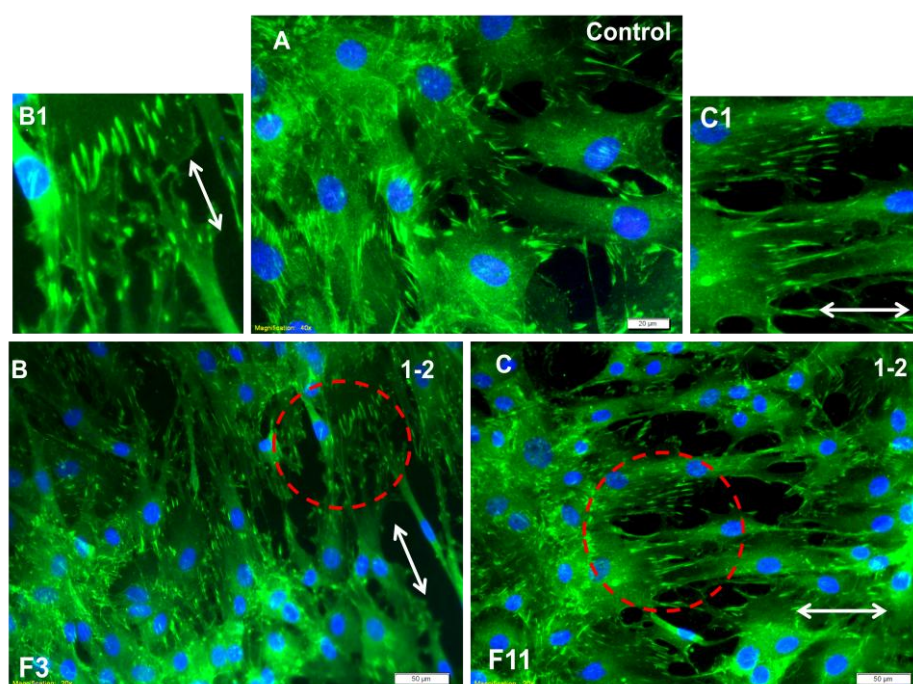
Figure 3.32. Fluorescence micrographs of anti-vinculin stained BMSCs. (A) on F3 and (B) on F11. White arrows show the direction of alignment. The pillar-to-pillar distance in micrometers is shown in the top right corner of each image. Enlarged images present the areas labelled with dashed circles (3.32B1-3.32C1).

On a smooth control surface, the focal adhesions appear to fan out from the center of the cell in all directions (Figure 3.32A). On the other hand, the focal adhesions of the cell grown on the anisotropic fields of the nanopillar array aligned with the shorter distance between the pillars (Figures 3.32B and 3.32C). Magnified images of FACs indicate strong alignment (Figures 3.32B1 and 3.32C1). Similar results have previously been reported on micro or nanogrooved surfaces (Teixeira et al., 2004, Charest et al., 2004, Biggs et al., 2010,

Lamers et al., 2010). There is only one report that showed the guidance of the cells by the pillars (Padeste et al., 2011). In this article, mouse neural stem cells seeded on anisotropically distributed nanopillars have shown to orient themselves accordingly. In addition to alignment of FACs, cell to cell contact seemed to be established between the cells elonagated succesively (Figure 3.32C1).

SEM micrographs of Saos-2 cells (Figure 3.33) supported the fluorescence micrography results (Figures 3.28 and 3.30) of insufficient Saos-2 spreading, especially observed on F1. Although some well spread cells were observed, most of the cells were still round (Figure 3.33A). The most notable observation with Saos-2 cells on the pillars was large numbers of filopodial extensions contacting the pillars. While the extensions were in peripheral (radial) on the most densely packed field F1 (Figure 3.33A), they became directional with increase of anisotropy (Figures 3.33B-D).
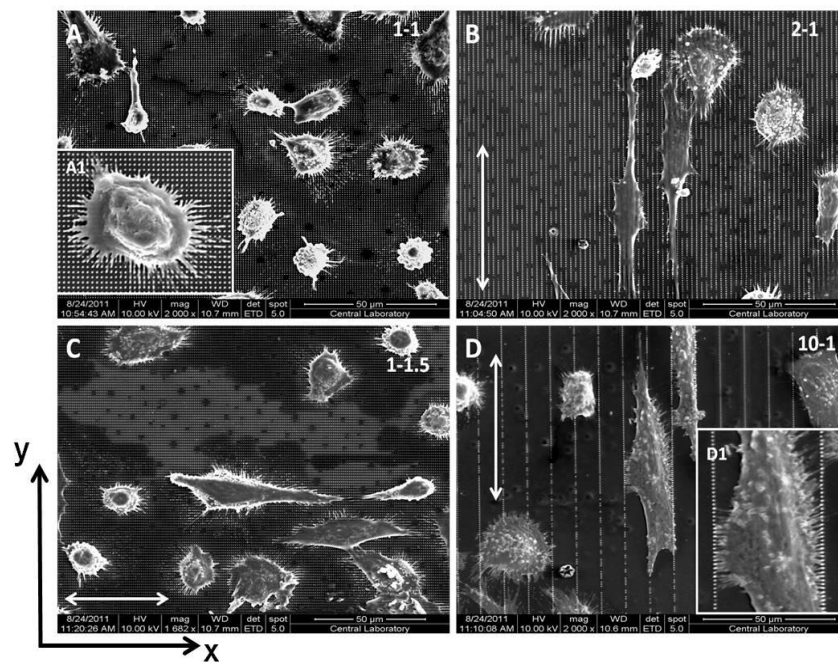
Figure 3.33. SEM images of Saos-2 cells in different fields. (A) Filopodial extensions on F1, (A1) Inset, magnified image of a Saos-2 cell adhered using filopodia onto densely covered F1, (B and C) Saos-2 cells in F3 and F6, respectively, (D) Saos-2 cells on F5, (D1) Inset, magnified view of Saos-2 cell on F5. The pillar-to-pillar distance in micrometers is indicated in the top right corner of each image. White arrows show the direction of alignment.

Like the BMSCs, the size of Saos-2 cell is too large to place themselves between even the largest interpillar spacing (10 µm). However, Saos-2 cells stretched themselves on two adjacent 10 µm spacings. Another interesting finding is the almost one-to-one interaction established between the filopodium and the individual nanopillars. Filopodia are linked to directed migration and abundant filopodia is a characteristic of invasive cancer cells. More importantly filopodia contain receptors for a variety of signalling molecules and for the ECM molecules. Since they are 0.1 - 0.2 µm wide in their size which is quite comparable to the low micro-high nano-sized pillars and thus influence of nanotopography on cell behavior is not surprising (Matilla et al., 2008). Although Saos-2 cells started to align in the direction anisotropy (Figures 3.33B-3.33D), filopodia-pillar binding was observed to be perpendicular to the direction of anisotropy (Figure 3.33D).

In order to see the orientation of FACs, vinculin was labelled with Anti-Vinculin antibodies for the Saos-2 cells grown on control and pillared surfaces (Figure 3.34). The control surface produced cells with focal adhesions that have random orientations as illustrated in Figure 3.34A. It has already been shown that Saos-2 cells avoid smooth areas, occupy densely packed fields but do not spread fully (Figures 3.28C, 3.28D, 3.33A). During the process of adhesion, a cell undergoes attachment, spreading, and the formation of stress fibers and focal adhesions. Thus, we may expect to observe "immature" focal adhesions on these fields. However, labelling of focal adhesion points with Anti-Vinculin stain showed dense FAC formations on the Saos-2 cells (Figure 3.34B). Especially the location of focal adhesion points in enlarged images is interesting. In Figure 3.34B1, radially distributed structures were observed as bright green protrusions/specks all over the cell surface. In addition, Figure 3.34 shows the population of Saos-2 cells with different degrees of spreading; some spherical (Figure 3.34B) and some well spread or aligned (Figure 3.34C). Anisotropy seems to affect the location of formation of focal adhesion points. They were found to be expressed at the front and end edge of the elongated cells (Figure 3.34C1).
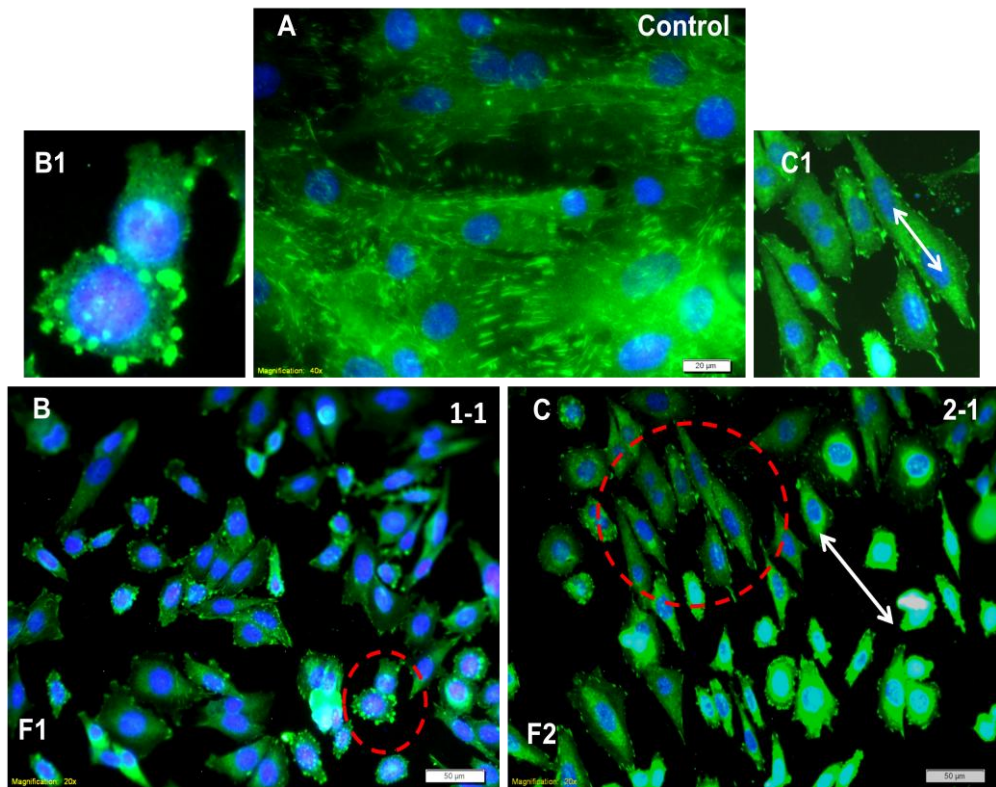
Figure 3.34. Fluorescence micrographs of anti-vinculin stained Saos-2 cells on F1 and F2 fields after 2 days. (A) Saos-2 on F1 and B) Saos-2 on F2, (A1 and B1) show enlarged images of the cells labelled with red circles. White arrows show the direction of alignment. The pillar-to-pillar distance in micrometers is shown in the top right corner of each image. Scale bars: A: 20 µm, B and C: 50 µm.

The orientation angles of the cells were measured by the analysis of fluorescently labelled images using the software NIH Image J and according to Teixeira et al., (2003) and Hu et al., (2005). The orientation angle is defined as the angle between the direction of the longest cord in the cell and the direction of the lines of nanopillars. For these calculations the SEM images of the cells grown on Fields 3 and 11 were used. The average orientation angle was between 6-8° for both cell types, and since any angle below 15° is accepted as aligned (Wojciak-Stothard et al. (1996), these cells in this set were considered to be well aligned. Thus, pillars in distances much smaller than the cells could orient both mesenchymal cells (BMSC) and the cells from the osteosarcoma cell line (Saos-2).

BMSCs used were from rat primary cell cultures and were untransformed mesenchymal stem cells. The Saos-2 cells, on the other hand, are derived from a human bone tumor (osteosarcoma). It is reported that cancer cells are softer, more elastic and deformable than normal cells (Lekka et al. 1999, Park et al. 2005, Li et al. 2008), and when a normal cell transforms into a cancerous cell, its stiffness, ability to attach, move and spread on substrates changes.

It has also been reported by Hart et al, (2007) that progenitor cells are more sensitive to nanoscale topography than differentiated cells. In their study, osteoprogenitor cells were tested on arrays of nanopits with 120 nm diameters and 300 nm center-to-center spacings. The results showed increased filopodia interaction with the surrounding nanoarchitecture leading to a decrease in cell spreading, focal adhesion complex formation and cytoskeletal organization. Similarly, a decrease was reported in the adhesion of osteoprogenitor cells upon seeding on ordered and symmetrical nano-topographies such as PMMA nanostructures fabricated by embossing in comparison to flat (control) surfaces. In contrast, randomly distributed nanoscale features increased cell adhesion (Dalby et al., 2006). In other studies, surface nanotopography was frequently observed to promote adhesion and proliferation (Lovmand et al., 2009), bone matrix synthesis and improve osseointegration of osteoblastic cells (Boyan et al., 1996, Cooper et al., 2000, Sul et al., 2009, Ballo et al., 2011). Similarly, osteoblast adhesion was shown to increase on nano-phase alumina, which was able to support over three times more cells than on conventional alumina (Webster et al., 2000).

Decrease in cellular adhesion is observed with increasing nanoprotrusion height (Sjostrom et al., 2009). Gallagher et al., (2002) have reported that nano-structured surfaces decrease adhesion of some cell types such as fibroblasts but others observed improved adhesion for muscle cells (Thapa et al., 2003) and astrocytes (Baac et al., 2004). Turner et al., (1997) reported preference of transformed astrocytes for wet-etched, smooth regions over "grassy" regions composed of nanometer-scale columnar structures while primary cortical astrocytes from neonatal rats preferred silicon grass.

Two studies report the preference of rat epitenon fibroblasts to adhere to flat regions compared to regions covered by regular arrays of nanopillars (60 nm high pillars, pillar-to-pillar spacings 100–300 nm) (Curtis et al., 2001, Wilkinson et al 2002). In addition, various research groups speculated that the distance of separation between nanostructures

critically influence the formation of focal contacts, and also cell adhesion (Curtis et al., 2001, Cavalcanti-Adam et al., 2007, Hirschfeld-Warneken et al., 2008).

Although there are many types of adhesion receptors on the cell surface, adhesion primarily involves members of the integrin family. Integrin receptors extend along the thickness of the cell membrane. They are approximately 10 nm wide and 10–100 times more prevalent on the surface of a cell than most other receptors types (Alberts et al., 2002). The larger, clustered structures of integrins and cytoplasmic proteins are called focal adhesions. They are typically 250-500 nm wide and 2-10 μm long (Sniadecki 2006). Patla et al., (2010) have investigated the membrane–cytoskeleton interaction at focal adhesions in a cell by using cryoelectron tomography and found that it is mediated through particles located at the cell membrane and attached to actin fibres. These particles were of 25 ± 5 nm in diameter, and the average distance between them was approximately 45 nm.

As can be deduced from the examples presented regarding cell adhesion on micro and nanotextured surfaces there is not a common trend. It appears to depend on dimension and organization of the surface design and the cell type.

Although nanopillar height is also important in focal adhesion formation, it is the pillar diameter and the spacing that determine whether the adherent cells position themselves on feature (pillar) tops or contact the smooth regions on the substrate (Sniadecki et al., 2006). The feature diameter is proposed to exceed 70 nm to facilitate integrin clustering. Milner and Siedlecki (2007) stated that nanoscale pillars disrupt the optimal lateral spacing of integrin clustering, and activation of proteins of the focal adhesion when the feature dimension is less than 70 nm and the feature spacing is in the 70 – 300 nm range. Other studies point to the disruption of adhesion reinforcement on these nanoprotrusions, and that the changes in the focal adhesion density stem from the innate ability of surface protrusions taller than 70 nm to inhibit protein reinforcement at the focal adhesion site (Lee et al., 2009). Similarly, findings of Arnold et al. (2004), and Cavalcanti-Adam et al. (2007) with materials with spacings between the adhesive dots more than 73 nm resulted in limited cell adhesion, cell spreading and focal adhesions. However, as the substrate features approach the micron scale integrin clustering and the anisotropic elongation of the adhesion plaque was restored (Biggs et al 2010).

Literature indicates that cytoskeletal and adhesion complex alignment is generally more evident on channel type patterns with ridge widths between 1 and 5 μm than with much

larger lateral dimensions (Teixeira et al., 2003, Karuri et al., 2004). Cells cultured on grooves with nanoscale widths, are reported to produce focal adhesions which are almost exclusively oriented obliquely to the topographic patterns (Teixeira et al., 2006). Rajnicek et al., (1997) have reported two types of neurons that with groove depths of 14 nm and widths as narrow as 1 μm. Similarly, several studies have shown that grooves with ≥ 100 nm spacing can achieve alignment of the cells parallel to direction of channels. For example, Rebollar et al. (2007) have reported that human embryonic kidney cells (HEK-293) and Chinese hamster ovary cells (CHO-K1) aligned on the grooved substrates having 200-430 nm periodicity and 30-100 nm depth. Tsai and Lin (2009) have shown that human hepatobalstoma cells aligned on nanogrooves (400 nm width and 100 nm depth). In a recent study the cutoff dimensions of groove-ridge type of substrate for the alignment of fibroblast has found to be even smaller, 100 nm width and 75 nm depth (Lamers et al., 2010). In the present design, both types of cells, BMSC and Saos-2, were shown to sense successive nanopillars and aligned along the direction of the narrower interpillar gaps. It may be that the cells considered these as discontinuous groove-ridge topography with 200 nm ridge width (=diameter of individual nanopillar), 1-10 μm groove width (broaden interpillar distance) and 900 nm groove depth. Figure 3.31 A revealed that even with the slight anisotropy the BMSCs started to orient themselves along the shorter distance by projecting filopodia. These were same response towards anisotropy when Saos-2 cells were tested (Figures 3.32B and 3.32C).

Crouch et al. (2009) investigated anisotropic cell behavior using human dermal fibroblasts on surfaces with different (depth to width) ratios. Their cell alignment and elongation were found to increase with increasing ratios. In another study ratios as small as 0.01 induced significant alignment, the ratio required for 95% alignment was 0.16 (Teixeira et al., 2006).

3.5.2   Effects of Protein Coating and Material Stiffness

3.5.2.1   The Effect of Fibronectin Coating on Cell Adhesion

In order to study and compare the effect of chemical cues against the physical ones, the patterned films were coated with the cell adhesive protein of the ECM, fibronectin (Fn), and adhesion and spreading of BMSCs were determined (Figure 3.35).
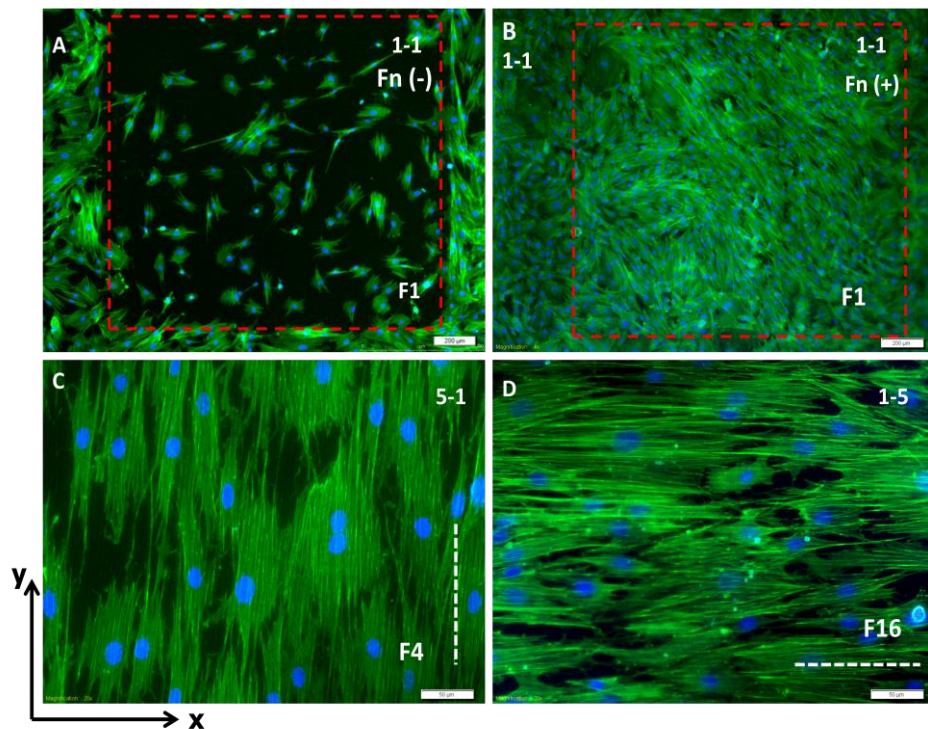
Figure 3.35. Fluorescence micrographs of BMSCs grown on uncoated and Fibronectin (Fn) coated P(L-D,L)LA films after 2 days incubation. (A) BMSCs on Fn free F1, (B) BMSCs occupied the highest density field F1 of the film, (C) BMSCs aligned along x axis in F4 on Fn coated film, (D) BMSCs aligned along y axis in F16 on Fn coated film. The pillar-to-pillar spacing in micrometers is indicated in the top right corner of each separate image. Stains: FITC-Phalloidin (green) for the cytoskeleton and DAPI (blue) for the nucleus. Scale bars of main micrographs: A, B: 200 μm; C, D: 50 μm.

By coating the surface of (P(L-D,L)LA) films the affinity of BMSCs towards the highly dense pillar fields (F1) which were avoided when untreated (Figure 3.35A) was significantly increased and these fields became equally populated (Figure 3.35B). These cells not only populated these areas but also spread and aligned along the direction of the narrower interpillar distance (Figures 3.35C and 3.35D).

Surface roughness at the nanoscale can be considered to be random patterns and is important in protein interactions that direct cell attachment activity, and therefore, tissue formation at implant surfaces in control of tissue formation at implant surfaces (Park and Webster, 2005). The RGD sequence is found in the composition of cell adhesive proteins

such as fibronectin or vitronectin and it is important in mediating cell adhesion to synthetic material surfaces (Sinha and Tuan, 1996). The nanofeatures could alter the conformation of these RGD-containing proteins, and affect cell adhesion and behavior (Cavalcanti et al., 2007). For example, Sutherland et al. (2001) reported that fibrinogen conformation is altered on nanopits as shown by platelet adhesion. Tsai et al., (2009) reported that osteoblast adhesion was reduced on grooved substrates (compared to planar controls) also due to this alteration of conformation of fibronectin. Thus, it may be concluded that physical cues of surface patterns could influence the effects of chemical cues.

In the present case addition of fibronectin onto the surfaces which were normally avoided by BMSC converted the surface to an acceptable surface.

3.5.2.2. The Effect of Stiffnes of the Film Material on Cell Adhesion

Another control over cell adhesion was achieved by changing the stiffness of the test material. Polymer P(L-D,L)LA is a rigid material where PLGA is of the same family but less crystalline and therefore has lower stiffness. When a blend of P(L-D,L)LA, and PLGA is made this material become less stiff then P(L-D,L)LA. In Figure 3.36A the BMSCs left the field F1 quite unpopulated whereas in Figure 3.36B the BMSCs occupied the F1 field more than before. The material in Figure 3.36A was the stiff P(L-D,L)LA and in Figure 3.36B it was the less stiff [P(L-D,L)LA:PLGA (60:40)] blend.
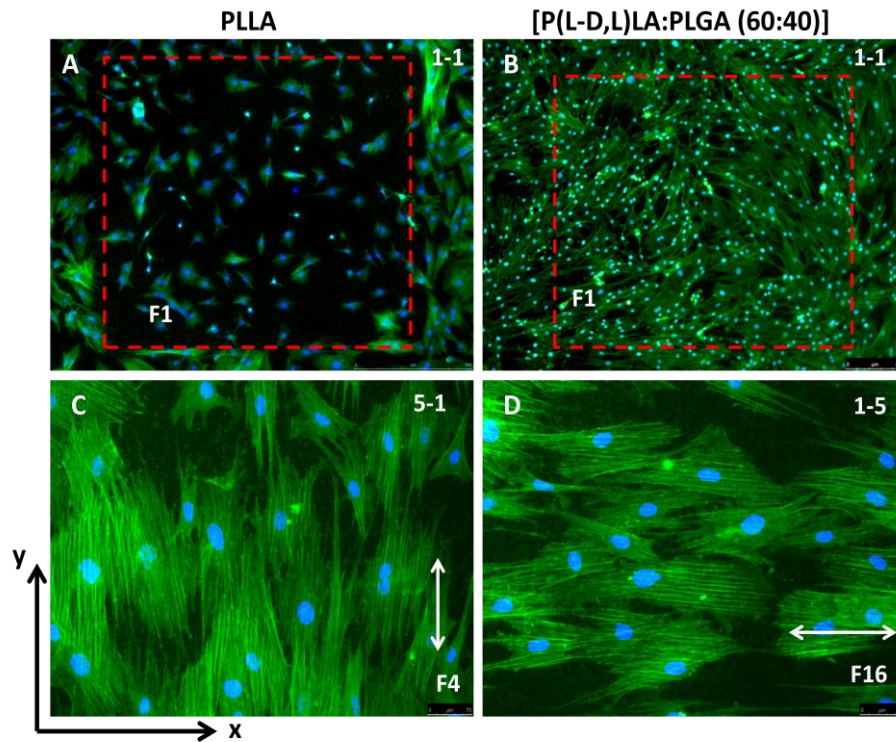
Figure 3.36. Fluorescence micrographs of BMSCs grown on films with different stiffness. (A) BMSCs on F1 made of P(L-D,L)LA, (B) BMSCs on F1 made of [P(L-D,L)LA:PLGA (60:40)] blends (C) BMSCs aligned along the x axis in F4 on blend film (D) BMSCs aligned along the y axis in F16 on blend film. The pillar-to-pillar spacing in micrometers is shown in the top right corner of each separate image. Stains: FITC-Phalloidin for the cytoskeleton and DAPI for the nucleus. Scale bars of main micrographs: A, B: 200 µm; C, D: 75 µm.

So, lower stiffness surface was more acceptable. This is probably because softer material responded to the forces applied by the cell and therefore the focal adhesion complexes were allowed to enhance adhesion. Substrate stiffness influences how strongly cells adhere, how much force they exert and their degree of spreading. But, responses to mechanical stimuli may be cell-type specific and depend on the nature of the adhesion receptor through the cell binds to its substrate. For instance motor neurons derived from embryonic mouse spinal cord extend neurites with extensive branches on soft but not hard surfaces (Flanagan et al., 2002). In contrast, smooth muscle cells, like fibroblasts, extend processes more avidly on hard surfaces but are round on soft materials (Engler et al., 2004).

Furthermore, substrate stiffness can also influence cellular differentiation. Integrins have bidirectional roles that is, they can transduce externally applied mechanical forces from the ECM to the cytoskeleton and to the nucleus (Yeung et al., 2005; Goffin et al., 2006; Pelham and Wang, 1997; Discher et al., 2005). All these behavioral changes may be due to response of adhesion ligands to the substrate stiffness which can in turn initiate changes actomyosin contractility and specific transcription events leading to regulation of adhesion receptor and lineage specific genes.

Thus, further studies on the relationship between physical environment and unique cell types could be important in designing implantable devices, polymers, stents, neural prosthetics, and hard tissue implants. Moreover, the preparation of analogous substrates in other materials such as metals, oxides and ceramics will be of particular interest as well defined models for surfaces of implant materials.

CHAPTER 4

CONCLUSIONS

In this study, it was possible to test the deformation of the nucleus and cell body in five types of cells; (adenosarcoma cell line MCF7, human osteosarcoma cell line (Saos-2), a healthy human bone cell line (hFOB 1.19), a stem cell (rat bone marrow stem cell, BMSC and one fibroblastic cell line (L929)) on Type 1 and Type 2 micropillars which differed in distribution of the pillars on the substrate surface. Fluorescence microscopy and SEM demonstrated that the nuclei of the two cancerous cell lines deform extensively on Type 1 and Type 2 pillars. Surprisingly, BMSCs showed the lowest nuclei deformation of all. Anti Lamin A staining of the most and the least deformable cells verified the intactness of their nuclear membrane. The distance between pillars and size of the cells determined whether the cells adhered to surface of the substrate or preferred to stay on top of the pillars.

When the two types of pillars were compared, symmetrically distributed Type 1 pillars were found in distinguishing the cancer cells from the less deformable cell types very effectively based on the extent of their nucleus deformation. Eventhough, the asymmetrically and more sparsely distributed Type 2 pillars also deformed the cancerous cells to some extent, quantitative analysis of nucleus deformation indicated that Type 1 pillars present a higher selection ability. Significant differences were found in the circularity of the nuclei on Type 2 pillars but, Type 1 pillars deformed cancerous cells by twice as much as their healthy counterparts or BMSCs. For all cell types the average cell area was also calculated to decrease when on micropillar covered surfaces. Similarly, in all cell types, the nucleus occupied equal or less area on patterned surfaces excepting hFOB 1.19.

Design and dimensions of Type 3 substrates were suitable to investigate the force with which the cells tugged at the pillars. The only parameter varied in this case was the stiffnesswere used. On the stiff P(L-D,L)LA substrate, there was no significant difference between the bending of the pillars due to tugging at them by Saos-2 or L929 cells.

However, on the softer substrate, [P(L-D,L)LA:PLGA (60:40)], Saos-2 was observed to bend pillars more than L929 cells and 20% more that it didi the stiff pillars.

The relationship between stiffness of the films and osteogenic differentiation of BMSCs was qualitatively (fluorescence microscopy) assessed. Rigid P(L-D,L)LA films were shown to enhance osteogenic differentiation of BMSCs. This result was supported by OPN deposition observed in the extracellular regions.

In order to find distribution of features that enhance or discourage adhesion and/or alignment of cells, an array that consisted of nanopillar covered fields, where the distance between the pillars are varied systematically, was used. BMSCs avoided the most densely nanopillar covered fields and occupied pattern-free regions and this continued until the separation was 2 µm. 2 µm seemed to be a threshold value for adhesion of BMSCs. Saos-2, on the other hand, occupied densely and sparsely patterned fields and the same threshold values for the adhesion of BMSCs seemed to be valid for the Saos-2 cells, too. Both BMSCs and Saos-2 cells started to align on the pillars if the distance in any direction was >1.5 µm. Coating of fibronectin onto the surfaces which were normally avoided by BMSC converted the surface to an acceptable surface. Decreasing the stiffness of the surface also made the surface more acceptable for attachment.

It appears that it might be possible to distinguish cancer cells from healthy cells by their adhesion on tailored surfaces, guide in a certain direction and to influence the differentiation. The findings of this study demonstrate the great potential and importance of the microenvironment on cell fate.

REFERENCES

Agrelo R., Setien F., Espada J., Artiga M.J., Rodriguez M., Perez-Rosado A., Sanchez-Aguilera A., Fraga M.F., Piris M.A., Esteller M. Inactivation of the lamin A/C gene by CpG island promoter hypermethylation in hematologic malignancies, and its association with poor survival in nodal diffuse large B-cell lymphoma. J Clin Oncol 2005; 23: 3940–3947.

Ahmed W.W., Wolfram T., Goldyn A.M., Bruellhoff K., Rioja B.A., Möller M., Spatz J.P., Saif T.A., Groll J., Kemkemer R. Myoblast morphology and organization on biochemically micro-patterned hydrogel coatings under cyclic mechanical strain. Biomaterials 2010; 31: 250–258.

Alberts B., Johnson A., Lewis J., Raff M., Roberts K., Walter P. Molecular biology of the cell. 4th edition. New York: Garland Science; 2002. The Extracellular Matrix of Animals.

Alves N.M., Pashkuleva I., Reis R.L., Mano J.F. Controlling cell behavior through the design of polymer surfaces. Small 2010; 6: 2208-2220.

Arnold M., Cavalcanti-Adam E.A., Glass R., Blummel J., Eck W., Kantlehner M., Kessler H., Spatz J. P. Activation of integrin function by nanopatterned adhesive interfaces. Chem Phys Chem 2004; 5: 383-388.

Arnsdorf E.J., Tummala P., Kwon R.Y., Jacobs C.R. Mechanically induced osteogenic differentiation – the role of RhoA, ROCKII and cytoskeletal dynamics. J Cell Sci 2009; 122(4): 546–555.

Asch B.B., Kamat B.R., Burstein N.A. Interactions of normal, dysplastic, and malignant mammary epithelial cells with fibronectin in vivo and in vitro. J Cancer Res 1981; 41: 2115-2125.

Baac H., Lee J.H., Seo J.M., Park T.H., Chung H., Lee S.D., Kim S.J. Submicron-scale topographical control of cell growth using holographic surface relief grating. Mater Sci Eng C 2004; 24: 209-212.

Ballo A., Agheli H., Lausma J., Thomsen P., Petronis S. Nanostructured model implants for in vivo studies: influence of well-defined nanotopography on de novo bone formation on titanium implants International Journal of Nanomedicine 2011; 6: 3415-3428.

Bao G. and Suresh S. Cell and molecular mechanics of biological materials. Nature Mater 2003; 2: 715–725.

Bausch A.R., Moller W., Sachmann E. Measurement of local viscoelasticity and forces in living cells by magnetic tweezers. Biophys J 1999; 76: 573–579.

Béduer A., Vieu C., Arnauduc F., Sol J.-L., Loubinoux I., Vaysse L. Engineering of adult human neural stem cells differentiation through surface Micropatterning Biomaterials 2012; 33: 504-514.

Beningo K.A. and Wang Yu-Li. Flexible substrata for the detection of cellular traction forces. TRENDS in Cell Biology 2002; 12(2): 79-84.

Ben-Ze'ev A. The cytoskeleton in cancer cells. Biochimica Biophys. Acta 1985; 780: 197-212.

Ben-Ze'ev A. Cytoskeletal and adhesion proteins as tumor suppressors. Curr Opin Cell Biol 1997; 9: 99-108.

Bhadriraju K. and Hansen L.K. Extracellular matrix and cytoskeleton-dependent changes in cell shape and stiffness Exp Cell Res 2002; 278: 92-100.

Bhattacharya D., Talwar S., Mazumder A., Shivashankar G.V. Spatio-temporal plasticity in chromatin organization in mouse cell differentiation and during Drosophila embryogenesis. Biophys J 2009; 96: 3832–3839.

Biggs M.J.P., Richards R.G., Gadegaard N., Wilkinson C.D.W., Dalby M.J. The effects of nanoscale pits on primary human osteoblast adhesion formation and cellular spreading. Journal of Materials Science: Materials in Medicine 2007; 18: 399-404.

Biggs M.J.P., Richards R.G., Gadegaard N., McMurray R.J., Affrosman, S., Wilkinson C.D., Oreffo R.O.C., Dalby, M.J. Interactions with nanoscale topography: adhesion quantification and signal transduction in cells of osteogenic and multipotent lineage. J Biomed Mater Res Part A, 2009; 91A: 195-208.

Biggs M.J., Richards R.G., Dalby M.J. Nanotopographical modification: a regulator of cellular function through focal adhesions. Nanomedicine 2010: 6(5); 619-633.

Binning G., Quate C.F., Gerber C. Atomic Force Microscope. Phys Rev Lett 1986: 56(9); 930-933.

Biswas A, Bayer I.S., Biris A.S., Wang T., Dervishi E., Faupel F. Advances in top–down and bottom–up surface nanofabrication:Techniques, applications & future prospects. Advances in Colloid and Interface Science 2012; 170: 2–27.

Boyan B.D., Hummert T.W., Dean D.D., Schwartz Z. Role of material surfaces in regulating bone and cartilage cell response. Biomaterials 1996; 17: 137-146.

Brammer K.S., Choi C., Frandsen C.J., Oh S., Jin S. Hydrophobic nanopillars initiate mesenchymal stem cell aggregation and osteo-differentiation Acta Biomaterialia 2011; 7: 683–690.

Branch D.W., Wheeler B.C., Brewer G.J., Leckband D.E. Long-term maintenance of patterns of hippocampal pyramidal cells on substrates of polyethylene glycol and microstamped polylysine. IEEE Trans Biomed Eng 2000; 47(3): 290–300.

Britland S., Morgan H., Wojciak-Stothard B., Riehle M., Curtis A, Wilkinson C. Synergistic and hierarchical adhesive and topographic guidance of BHK cells. Exp Cell Res 1996; 228: 313-325.

Broers J.L., Raymond Y., Rot M.K., Kuijpers H., Wagenaar S.S., Ramaekers F.C. Nuclear A-type lamins are differentially expressed in human lung cancer subtypes. Am J Pathol 1993; 143: 211-220.

Buda A., Pignatelli M. Cytoskeletal network in colon cancer: from genes to clinical application. Int J Biochem Cell Biol 2004; 36: 759-765.

Burridge K., and Charanowska-Wodnick M. Focal adhesions, contractility, and signaling. Annu Rev Cell Dev Biol 1996; 12: 463-519.

Buxboim A., Ivanovska I.L., Discher D.E. Matrix elasticity, cytoskeletal forces and physics of the nucleus: How deeply do cells 'feel' outside and in? Journal of Cell Science 2010; 123: 297-308.

Caplan A.I. Mesenchymal stem cells. J Orthop Res 1991; 9: 641–650.

Carragher N.O. and Frame M.C. Focal adhesion and actin dynamics: a place where kinases and proteases meet to promote invasion. TRENDS in Cell Biology 2004; 14: 241-249.

Cassie A.B.D. and Baxter S. Wettability of porous surfaces. Trans Faraday Soc 1944; 40: 546-551.

Cavalcanti-Adam E.A., Volberg T., Micoulet A., Kessler H., Geiger B., Spatz J.P. Cell spreading and focal adhesion dynamics are regulated by spacing of integrin ligands. Biophysical Journal 2007; 92: 2964-2974.

Chakraborty J. and Von Stein G.A. Pleomorphism of human prostatic cancer cells (DU 145) in culture—The role of cytoskeleton. Exp Mol Pathol 1996; 44: 235-245.

Charest J.L., Bryant L.E., Garcia A.J., King W.P. Hot embossing for micropatterned cell substrates Biomaterials 2004; 25: 4767-4775.

Charest J.L., Eliason M.T., Garcia A.J., King W.P. Combined microscale mechanical topography and chemical patterns on polymer cell culture substrates. Biomaterials 2006; 27: 2487–2494.

Chau J.F., Leong W.F., Li B. Signaling pathways governing osteoblast proliferation, differentiation and function. Histol Histopathol 2009; 24(12):1 593-1606.

Chen C.S., Mrksich M., Huang S., Whitesides G.M., Ingber D.E. Geometric control of cell life and death. Science 1997; 276: 1425-1428.

Chiu G.L.T. and Shaw J.M. Optical Lithography: Introduction. IBM J Res Develop 1997; 41(1/2): 3-6.

Christopherson G.T., Song H., Mao H.Q. The influence of fiber diameter of electrospun substrates on neural stem cell differentiation and proliferation. Biomaterials 2009; 30: 556–564.

Clark P., Connolloy P., Curtis A.S., Dow J.A., Wilkinson C.D. Topographical control of cell behaviour. I. Simple step cues. Development 1987; 99: 439-448.

Clark P., Connolloy P., Curtis A.S., Dow J.A., Wilkinson C.D. Topographical control of cell behaviour. II. Multiple grooved substrata. Development 1990; 108: 635-644.

Clark P., Connolly P., Curtis A.S., Dow J.A., Wilkinson C.D. Cell guidance by ultrafine topography in vitro. J Cell Sci 1991; 99(Pt.): 73–77.

Clark E.A. and Brugge J.S. Integrins and signal transduction pathways: the road taken. Science 1995; 268: 233-229.

Constantinescu D., Gray H.L., Sammak P.J., Schatten G.P., Csoka A.B. Lamin A/C expression is a marker of mouse and human embryonic stem cell differentiation. Stem Cells 2006; 24: 177-185.

Cooper L.F. A role for surface topography in creating and maintaining bone at titanium endosseous implants. J Prosthet Dent 2000; 84: 522-534.

Craighead H.G., Turner S.W., Davis R.C., James C.D., Perez A.M., St. John PM, Isaacson M.S., Kam L., Shain W., Turner J.N., Banker G. Chemical and topographical surface modification for control of central nervous system cell adhesion. J Biomed Microdev 1998; 1(1): 49-64.

Creekmore A.L., Silkworth W.T., Cimini D., Jensen R., Roberts P.C., Schmelz E.M. Changes in gene expression and cellular organization in a model of progressive ovarian cancer. PLoSOne 2011; 6: 1-16.

Cross S.E., Jin Y.-S., Rao, J.Y. Gimzewski J.K. Applicability of AFM in cancer detection Nature Nanotechnology 2009; 4: 72-73.

Crouch A.S., Miller D., Luebke K.J., Hu W. Correlation of anisotropic cell behaviors with topographic aspect ratio. Biomaterials 2009; 30: 1560-1567.

Curtis, A.S.G., and Varde, M. Control of cell behaviour: Topological factors. J. Natl Cancer Res Inst 1964; 33: 15-26.

Curtis A.S.G. and Clark P. The effects of topographic and mechanical properties of materials on cell behaviour. Crit Rev Bicompat 1990; 5: 343-362.

Curtis A.S.G. and Wilkinson C. Topographical control of cells. Biomaterials 1997; 18: 1573-1583.

Curtis A.S.G., Casey B., Gallagher J.O., Pasqui D., Wood M.A., Wilkinson C.D.W. Substratum nanotopography and the adhesion of biological cells. Are symmetry or regularity of nanotopography important? Biophysical Chemistry 2001; 94: 275-283.

Curtis A.S.G., Gadegaard N., Dalby MJ, Riehle MO, Wilkinson CDW, Aitchison G. Cells react to nanoscale order and symmetry in their surroundings. IEEE Trans Nanobioscience 2004; 3: 61-65.

da Silva Meirelles L., Chagastelles P.C., Nardi N.B. Mesenchymal stem cells reside in virtually all post-natal organs and tissues. J Cell Sci 2006; 119: 2204-2213.

Dahl K.N., Kahn S.M., Wilson K.L., Discher D.E. The nuclear envelope lamina network has elasticity and a compressibility limit suggestive of a molecular shock absorber. J Cell Sci 2004; 117: 4779-4786.

Dalby M.J., Riehle M.O., Yarwood S.J., Wilkinson C.D., Curtis A.S. Nucleus alignment and cell signaling in fibroblasts: response to a micro-grooved topography. Exp Cell Res 2003; 284(2): 274–282.

Dalby M.J., Giannaras D., Riehle M.O., Gadegaard N., Affrossman S., Curtis, A.S.G. Rapid fibroblast adhesion to 27 nm high polymer demixed nano-topography. Biomaterials 2004; 25: 77-83.

Dalby M.J. Topographically induced direct cell mechanotransduction. Medical Engineering and Physics 2005; 27: 730-742.

Dalby M.J, McCloy D., Robertson M., Wilkinson C.D.W and Oreffo R.O.C. Osteoprogenitor response to defined topographies with nanoscale depths. Biomaterials 2006; 27: 1306-1315.

Dalby M.J., McCloy D., Robertson M., Agheli H., Sutherland D., Affrossman S., Oreffo R.O.C. Osteoprogenitor response to semi-ordered and random nanotopographies. Biomaterials 2006; 27 (15): 2980-2987.

Dao M., Lim C.T., Suresh S. Mechanics of the human red blood cell deformed by optical tweezers. J Mech Phys Solids 2003; 51: 2259-2280.

Darling E.M., Zauscher S., Block J.A., Guilak F. A thin-layer model for viscoelastic, stress-relaxation testing of cells using atomic force microscopy: do cell properties reflect metastatic potential? Biophys J 2007; 92: 1784–1791.

Davidson P.M., Ozcelik H., Hasirci V., Reiter G., Anselme K. Microstructured Surfaces Cause Severe but Non-Detrimental Deformation of the Cell Nucleus. Adv Mater 2009; 21: 3586-3590.

Dechat T., Pfleghaar K., Sengupta K., Shimi T., Shumaker D.K., Solimando L., Goldman R.D. Nuclear lamins: major factors in the structural organization and function of the nucleus and chromatin. Genes Dev 2008, 22: 832-853.

DeMay R.M. The Art and Science of Cytopathology, American Society of Clinical Pathologists Press, Chicago, 1996.

Dervishi E., Li Z., Watanabe F., Biswas A., Xu Y., Biris A.R., Saini V., Biris A.S. Large-scale graphene production by RF-cCVD method. Chem Commun 2009; 27: 4061-4063.

Discher D.E., Janmey P., Wang Y-L. Tissue cells feel and respond to the stiffness of their substrate. Science 2005; 310: 1139-1143.

Domb A.J., Kumar N. Biodegradable polymers in clinical use and clinical development John Wiley & Sons Inc. New Jersey, Canada. 2011

Dumas V., Perrier A., Malaval L., Laroche N., Guignandon A., Vico L., Rattner A. The effect of dual frequency cyclic compression on matrix deposition by osteoblast-like cells grown in 3D scaffolds and on modulation of VEGF variant expression. Biomaterials 2009; 30(19): 3279-3288.

Dunn G.A., Brown A.F. Alignment of fibroblasts on grooved surfaces described by a simple geometric transformation. J Cell Sci 1986; 83: 313–340.

Eliason M.T., Charest J.L., Simmons B.A., Garcia A.J., King W.P. Nanoimprint fabrication of polymer cell substrates with combined microscale and nanoscale topography. Journal of Vacuum Science & Technology B: Microelectronics and Nanometer Structures 2007; 25: L31-L34.

Engler A.J., Richert L.,Wong J.Y., Picart C., and Discher D.E. Surface probe measurements of the elasticity of sectioned tissue, thin gels and polyelectrolyte multilayer films: correlations between substrate stiffness and cell adhesion. Surf Sci 2004; 570: 142-154.

Engler A.J., Sen S., Sweeney H.L., Discher D.E. Matrix elasticity directs stem cell lineage specification. Cell 2006; 126: 677-689.

Feynman R.P. There's Plenty of Room at the Bottom. Journal of Microeleciromechanical Systems 1992; 1: 60-66.

Fitzgerald, M. Ten emerging technologies: nanobiomechanics. Technol. Rev. 2006; 109: 67.

Flanagan L.A., Ju Y.E., Marg B., Osterfield M., Janmey P.A. Neurite branching on deformable substrates. Neuroreport 2002; 13: 2411-2415.

Flemming R.G., Murphy C.J., Abrams G.A., Goodman S.L. and Nealey P.F. Effects of synthetic micro- and nano-structured surfaces on cell behavior Biomaterials 1999; 20: 573-588.

Flanagan L.A., Ju Y.E., Marg B., Osterfield M., Janmey P.A. Neurite branching on deformable substrates. Neuroreport 2002; 13: 2411-2415.

French R.H. and Tran H.V. Immersion Lithography: Photomask and wafer-level materials. Annu Rev Mater Res 2009; 39: 93-126.

Fu J., Wang Y.K., Yang M.T., Desai R.A., Yu X., Liu Z., Chen C.S. Mechanical regulation of cell function with geometrically modulated elastomeric substrates. Nature Methods 2010; 7(9): 733-736.

Fuchs E., Tumbar T., Guasch G. Socializing with the neighbors: Stem cells and their niche. Cell 2004; 116: 769–778.

Gallagher J.O., McGhee K.F., Wilkinson C.D.W., Riehle M.O. Interaction of animal cells with ordered nanotopography. IEEE Trans Nanobiosci 2002; 1: 24-28.

Gardel M.L., Shin J.H., MacKintosh F.C., Mahadevan L., Matsudaira P., Weitz D.A. Elastic behavior of cross-linked and bundled actin networks. Science 2004; 304: 1301-1305.

Gates B.D., Xu Q., Stewart M., Ryan D., Willson C.G., Whitesides G.M. New Approaches to Nanofabrication: Molding, Printing, and Other Techniques. Chem Rev 2005; 105: 1171-1196.

Ge C., Xiao G., Jiang D., Franceschi R.T. Critical role of the extracellular signalregulated kinase-MAPK pathway in osteoblast differentiation and skeletal development. J Cell Biol 2007; 176: 709–718.
George S.M., Atomic Layer Deposition: An Overview, Chem Rev 2010; 110: 111-131.

Gerecht S., Bettinger C.J., Zhang Z., Borenstein J.T., Vunjak-Novakovic G., Langer R. The effect of actin-disrupting agents on contact guidance of human embryonic Stem Cells. Biomaterials 2007; 28: 4068-4077.

Ghibaudo M., Saez A, Trichet L. Xayaphoummine A., Browaeys J., Silberzan P., Buguin A., Ladoux B. Traction forces and rigidity sensing regulate cell functions. Soft Matter 2008; 4: 1836-1843.

Ginger D.S. Zhang H. Mirkin C.A. The evolution of dippen nanolithography. Angew Chem Int Ed Engl 2004; 43: 30-45.

Gittens R.A., McLachlan T., Olivares-Navarrete R., Cai Y., Berner S., Tannenbaum R., Schwartz Z., Sandhage K.H., Boyan B.D. The effects of combined micron-submicron-scale surface roughness and nanoscale features on cell proliferation and differentiation Biomaterials 2011; 32: 3395-3403.

Glawe J.D., Hill J.B., Mills D.K., McShane M.J. Influence of channel width on alignment of smooth muscle cells by high-aspect-ratio microfabricated elastomeric cell culture scaffolds. J Biomed Mater Res A 2005; 75(1): 106-114.

Goffin J.M., Pittet P., Csucs G., Lussi J.W., Meister J.J., Hinz B. Focal adhesion size controls tension-dependent recruitment of alpha-smooth muscle actin to stress fibers. J Cell Biol 2006; 172: 259-268.

Graziano A., d'Aquino R. Cusella-De Angelis M.G., Laino G., Piattelli A., Pacifici M., De Rosa A., Papaccio G. Concave pit-containing scaffold surfaces improve stem cell derived osteoblast performance and lead to significant bone tissue formation. PloS One 2007; 2(6): 1-9.

Guck J., Ananthakrishnan R., Mahmood H., Moon T.J., Cunningham C.C., Kas J. The optical stretcher: A novel laser tool to micromanipulate cells. Biophys J 2001; 81: 767-784.

Guck J., Schinkinger S., Lincoln B. Wottawah F., Ebert S., Romeyke M., Lenz D., Erickson H.M., Ananthakrishnan R., Mitchell D., Käs J., Ulvick S., Bilby C. Optical deformability as an inherent cell marker for testing malignant transformation and metastatic competence, Biophysical Journal 2005; 88: 3689-3698.

Hadjipanayi E., Mudera V., Brown R.A. Guiding cell migration in 3D: a collagen matrix with graded directional stiffness. Cell Motil Cytoskeleton 2009a; 66: 121-128

Hadjipanayi E, Mudera V, Brown RAJ Close dependence of fi broblast proliferation on collagen scaffold matrix stiffness. Tissue Eng Regen Med 2009b; 3: 77-84.

Hampoelz B. and Lecuit T. Nuclear mechanics in differentiation and development. Curr Opin Cell Biol 2011; 23(6): 668-675.

Haq F., Anandan V., Keith C., Zhang G. Neurite development in PC12 cells cultured on nanopillars and nanopores with sizes comparable with filopodia. Int J Nanomedicine. 2007; 2(1): 107–115.

Harrison R.G. The cultivation of tissues in extaneous media as a method of morphogenetic study. Anat Rec 1912; 6: 181-193.

Hart A., Gadegaard N., Wilkinson C.D., Oreffo R.O.C., Dalby M.J. Osteoprogenitor response to low-adhesion nanotopographies originally fabricated by electron beam lithography. J Mater Sci Mater Med 2007; 18: 1211-1218.

Hasirci V. and Kenar H. Novel surface patterning approaches for tissue engineering and their effect on cell behavior. Nanomedicine 2006; 1: 73-90.

Hirschfeld-Warneken V.C., Arnold M., Cavalcanti-Adam A., López-García M., Kessler H., and Spatz J.P. Cell adhesion and polarisation on molecularly defined spacing gradient surfaces of cyclic RGDfK peptide patches. Eur J Cell Biol 2008; 87: 743-750.

Hochmuth R.M. Micropipette aspiration of living cells. J. Biomechanics 2000; 33: 15-22.

Holthaus M.G., Stolle J., Treccani L., Rezwan K. Orientation of human osteoblasts on hydroxyapatite-based microchannels Acta Biomaterialia 2012; 8: 394-403.

Houseman, B.T. and Mrksich, M.The Microenvironment of ımmobilized arg-gly-asp peptides is an ımportant determinant of cell adhesion. Biomaterials 2001; 22: 943-955.

Houtchens G.R., Fostera M.D., Desai T.A., Morgan E.F., Wong J.Y. Combined effects of microtopography and cyclic strain on vascular smooth muscle cell orientation. Journal of Biomechanics 2008; 4: 762–769.

http://www. 2009.igem.org

Hu W., Yim E., Reano R., Leong K., Pang S.W. Effects of nanoimprinted patterns in tissue-culture polystyrene on cell behavior. J Vac Sci Technol 2005; 23(6): 2984-2989.

Huang S. and. Ingber D.E. Shape-dependent control of cell growth, differentiation, and apoptosis: switching between attractors in cell regulatory networks. Experimental Cell Research 2000; 261, 91-103

Huang N.F., Patlolla B., Abilez O., Sharma H., Rajadas J., Beygui R.E.,. Zarins C.K., Cooke J.P. A matrix micropatterning platform for cell localization and stem cell fate determination. Acta Biomaterialia 2010; 6: 4614–4621.

Hudson M.E., Pozdnyakova I., Haines K., Mor G., Snyder M. Identification of differentially expressed proteins in ovarian cancer using high-density protein microarrays. Proc Natl Acad Sci 2007; 104: 17494-17499.

Huie J.C. Guided molecular self-assembly: a review of recent efforts. Smart Mater Struct 2003; 12: 264-271.

Hulmes D.J.S. Building collagen molecules, fibrils, and suprafibrillar structures. J Struct Biol 2002; 137: 2-10.

Ingber D. Integrins as mechanochemical transducers. Curr Opin Cell Biol 1991; 3: 841-848.

Ingber D.E. Integrins, tensegrity, and mechanotransduction. Gravit Space Biol Bull 1997; 10: 49-55.

Itano N., Okamoto S., Zhang D., Lipton S.A., Ruoslahti E. Cell spreading controls endoplasmic and nuclear calcium: a physical gene regulation pathway from the cell surface to the nucleus, Proc Natl Acad Sci 2003; 100: 5181–5186.

Ito Y. Surface micropatterning to regulate cell functions Biomaterials 1999; 20: 2333-2342.

Jaalouk D.E. and Lammerding J. Mechanotransduction gone awry. Nature Reviews Molecular Cell Biology 2009; 10: 63-73.

Jadlowiec J., Koch H., Zhang X., Campbell P.G., Seyedain M., Sfeir C. Phosphophoryn regulates the gene expression and differentiation of NIH3T3, MC3T3- E1, and human mesenchymal stem cells via the integrin/MAPK signaling pathway. J Biol Chem 2004; 279: 53323–53330.

Jaiswal R.K., Jaiswal N., Bruder S.P., Mbalaviele G., Marshak D.R., Pittenger M.F. Adult human mesenchymal stem cell differentiation to the osteogenic or adipogenic lineage is regulated by mitogen-activated protein kinase. J Biol Chem 2000; 275:9645-9652.

James C.D., Davis R., Meyer M., Turner A., Turner S., Withers G., Kam L., Banker G., Craighead H., Isaacson M., Turner J., Shain W. Aligned microcontact printing of micrometer-scale poly-L-lysine structures for controlled growth of cultured neurons on planar microelectrode. IEEE Trans Biomed Eng 2000; 47(1): 17-21.

Jing G., Wang Y., Zhou T., Perry S.F., Grimes M.T., Tatic-Lucic S. Cell patterning using molecular vapor deposition of self-assembled monolayers and lift-off technique. Acta Biomaterialia 2011; 7: 1094-1103.

Kane R.S., Takayam S., Ostuni E., Ingber D.E., Whitesides G.M. Patterning proteins and cells using soft lithography. Biomaterials 1999; 20: 2363-2376.

Kantawong F., Burgess K.E.V., Jayawardena K., Hart A., Burchmore R.J., Gadegaard N., Oreffo R.O.C., Dalby, M.J. Whole proteome analysis of osteoprogenitor differentiation induced by disordered nanotopography and mediated by ERK signalling. Biomaterials 2009; 30 (27): 4723-4731.

Karuri N.W., Liliensiek S., Teixeira A.I., Abrams G., Campbell S., Nealey P.F., Murphy C.J. Biological length scale topography enhances cell-substratum adhesion of human corneal epithelial cells. Journal of Cell Science, 2004; 117(15): 3153-3164.

Kemkemer R., Jungbauer S., Kaufmann D., Gruler H. Cell orientation by a microgrooved substrate can be predicted by automatic control theory. Biophys J 2006; 90(12): 4701-4711.

Kenar H., Köse G.T., and Hasirci V. In vitro bone tissue engineering on patterned biodegradable polyester blends. Biomaterials 2006; 27: 885-895.

Keselowsky, B.G., Collard, D.M. & Garcia, A.J. Integrin binding specificity regulates biomaterial surface chemistry effects on cell differentiation. Proc Natl Acad Sci USA 2005; 102: 5953-5957.

Ketene A.N., Schmelz E.M., Roberts P.C., Agah M. The effects of cancer progression on the viscoelasticity of ovarian cell cytoskeleton structures Nanomedicine 2012; 8(1): 93-102.

Kilian K.A., Bugarija B., Lahn B.T., Mrksich M. Geometric cues for directing the differentiation of mesenchymal stem cells Proc Natl Acad Sci USA 2010; 107: 4872–4877.
Kim B.S. and Mooney D.J. Scaffolds for engineering smooth muscle under cyclic mechanical strain conditions. Journal of Biomechanical Engineering 2000; 122: 210–215.

Kim E.J., Boehm C.A., Mata A., Fleischman A.J., Muschler G.F., Roy S. Post microtextures accelerate cell proliferation and osteogenesis. Acta Biomaterialia 2010; 6: 160–169.

King W.P., Kenny T.W., Goodson K.E., Cross G., Despont M., Dürig U., Rothuizen H., Binnig G.K., Vettiger P. Atomic force microscope cantilevers for combined thermomechanical data writing and reading. Appl Phys Lett 2001; 78: 1300-1302.

Klees R.F., Salasznyk R.M., Kingsley K., Williams W.A., Boskey A., Plopper G.E. Laminin-5 induces osteogenic gene expression in human mesenchymal stem cells through an ERK-dependent pathway. Mol Biol Cell 2005; 16: 881-890.

Kolf C.M., Cho E., Tuan R.S. Mesenchymal stromal cells. Biology of adult mesenchymal stem cells: Regulation of niche, self-renewal and differentiation. Arthritis Res Ther 2007; 9: 204-215.
Krampera M., Marconi S., Pasini A., Galiè M., Rigotti G., Mosna F., Tinelli M., Lovato L., Anghileri E., Andreini A., Pizzolo G., Sbarbati A., Bonetti B. Induction of neural-like differentiation in human mesenchymal stem cells derived from bone marrow, fat, spleen and thymus. Bone 2007; 40: 382-390.

Krauss S.W., Lo A.J., Short S.A., Koury M.J., Mohandas N., Chasis J.A. Nuclear substructure reorganization during late stage erythropoiesis is selective and does not involve caspase cleavage of major nuclear substructural proteins. Blood 2005; 106: 2200-2205.

Krieg M., Arboleda-Estudillo Y., Puech P.H., Käfer J., Graner F., Müller D.J., Heisenberg C.P. Tensile forces govern germ-layer organization in zebrafish. Nat Cell Biol 2008; 10(4): 429-436.

Kubo K., Tsukimura N., Iwasa F., Ueno T., Saruwatari L., Aita H., Chiou W-A., Ogawa T. Cellular behavior on TiO2 nanonodular structures in a micro-to-nanoscale hierarchy model Biomaterials 2009; 30: 5319–5329.

Kumar A., Whitesides G.M., Features of gold having micrometer to centimeter dimensions can be formed through a combination of stamping with an elastomeric stamp and an alkanethiol ''ink'' followed by chemical etching. Appl. Phys Lett 1993: 63 (14): 2002-2006.

Kumar A., Biebuyck H.A., Whitesides G.M. Patterning self-assembled- monolayers: applications in materials science. Langmuir 1994; 10(5): 1498–1511.

Lamers E., Walboomers X.F., Domanski M. , Riet J.-te, van Delft Falco C.M.J.M., Luttge R., Winnubst L.A.J.A., Gardeniers Han J.G.E., Jansen J.A. The influence of nanoscale grooved substrates on osteoblast behavior and extracellular matrix deposition. Biomaterials 2010; 31: 3307-3316.

Lammerding J, Fong L.G., Ji J.Y., Reue K., Stewart C.L., Young S.G., Lee R.T. Lamins A and C but not lamin B1 regulate nuclear mechanics. J Biol Chem. 2006; 281: 25768-25780.

Le Blanc K. Immunomodulatory effects of fetal and adult mesenchymal stem cells. Cytotherapy 2003; 5: 485-489.

Lee J., Chu B.H., Chen K.H., Ren F., Lele T.P. Randomly oriented, upright SiO_2 coated nanorods for reduced adhesion of mammalian cells. Biomaterials 2009; 30: 4488-4493.

Lee M.R., Kwon K.W., Jung H., Kim H.N., Suh K.Y., Kim K., Kim K-S. Direct differentiation of human embryonic stem cells into selective neurons on nanoscale ridge/groove pattern arrays. Biomaterials 2010; 31: 4360-4366.

Lekka M., Laidler P., Gil D., Lekki J., Stachura Z., Hrynkiewicz A.Z. Elasticity of normal and cancerous human bladder cells studied by scanning force microscopy. Eur. Biophys. J. 1999; 28 (4): 312-316.

Leung L., Chan C., Baek S. Naguib H. Comparison of morphology and mechanical properties of PLGA bioscaffolds Biomed Mater 2008; 3: 1-9.

Li B., Xie L., Starr Z.C., Yang Z., Lin Jeen-Shang, Wang James H-C. Development of micropost force sensor array with culture experiments for determination of cell traction forces. Cell Motility and the Cytoskeleton 2007; 64: 509-518.

Li X.Y., Ota I., Yana I., Sabeh F., Weiss S.J. Molecular dissection of the structural machinery underlying the tissue-invasive activity of membrane type-1 matrix metalloproteinase. Mol Biol Cell 2008; 19: 3221-3233.

Lim, C.T., Zhou E.H., Li A., Vedula S.R.K., Fu H.X. Experimental techniques for single cell and single molecule biomechanics. Mat. Sci. Eng. C 2006; 26: 1278-1288.

Lincoln B., Erickson H.M., Schinkinger S., Wottawah F., Mitchell D., Ulvick S., Curt Bilby C., Guck J. Deformability-Based Flow Cytometry. Cytometry Part A 2004; 59A; 203-209.

Lindberg U., Karlsson R., Lassing I., Schutt C.E., Hoglund A.S. The microfilament system and malignancy. Semin Cancer Biol 2008; 18: 2-11.

Liu S., Calderwood D.A., Ginsberg M.H. Integrin cytoplasmic domain-binding proteins. J Cell Sci 2000; 113(Pt 20): 3563-3571.

Liu W.F. and Chen C.S. Engineering biomaterials to control cell function Materials Today 2005; 8: 28-35.

Lo C.M., Wang H.B., Dembo M., Wang L.Y. Cell movement is guided by the rigidity of the substrate. Biophys J 2000; 79: 144-152.

Loesberg W., Riet J., Delft Fv., Schon P., Figdor C., Speller S., van Loon J.J., Walboomers X.F., Jansen J.A. The threshold at which substrate nanogroove dimensions may influence fibroblast alignment and adhesion. Biomaterials 2007; 28: 3944-3951.

Loesberg W.A., Walboomers X.F., van Loon J.J., Jansen J.A. The effect of combined cyclic mechanical stretching and microgrooved surface topography on the behavior of fibroblasts. J Biomed Mater Res A 2005; 75(3): 723-732.

Lord M.S., Foss M., Besenbacher F. Influence of nanoscale surface topography on protein adsorption and cellular response. Nano Today 2010; 5: 66-78

Lovmand J., Justesen J., Foss M., Lauridsen R. H., Lovmand M., Modin C. Besenbacher F., Pedersen F. S., Duch M. The use of combinatorial topographical libraries for the screening of enhanced osteogenic expression and mineralization, Biomaterials 2009; 30(11): 2015-2022.

Lussi J.W., Michel R., Reviakine I., Falconnet D., Goessl A., Csucs G., Hubbell J.A., Textor M. A novel generic platform for chemical patterning of surfaces Progress in Surface Science 2004; 76: 55-69.

Magnani A., Priamo A., Pasqui D., Barbucci R. Cell behaviour on chemically microstructured surfaces. Materials Science and Engineering C 2003; 23: 315-328.

Mahoney M.J., Chen R.R., Tan J., Saltzman W.M. The influence of microchannels on neurite growth and architecture. Biomaterials 2005; 26: 771-778.

Maloney J.M., Nikova D., Lautenschlager F., Clarke E., Langer R., Guck J., Van Vliet K.J. Mesenchymal stem cell mechanics from the attached to the suspended state. Biophysical Journal 2010; 99: 2479-2487.

Maniotis A.J., Chen C.S., and Ingber D.E. Demonstration of mechanical connections between integrins, cytoskeletal filaments, and nucleoplasm that stabilize nuclear structure. Proc Natl Acad Sci 1997; 94: 849–854.

Martínez E., Lagunas A., Mills CA, Rodríguez-Seguí S., Estévez M., Oberhansl S., J Comelles J., Samitier J. Stem cell differentiation by functionalized micro and nanostructured surfaces. Nanomedicine 2009; 4: 65-82.

Matsuzaka K., Walboomers F., de Ruijter A., Jansen J.A. Effect of microgrooved poly-l-lactic (PLA) surfaces on proliferation, cytoskeletal organization, and mineralized matrix formation of rat bone marow cells. Clin Oral Implants Res 2000; 11: 325-333.

Mattila P.K. and Lappalainen P. Filopodia: molecular architecture and cellular functions. Nature 2008; 9: 446-454.

Mattotti M., Alvarez Z., Ortega J.A., Planell J.A., Engel E., Alcántara S. Inducing functional radial glia-like progenitors from cortical astrocyte cultures using micropatterned PMMA. Biomaterials 2012; 33: 1759-1770.

McBeath R., Pirone D.M., Nelson C.M., Bhadriraju K, Chen C.S. Cell shape, cytoskeletal tension, and RhoA regulate stem cell lineage commitment. Dev Cell 2004; 6: 483-495.

McBride S.H., Falls T., Knothe Tate M.L. Modulation of stem cell shape and fate: Mechanical modulation of cell shape and gene expression. Tissue Eng A 2008; 14: 1573-1580.

McNamara L., Sjöström T., Burgess K.E., Kim J.J., Liu E., Gordonov S., Moghe P.V., Meek R.M., Oreffo R.O., Su B., Dalby M.J. Skeletal stem cell physiology on functionally distinct titania nanotopographies. Biomaterials 2011; 32(30): 7403-7410.

McNamara L.E., McMurray R.J., Biggs M.J.P., Kantawong F., Oreffo R.O.C., Dalby, M.J. Nanotopographical control of stem cell differentiation. Journal of Tissue Engineering 2010; 18: 1-13.

Mendonca G., Mendonca D.B.S, Aragao F.J.L, Cooper L.F. The combination of micron and nanotopography by h2so4/h2o2 treatment and its effects on osteoblast-specific gene expression of hmscs. J Biomed Mater Res 2010; 94A(1): 169-179.

Meshorer E., Yellajoshula D., George E., Scambler P.J., Brown D.T., Misteli T. Hyperdynamic plasticity of chromatin proteins in pluripotent embryonic stem cells. Dev Cell 2006; 10: 105-116.

Meyle J., Gultig K., Brich M., Hammerle H., Nisch W. Contact guidance of fibroblasts on biomaterial surfaces. J Mater Sci Mater Med 1994; 5: 463-466.

Migliorini E., Grenci G., Ban J., Pozzato A., Tormen M., Lazzarino M., Torre V., Ruaro M.E. Acceleration of neuronal precursors differentiation induced by substrate nanotopography. Biotechnology & Bioengineering 2011; 108(11): 2736-2746.

Mijailovich S.M., Kojic M., Zivkovic M., Fabry B., Fredberg B. A finite element model of cell deformation during magnetic bead twisting. J Appl Physiol 2002; 93: 1429-1436.

Miller C., Jeftinija S., Mallapragada S. Synergistic effects of physical and chemical guidance cues on neurite alignment and outgrowth on biodegradable polymer substrates. Tissue Eng 2002; 8(3): 367-378.

Mills J.P., Qie L., Dao M., Lim C.T. and Suresh S. Nonlinear elastic and viscoelastic deformation of the human red blood cell with optical tweezers. Mech Chem Biosyst 2004; 1: 169-180.

Milner K.R. and Siedlecki C.A. Submicron poly(L-lactic acid) pillars affect fibroblast adhesion and proliferation. J Biomed Mater Res A 2007; 82: 80-91.

Minne S.C., Yaralioglu G., Manalis S.R., Adams J.D., Atalar A., Quate C.F. Automated parallel high speed atomic force microscopy1998, Appl Phys Lett 72, 2340-2342.

Moon J.H., Yang Seung-Man, Pine D.J., Chang W-S. Multiple-exposure holographic lithography with phase shift Appl Phys Lett 2004; 85: 4184-4186.

Moss S.F., Krivosheyev V., de Souza A., Chin K., Gaetz H.P., Chaudhary N., Worman H.J., Holt PR. Decreased and aberrant nuclear lamin expression in gastrointestinal tract neoplasms. Gut 1999; 45:723-729.

Murphy W.L., Hsiong S., Richardson T.P., Simmons C.A., Mooney D.J. Effects of a bone-like mineral film on phenotype of adult human mesenchymal stem cells in vitro. Biomaterials 2004; 26: 303-310.

Nakagawa S., Pawelek P., Grinnell F. Extracellular matrix organization modulates fibroblast growth and growth factor responsiveness. Exp Cell Res 1989; 182: 572-582.

Ochalek T., Nordt F.J., Tullberg K., Burger M.M. Correlation between cell deformability and metastatic potential in B16-F1 melanoma cell variants. Cancer Res 1988; 48: 5124-5128.

Ogawa T., Saruwatari L., Takeuchi K., Aita H., Ohno N. Ti nano-nodular structuring for bone integration and regeneration. J Dent Res 2008; 87: 751-756.

Ohara P.T. and Buck R.C. Contact guidance in vitro. A light, transmission, and scanning electron microscopic study. Exp Cell Res 1979; 121(2): 235-249.

Okada S., Ito H., Nagai A., Komotori J., Imai H. Adhesion of osteoblast-like cells on nanostructured hydroxyapatite Acta Biomaterialia 2010; 6: 591-597.

Overby D.R, Matthews B.D, Alsberg E., Ingber D.E. Novel dynamic rheological behavior of individual focal adhesions measured within single cells using electromagnetic pulling cytometry. J Acta Biomaterialia 2005; 1: 295-303.

Ozturk N., Girotti A., Kose G.T., Rodríguez-Cabello J.C., Hasirci V. Dynamic cell culturing and its application to micropatterned, elastin-like protein-modified poly(N-isopropylacrylamide) scaffolds. Biomaterials 2009; 30: 5417-5426.

Padeste C., Özçelik H., Ziegler J., Schleunitz A., Bednarzik M., Yücel D., Hasırcı V. Replication of high aspect ratio pillar array structures in biocompatible polymers for tissue engineering applications. Microelectronic Engineering 2011; 88: 1836-1839.

Pajerowski J.D., Dahl K.N., Zhong F.L., Sammak P.J., Discher D.E.. Physical plasticity of the nucleus in stem cell differentiation. Proc Nat Acad Sci 2007; 104: 15619-15624.

Palin E., Liu H.N., Webster T.J. Mimicking the nanofeatures of bone increases bone-forming cell adhesion and proliferation. Nanotechnology 2005; 16(9): 1828-1835.

Park G.E., Webster T.J. A review of nanotechnology for the development of better orthopedic implants. J Biomed Nanotechnol 2005; 1: 18-29.

Park S., Koch D., Cardenas R., Kas J., Shih C.K. Cell motility and local viscoelasticity of fibroblasts. Biophys J 2005; 89: 4330-4442.

Park S.A, Kim I.A., Lee Y.J., Shin J.W., Kim C-R., Kim J.K., Yang Y., Shin J-W. Biological responses of ligament fibroblasts and gene expression profiling on micropatterned silicone substrates subjected to mechanical stimuli. Journal of Bioscience and Bioengineering 2006; 102: 402-412.

Patel S., Thakar R.G., Wong J. McLeod S.D., Li S. Control of cell adhesion on poly(methyl methacrylate). Biomaterials 2006; 27: 2890–2897.

Patla I., Volberg T., Elad N., Hirschfeld-Warneken V., Grashoff C., Fässler R., Spatz J. P., Geiger B. and Medalia O. Dissecting the molecular architecture of integrin adhesion sites by cryo-electron tomography. Nature Cell Biology 2010; 12(9): 909-916.

Pelham R.J Jr, Wang Y. Cell locomotion and focal adhesions are regulated by substrate flexibility. Proc Natl Acad Sci 1997; 94: 13661-13665.

Peng R., Yao X., Ding J. Effect of cell anisotropy on differentiation of stem cells on micropatterned surfaces through the controlled single cell adhesion. Biomaterials 2011; 32: 8048-8057.

Perennes F., Marmiroli B., Tormen M., Matteucci M., Di Fabrizio E. Replication of Deep X-ray Lithography fabricated microstructures through casting of soft material Journal of Micro/Nanolithography MEMS and MOEMS 2006: 5 (1): 011007-6.

Phinney D.G. Building a consensus regarding the nature and origin of mesenchymal stem cells. J Cell Biochem Suppl 2002; 38: 7–12.

Piner R.D., Zhu J., Xu F., Hong S., Mirkin C.A. Dip-Pen Nanolithography. Science 1999: 283; 661-663.

Pittenger M.F., Mackay A.M., Beck S.C., Jaiswal R.K., Douglas R., Mosca J.D., Moorman M.A., Simonetti D.W., Craig S., Marshak D.R. Multilineage potential of adult human mesenchymal stem cells. Science 1999; 284: 143-147.

Prodanov L., Riet J., Lamers E., Domanski M., Luttge R., van Loon J.J.W.A.,. Jansen J.A, Walboomers X.F. The interaction between nanoscale surface features and mechanical loading and its effect on osteoblast-like cells behavior. Biomaterials 2010; 31: 7758-7765.

Prunet-Marcassus B., Cousin B., Caton D., André M., Pénicaud L., Casteilla L. From heterogeneity to plasticity in adipose tissues: Site-specific differences. Exp Cell Res 2006; 312: 727-736.

Rajnicek A.M., Britland S., McCaig C.D. Contact guidance of CNS neurites on grooved quartz: influence of groove dimensions, neuronal age and cell type. J Cell Sci 1997; 110(Part 23): 2905-2913.

Rajnicek A.M., McCaig C.D. Guidance of CNS growth cones by substratum grooves and ridges: Effects of inhibitors of the cytoskeleton, calcium channels and signal transduction pathways. J Cell Sci 1997; 110: 2915-2924.

Ranella A., Barberoglou M., Bakogianni S., Fotakis C., Stratakis E. Tuning cell adhesion by controlling the roughness and wettability of 3D micro/nano silicon structures. Acta Biomaterialia 2010; 6: 2711-2720.

Raz A., and Geiger B. Altered organization of cell-substrate contacts and membrane-associated cytoskeleton in tumor cell variants exhibiting different metastatic capabilities. Cancer Res 1982; 42: 5183-5190.
Rebollar E., Frischauf I., Olbrich M., Peterbauer T., Hering S., Preiner J., Hinterdorfer P., Romanin C., Heitz J. Proliferation of aligned mammalian cells on laser nanostructured polystyrene Biomaterials 2008; 29: 1796-1806.

Recknor J.B., Recknor J.C., Sakaguchi D.S., Mallapragada S.K. Oriented astroglial cell growth on micropatterned polystyrene substrates. Biomaterials 2004; 25: 2753-2767.

Recknor J.B., Sakaguchi D.S., Mallapragada S.K. Directed growth and selective differentiation of neural progenitor cells on micropatterned polymer substrates. Biomaterials 2006; 27(22): 4098-4108.

Relan N.K., Yang Y., Beqaj S., Miner J.H., Schuger L. Cell elongation induces laminin alpha2 chain expression in mouse embryonic mesenchymal cells: role in visceral myogenesis, J Cell Biol 1999; 147: 1341-1350.

Remmerbach T.W., Wottawah F., Dietrich J., Lincoln B., Wittekind C. Guck J. Oral Cancer Diagnosis by Mechanical Phenotyping Cancer Res 2009; 69: 1728-1732.

Rodriguez J.P., Gonzalez M., Rios S., Cambiazo V. Cytoskeletal organization of human mesenchymal stem cells (MSC) changes during their osteogenic differentiation. J Cell Biochem 2004; 93(4): 721-731.

Rogers J.A. and Nuzzo R.G. Recent progress in soft lithography. Materials Today 2005; 8 (2): 50-56.

Rowat A.C., Lammerding J., Herrmann H., Aebi U. Towards an integrated understanding of the structure and mechanics of the cell nucleus. BioEssays 2008; 30: 226-236.

Schaller M.D., Borgman C.A., Cobb B.S., Vines R.R., Reynolds A.B., Parsons J.T. pp125FAK a structurally distinctive protein-tyrosine kinase associated with focal adhesions. Proc Natl Acad Sci 1992; 89: 5192-5196.

Schape J., Prausse S., Radmacher M., Stick R. Influence of lamin A on the mechanical properties of amphibian oocyte nuclei measured by atomic force microscopy. Biophys J 2009; 96:4319-4325.

Schellenberg F. A little light magic. IEEE Spectrum 2003; 40: 34-39.

Schift H., Saxer S., Park S., Padeste C., Piles U., Gobrecht J. Controlled co-evaporation of silanes for nanoimprint stamps. Nanotechnology 2005; 16: 171-175.

Schift H., Saxer S., Park S., Padeste C., Piles U., Gobrecht J. Controlled co-evaporation of silanes for nanoimprint stamps. Nanotechnology 2005; 16: 171-175.

Schoen I., Hu W., Klotzsch E, Vogel V. Probing cellular traction forces by micropillar arrays: contribution of substrate warping to pillar deflection Nano Lett. 2010; 10 (5): 1823-1830.

Settleman J. Tension precedes commitment - even for a stem cell. Mol Cell 2004; 14: 148-150.

Shah-Yukovich E.M., and Nelson A.C. Characterization of solid tumor microvasculature: a three-dimensional analysis using the polymer casting technique. Lab Invest 1988; 58: 236-244.

Shimi T., Pfleghaar K., Kojima S., Pack C.G., Solovei I., Goldman A.E., Adam S.A., Shumaker D.K., Kinjo M., Cremer T. Goldman R.D. The A- and B-type nuclear lamin networks: microdomains involved in chromatin organization and transcription. Genes Dev 2008; 22: 3409-3421.

Shingi H., Masato S., Eiichi T., Hideki M. Metal nanogap devices fabricated by conventional photolithography and their application to deoxyribose nucleic acid analysis. J Vac Sci & Tech B: Microelectronics and Nanometer Structures 2003: 21; 2937-2940.

Silva G.A., Czeisler C., Niece K.L., Beniash E., Harrington D.A., Kessler J.A., Stupp S.I. Selective differentiation of neural progenitor cells by high-epitope density nanofibers. Science 2004; 303: 1352-1355.

Sinha R.K., Tuan R.S. Regulation of human osteoblast integrin expression by orthopedic implant materials. Bone 1996; 18: 451-457.

Sjostrom T., Dalby M.J., Hart A., Tare R., Oreffo R.O.C., Su B. Fabrication of pillar-like titania nanostructures on titanium and their interactions with human skeletal stem cells. Acta Biomaterialia 2009; 5: 1433-1441.

Sniadecki N.J., Desai R.A., Ruiz S.A., Chen C.S. Nanotechnology for Cell–Substrate Interactions. Annals of Biomedical Engineering 2006; 34(1): 59-74.

Song G., Ju Y., Shen X., Luo Q., Shi Y., Qin J. Mechanical stretch promotes proliferation of rat bone marrow mesenchymal stem cells. Colloids Surf B Biointerfaces 2007; 58(2): 271-277.

Sorensen A., Alekseeva T., Katechia K., Robertson M., Riehled M.O., Barnett S.C. Long-term neurite orientation on astrocyte monolayers aligned by microtopography. Biomaterials 2007; 28: 5498-5508.

Spatz J.P. and Geiger B. Molecular Engineering of cellular environments: cell adhesion to nano-digital surfaces. Methods in Cell Biology 2007; 83: 89-111.

Standley, P.R., Cammarata A., Nolan B.P., Purgason C.T., Stanley M.A. Cyclic stretch induces vascular smooth muscle cell alignment via NO signaling. American Journal of Physiology— Heart and Circulatory Physiology 2002; 283: H1907-H1914.

Sul Y.T., Kang B.S., Johansson C., Um H.S., Park C.J., Albrektsson T. The roles of surface chemistry and topography in the strength and rate of osseointegration of titanium implants in bone. J Biomed Mater Res A 2009; 89: 942-950.

Suresh S. Biomechanics and biophysics of cancer cells. Acta Biomater 2007; 3: 413-438.

Suresh S., Spatz J., Mills J.P., Micoulet A., Dao M., Lim C.T., Beil M.T., Seufferlein T. Connections between single-cell biomechanics and human disease states: gastrointestinal cancer and malaria. Acta Biomater 2005; 1: 15-30.

Sutherland D.S., Broberg M., Nygren H., Kasemo B. Influence of nanoscale surface topography and chemistry on the functional behaviour of an adsorbed model macromolecule. Macromol Biosci 2001; 1: 270-273.

Tan J.L., Tien J., Pirone D.M., Gray D.S., Bhadriraju K., Chen C.S. Cells lying on a bed of microneedles: an approach to isolate mechanicalforce. Proc Natl Acad Sci 2003; 100: 1484-1489.

Teixeira A.I., Abrams G.A., Bertics P.J., Murphy C.J., Nealey P.F. Epithelial contact guidance on well defined micro and nanostructured substrates. J Cell Sci 2003; 116: 1881-1892.

Teixeira A.I., Nealey P.F., Murphy C.J. Responses of human keratocytes to micro and nanostructured substrates. J Biomed Mater Res A 2004; 71A (3), 369-376.

Teixeira A.I., McKie G.A., Foley J.D., Bertics P.J., Nealey P.F., Murphy C.J. The effect of environmental factors on the response of human corneal epithelial cells to nanoscale substrate topography. Biomaterials 2006; 27: 3945-3954.

Thakar R.G., Ho F., Huang N.F., Liepmann D., Li S. Regulation of vascular smooth muscle cells by micropatterning. Biochem Biophys Res Commun 2003; 307: 883-890.

Thapa A., Webster T.J., Haberstroh K.M. Polymers with nanodimensional surface features enhance bladder smooth muscle cell adhesion. J Biomed Mater Res 2003; 67A (4): 1374-1383.

Thomas C.H., Collier J.H., Sfeir C.S., Healy K.E. Engineering gene expression and protein synthesis by modulation of nuclear shape, Proc Natl Acad Sci 2002; 99: 1972–1977.

Thoumine O., Ott A., Cardoso O., Meister J.J. Microplates: a new tool for manipulation and mechanical perturbation of individual cells. J Biochem Biophys Meth 1999; 39: 47-62.

Titushkin I. and Cho M. Modulation of Cellular Mechanics during Osteogenic Differentiation of Human Mesenchymal Stem Cells, Biophysical Journal 2007; 93: 3693-3702.

Tsai W-B and Lin J-H. Modulation of morphology and functions of human hepatoblastoma cells by nano-grooved substrata Acta Biomaterialia 2009; 5:1442-1454.

Tsai W-B, Ting Y-C, Yang J-Y, Lai J-Y, Liu H-L. Fibronectin modulates the morphology of osteoblast-like cells (MG-63) on nano-grooved substrates. J Mater Sci Mater Med 2009; 20: 1367-1378.

Tseng A.A, Removing material using atomic force microscopy with single- and multiple-tip sources. Small 2011; 7(24): 3409-3427.

Tseng A.A., Notargiocamo A., Chen T.P. Nanofabrication by scanning probe microscope lithography. J Vac Sci Technol B 2005: 23(3); 877-894.

Tsuruma A., Tanaka M., Yamamoto S., Fukushima N., Yabu H., Shimomura M. Topographical control of neurite extension on stripe-patterned polymer films. Colloids and Surfaces A: Physicochem Eng Aspects 2006; 284-285: 470-474.

Turner S., Kam L., Isaacson M. and Craighead H. G., Shain W., Turner J. Cell attachment on silicon nanostructures. J Vac Sci Technol B 1997; 15(6): 2848-2854.

Uccelli A., Moretta L. Pistoia V. Mesenchymal stem cells in health and disease. Nature Reviews Immunology 2008; 8: 726-736.

Van Vliet K.J., Bao G, Suresh S. The biomechanics toolbox: experimental approaches to living cells and biomolecules. Acta Mater 2003; 51: 5881-5905.

Vogel V. and Sheetz M. Local force and geometry sensing regulate cell functions. Nat Rev Mol Cell Biol 2006; 7: 265-275.

Wang H.B, Dembo M., Wang Y.L. Substrate flexibility regulates growth and apoptosis of normal but not transformed cells. Am J Physiol Cell Physiol 2000; 279: 1345-1350.

Wang J.H., Grood E.S., Florer J., Wenstrup R. Alignment and proliferation of MC3T3-E1 osteoblasts in microgrooved silicone substrata subjected to cyclic stretching. Biomaterials 2000; 33: 729-735.

Wang J.H., Yang G., Li Z., Shen W. Fibroblast response to cyclic mechanical stretching depends on cell orientation to the stretching direction. Biomaterials 2004; 37: 573–576.

Wang P-Y., Yu J., Lin J-H., Tsai W-B. Modulation of alignment, elongation and contraction of cardiomyocytes through a combination of nanotopography and rigidity of substrates. Acta Biomaterialia 2011; 7: 3285–3293.

Ward K.A., Li W.I., Zimmer S., Davis T. Viscoelastic properties of transformed cells: role in tumor cell progression and metastasis formation. Biorheology 1991; 28: 301-313.

Webster T.J., Ergun C., Doremus R.H., Siegel R.W., Bizios R. Enhanced functions of osteoblasts on nanophase ceramics. Biomaterials 2000; 21: 1803-1810.

Weiner S., and Wagner H.D. The material bone: structure mechanical function relations. Ann Rev Mat Sci 1998; 28: 271–298.

Weiss P. Experiments on cell and axon orientation in vitro: the role of collodial exudates in tissue orgnization. J Exp Zool 1945; 100: 253-386.

Wenzel R.N. Resistance of solid surfaces to wetting by water. Ind Eng Chem 1936; 28: 988-994.

Wheeler B.C., Corey J.M., Brewer G.J., Branch D.W. Microcontact printing for precise control of nerve cell growth in culture. Biomech Eng 1999; 121: 73-78.

Whitesides G.M., Stroock A.D. Flexible methods for microfluidics. Phys. Today 2001; 54: 42-48.
Wiederrecht G. Handbook of nanofabrication, 1st Ed. Elsevier Press, Amsterdam, Boston, 2010.

Wilkinson A., Hewitt R.N., McNamara L.E., McCloy D., Dominic Meek R.M., Dalby, M.J. Biomimetic microtopography to enhance osteogenesis in vitro. Acta Biomaterialia 2011; 7 (7): 2919-2925.

Wilkinson C.D.W., Riehle M., Wood M., Gallagher J., Curtis A.S.G. The use of materials patterned on a nano- and micro-metric scale in cellular engineering. Mater Sci Eng C 2002; 19: 263-269.

Willis N.D., Cox T.R., Rahman-Casans S.F., Smits K., Przyborski S.A., van den Brandt P., van Engeland M., Weijenberg M., Wilson R.G., de Bruine A., C.J. Hutchison. Lamin A/C is a risk biomarker in colorectal cancer. PLoS One 2008; 3: e2988.

Winer J, Janmey P, McCormick M, Funaki M. Bone marrow-derived human mesenchymal stem cells become quiescent on soft substrates but remain responsive to chemical or mechanical stimuli. Tissue Eng Part A. 2009; 15:147–154.

Wojciak-Stothard, B., Curtis, A. S., Monaghan, W., McGrath, M., Sommer, I. and Wilkinson, C. D. Role of the cytoskeleton in the reaction of fibroblasts to multiple grooved substrata. Cell Motil Cytoskeleton 1995; 31: 147-158.

Wojciak-Stothard B., Curtis A., Monaghan W., MacDonald K. and Wilkinson C. Guidance and activation of murine macrophages by nanometric scale topography. Exp Cell Res.996; 223: 426-435.

Wong J.Y., Leach J.B., Brown X.Q. Balance of chemistry, topography, and mechanics at the cell–biomaterial interface: Issues and challenges for assessing the role of substrate mechanics on cell response Surf. Sci. 2004; 570: 119-133.

Woodbury D., Schwarz E.J., Prockop D.J., Black I.B. Adult rat and human bone marrow stromal cells differentiate into neurons J Neurosci Res 2000; 61: 364–370.

Wottawah F., Schinkinger S., Lincoln B., Ebert S., Müller K., Sauer F., Travis K., Guck J. Characterizing single suspended cells by optorheology Acta Biomaterialia 2005; 1: 263–271.

Wozniak MA, Modzelewska K, Kwong L, Keely PJ. Focal adhesion regulation of cell behavior. Biochim Biophys Acta 2004; 1692(2, 3): 103–119.

Wu B. and Kumar A. Extreme Ultraviolet Lithography. Extreme ultraviolet lithography: A review. J Vac Sci Technol B 2007; 25: 1743-1761.

Wyckoff J.B., Jones J.G., Condeelis J.S., Segall J. E. A critical step in metastasis: in vivo analysis of intravasation at the primary tumor. Cancer Res 2000; 60: 2504-2511.

Xia Y. and Whitesides G.M. Soft Lithography. Annual Review of Materials Science. 1998; 28: 153-184.

Xie J.W., Willerth S.M., Li X.R., Macewan M.R., Rader A., Sakiyama-Elbert S.E, Xia Y. The differentiation of embryonic stem cells seeded on electrospun nanofibers into neural lineages. Biomaterials 2009; 30: 354–362.

Xiu Y.H., Hess D.W., Wong C.P., UV and thermally stable superhydrophobic coatings from sol-gel processing. Journal of Colloid and Interface Science 2008; 326: 465-470.

Yang F., Murugan R., Wang S., Ramakrishna S. Electrospinning of nano/micro scale poly(L-lactic acid) aligned fibers and their potential in neural tissue engineering. Biomaterials 2005; 26: 2603-2610.

Yang J-Y, Ting Y-C, Lai J-Y, Liu H-L, Fang H-W, Tsai W-B. Quantitative analysis of osteoblast-like cells (MG63) morphology on nanogrooved substrata with various groove and ridge dimensions. J Biomed Mater Res A 2009; 90A: 629–640.

Yang M.T., Sniadecki N.J., Chen C.S. Geometric considerations of micro- to nanoscale elastomeric post arrays to study cellular traction forces. Advanced Materials 2007; 19: 3119-3123.

Yao L., Wang S., Cui W., Sherlock R., O'Connell C., Damodaran G., Gorman A., Windebank A., Pandit A. Effect of functionalized micropatterned PLGA on guided neurite growth. Acta Biomaterialia 2009; 5: 580–588.

Ye X., Liu H., Ding Y, Li H, Lu B. Research on the cast molding process for high quality PDMS molds. Microelectronic Engineering 2009; 86(3): 310-313.

Yilgor P., Hasirci N., Hasirci V. Sequential BMP-2/BMP-7 delivery from polyester nanocapsules. J. Biomed. Mater. Res. Part A, 2010; 93: 528-536.

Yim E.K.F., Reano R.M., Pang S.W., Yee A.F., Chen C.S., Leong K.W. Nanopattern-induced changes in morphology and motility of smooth muscle cells. Biomaterials 2005; 26: 5405-5413.

Yim E.K.F., Pang S.W., Leong K.W. Synthetic nanostructures inducing differentiation of human mesenchymal stem cells into neuronal lineage. Exp Cell Res 2007; 313: 1820-1829.

Yourek G., Hussain M.A., Mao J.J. Cytoskeletal changes of mesenchymal stem cells during differentiation. ASAIO J. 2007; 53(2): 219-228.

Yu H., Xiong S., Yong T.C., Leong W.S., Tan L.P. A novel and simple microcontact printing technique for tacky, soft substrates and/or complex surfaces in soft tissue engineering. Acta Biomaterialia 2012; 8: 1267–1272

Yücel D., Kenar H., Sethu P., Parashurama N., Hasirci V., Kaplan D., Toner M. Expression of Neural and Cardiomyogenic Lineage Markers by Mesenchymal Stem Cells from Human Bone Marrow and Wharton's Jelly. "2nd Annual Methods in Bioengineering Conference", (2007).

Yucel D., Kose G.T., Hasirci, V. Tissue engineered, guided nerve tube consisting of aligned neural stem cells and astrocytes. Biomacromolecules 2010; 11: 3584-3591.

Zhang J., Venkataraman S., Xu H., Song Yoon-Kyu Song, Hyun-Kon,. Palmore G.T.R., Fallon J., Nurmikko A.V. Combined topographical and chemical micropatterns for templating neuronal networks Biomaterials 2006; 27: 5734-5739.

Zhu B., Lu Q., Yin J., Hu J., Wang Z. Alignment of osteoblast-like cells and cell-produced collagen matrix induced by nanogrooves. Tissue Eng 2005; 11 (5, 6): 825-834.

Zink D., Fischer A.H., Nickerson J.A. Nuclear structure in cancer cells. Nat Rev Cancer 2004; 4: 677-687.

Zorlutuna P., Elsheikh A., Hasirci V. Nanopatterning of collagen scaffolds improve the mechanical properties of tissue engineered vascular grafts. Biomacromolecules 2009; 10: 814-821.

CURRICULUM VITAE

PERSONAL INFORMATION

Surname, Name: Özçelik, Hayriye
Nationality: Turkish (T.C.)
Date and Place of Birth: 24 January, 1977, Ankara, Turkey
Marital Status: Single
Phone: +90 312 210 51 89
Fax: +90 312 210 15 42
E-mail: inthecell@gmail.com, inthecell@hotmail.com

EDUCATION

Degree	Institution	Year of Graduation
MS	METU, Dept. of Biotech.	2004
BS	METU, Dept of Biology	2000

ACADEMIC EXPERIENCE

Year	Place	Enrollment
2007-2012	METU, Biotech. Res. Unit	Full time Researcher
2001-2004	METU, Biotech.Res. Unit	Full time Researcher

FOREIGN LANGUAGES: Advanced English

WORK EXPERIENCE

Year	Place	Enrollment
2002-2004	TÜBİTAK-BİTAV	Researcher and scientific text writer
2005-2006	Bilkent University, Department of Molecular Biology and Genetics.	Research Associate

RESEARCH EXPERIENCE ABROAD

Year	Place	Enrollment
15 June-15 August 2009	Paul Scherrer Institut Lab. for Micro and Nanotechnology	Research on production of high aspect ratio nanopillar arrays

PUBLICATIONS

Oral Presentations

2011   **H. Özçelik**, C. Padeste, V. Hasırcı, Cell Adhesion Behavior of Bone Marrow Stem Cells on Fibronectin-Coated Nanopillar Arrays, 24th European Conference on Biomaterials ESB 2011, September, 4-8, 2011, Dublin, IRELAND**.**

2011   **H. Özçelik**, C. Padeste, V. Hasırcı, Deformation of Nuclei and Microstructures: Evidence of Different Mechanoresponsiveness of Cancer and Non Cancerous Cells, V European Chapter of the Tissue Engineering and Regenerative Medicine International Society (TERMIS), June 7-10, 2011, Granada, SPAIN

2010   **H. Özçelik**, J. Ziegler, A. Schleunitz, M. Bednarzik, C. Padeste, V. Hasırcı, The Role of Nanopillars on Adhesion and Orientation of Saos-2 and Bone Marrow Stem Cells, 23rd European Conference on Biomaterials ESB 2010, September 11-15, 2010, Tampere, FINLAND.

2010   C. Padeste, **H. Özçelik**, J. Ziegler, A. Schleunitz, M. Bednarzik, V. Hasırcı,

Replication of high aspect ratio pillar array structures in biocompatible polymers for tissue engineering applications, 36th International Conference on Micro & Nano Engineering, September 19-22, 2010, Genda, ITALY.

2010   C. Padeste, H. Schift, A. Schleunitz, V. Trabadelo, **H. Özçelik**, V. Hasirci, J. Ziegler, S. Neuhaus, and H. Solak, Large area nanostructures for application in biology and bio-analytics, 1st First Cross Border Conference on NanoSciences and Materials for Health (Nano SMH), June 21-25, 2010, Nancy, FRANCE

Journal Papers

2011   C. Padeste , H. Özçelik , J. Ziegler, A. Schleunitz, M. Bednarzik , D. Yücel, V. Hasırcı**,** Replication of high aspect ratio pillar array structures in biocompatible polymers for tissue engineering applications, Microelectronic Engineering 88: 1836–1839.

2009   P.M.Davidson, H.Özcelik, V.Hasirci, G.Reiter, K.Anselme, Microstructured Surfaces Cause Severe but Non-Detrimental Deformation of the Cell Nucleus, Adv Mater 21: 3586-3590**.**

Patents

2012   A grid containin systematically distributed micro-nanopillar coated fields to control cell adhesion. Patent filing was already done for PCT (international application) to the Turkish Patent Institute in the name of both institutions (Middle East Technical Univ, TR- and Paul Scherrer Institute, CH) through the appointed patent attorney on 26 April 2012 File No: 2012-G-136420 for PCT.